
Electronic Thesis and Dissertation Repository

8-21-2015 12:00 AM

Design and Control of Robotic Systems for Lower Limb Stroke Rehabilitation

Aaron Yurkewich
The University of Western Ontario

Supervisor
Dr. Rajni Patel
The University of Western Ontario

Graduate Program in Electrical and Computer Engineering
A thesis submitted in partial fulfillment of the requirements for the degree in Master of
Engineering Science
© Aaron Yurkewich 2015

Follow this and additional works at: <https://ir.lib.uwo.ca/etd>



Part of the [Biomechanical Engineering Commons](#)

Recommended Citation

Yurkewich, Aaron, "Design and Control of Robotic Systems for Lower Limb Stroke Rehabilitation" (2015).
Electronic Thesis and Dissertation Repository. 3077.
<https://ir.lib.uwo.ca/etd/3077>

This Dissertation/Thesis is brought to you for free and open access by Scholarship@Western. It has been accepted for inclusion in Electronic Thesis and Dissertation Repository by an authorized administrator of Scholarship@Western. For more information, please contact wlsadmin@uwo.ca.

DESIGN AND CONTROL OF ROBOTIC SYSTEMS FOR LOWER LIMB
STROKE REHABILITATION

Monograph

by

Aaron P. Yurkewich

Graduate Program in Electrical & Computer Engineering

A thesis submitted in partial fulfillment
of the requirements for the degree of
Master's in Engineering Science

The School of Graduate and Postdoctoral Studies
The University of Western Ontario
London, Ontario, Canada

© Aaron Yurkewich 2015

Abstract

Lower extremity stroke rehabilitation exhausts considerable health care resources, is labor intensive, and provides mostly qualitative metrics of patient recovery. To overcome these issues, robots can assist patients in physically manipulating their affected limb and measure the output motion. The robots that have been currently designed, however, provide assistance over a limited set of training motions, are not portable for in-home and in-clinic use, have high cost and may not provide sufficient safety or performance. This thesis proposes the idea of incorporating a mobile drive base into lower-limb rehabilitation robots to create a portable, inherently safe system that provides assistance over a wide range of training motions. A set of rehabilitative motion tasks were established and a six-degree-of-freedom (DOF) motion and force-sensing system was designed to meet high-power, large workspace, and affordability requirements. An admittance controller was implemented, and the feasibility of using this portable, low-cost system for movement assistance was shown through tests on a healthy individual. An improved version of the robot was then developed that added torque sensing and known joint elasticity for use in future clinical testing with a flexible-joint impedance controller.

Keywords

Stroke Rehabilitation, Rehabilitation Robotics, Lower Extremity Rehabilitation, Human Machine Interaction, Multi-Degree-of-Freedom Design and Control.

Co-Authorship Statement

Chapter 2:

- A.Yurkewich – provided the concept, explanation, presentation and CAD design of this lower-limb robotic system that were used in a successful funding proposal (PI: Dr. R.V. Patel) to fund this project, designed, manufactured, debugged and validated the entire system, including the mobile base, 3-DOF platform, force sensing system, electronic circuitry, mathematical models, robot control architecture, and software implementation, performed all experiments and wrote the full conference manuscript, reviewed and submitted the manuscript
- F. Atashzar – contributed to the development of the successful funding proposal (PI: Dr. R.V. Patel) that funded this project, helped in the selection of the omni-drive mechanism over alternatives and the pressure sensors chosen for the sensorized footplate, reviewed the manuscript
- A. Ayad – reviewed and gave suggestions on the final mechanical design of the six-DOF robot, helped in the in-house manufacturing and assembly of the robot, and in the design and manufacture of the custom circuit board

Acknowledgments

During my Master's research I gained generous support and guidance from our rehabilitation group, the Canadian Surgical Technologies and Advanced Robotics (CSTAR) research team, the AGE-WELL NCE research group, and the staff and students within the Western University community.

I would like to thank my supervisor, Dr. Rajni Patel, for his mentorship throughout my research development. He has been a major motivator during my undergraduate and Masters' research and discussing ideas and goals with him has broadened my perspectives and knowledge in health care robotics research greatly.

To develop the robotic systems designed, manufactured, and implemented the input and support of many colleagues was helpful in improving the system and moving it forward.

Chris Vandelaar of the University Machine Services provided design and manufacturing experience that added rigidity and longevity to the robot structure. He also provided machining training so the robot could be manufactured in-house.

Ahmed Ayad, a research volunteer and undergraduate student played an instrumental role in the circuit board design and robot manufacture stages and Ran Xu, a fellow graduate student at CSTAR provided insight in the control of the robot.

Eugen Porter of the Western University Electronics Shop has been a mentor to me during my University education, introduced me to robotics and has always been an encouraging friend that is full of ideas. He has inspired me to love learning and mentor younger students in developing their knowledge and teamwork skills.

Thank you to my family and my girlfriend Emily, as well as her family, for their love and support, and for helping me reflect on the bigger picture of my work.

Table of Contents

Abstract	ii
Co-Authorship Statement.....	iii
Acknowledgments.....	iv
Table of Contents	v
List of Tables	viii
List of Figures	ix
List of Appendices	xiii
List of Symbols	xiv
Chapter 1	2
1 Introduction	2
1.1 Effects of Stroke on Neuromuscular Deficit.....	2
1.2 Clinical Therapy & Rehabilitative Impact	4
1.3 Limitations & Challenges of Current Therapy	6
1.4 Motivation.....	8
1.4.1 Socio-Economic Impact of Robotic Stroke Therapy	8
1.4.2 Therapy Techniques.....	10
1.4.3 Rehabilitation Tasks for Clinical & At-Home Therapy.....	11
1.5 Robotic Therapy for Lower-Limb Rehabilitation.....	13
1.6 Thesis Outline and Organization	16
Chapter 2.....	18
2 Six-Degree-of-Freedom Robotic System for Lower-Limb Stroke Rehabilitation.....	18
2.1 Mechanical Design & Manufacturing.....	20
2.2 Mathematical Modeling	25

2.2.1	Inverse Kinematic Model.....	26
2.2.2	Inverse Jacobian Formulation	28
3.2.3	Forward Kinematics.....	30
2.3	Custom Designed Six-DOF Force Sensor	31
2.3.1	Sensor Design	31
2.3.2	Sensor Optimization.....	34
2.3.3	Sensor Calibration and Evaluation.....	35
2.4	Electrical Design.....	41
3.4.1	Overview of Communication Flow	42
2.4.1	Custom Circuitry Design & Module Implementation	43
2.5	Robot Control.....	53
2.5.1	Trajectory Control.....	54
2.5.2	Admittance Control.....	56
2.6	Summary of Six-DOF Rehabilitation System.....	57
Chapter 3	58
3	Flexible Mobile Robotic System for In-Home Stroke Rehabilitation Motion Assistance and Assessment.....	58
3.1	Mechanical Design.....	61
3.2	Custom Flexible Sensor for Joint Torque Sensing and Three-DOF Force Sensing.....	64
3.2.1	Sensor Design	64
3.3	Robot Control & Mathematical Modeling.....	74
4	Concluding Remarks and Future Work	79
4.1	Thesis Contributions	79
4.2	Discussion	80
4.3	Future Work	81

5	References	84
	Appendices.....	90
	Curriculum Vitae	96

List of Tables

Table 1: Robot Specifications List.....	20
Table 2: Planar Motion Mechanism Decision Matrix.....	21
Table 3: Drive Base Actuator Selection Chart.....	23
Table 4: Translation & Rotation Robot Specifications.....	25
Table 5: ATI Delta-NET Force/Torque Sensor Specifications, Sensor Comparison	39
Table 6: Custom Force/Torque Sensor Specifications.....	39
Table 7: ATI Gamma Force/Torque Sensor Specifications, Used for Calibration.....	40
Table 8: Required Specifications for Microcontroller	51

List of Figures

Figure 1: Sitting Knee Extension Task Prescribed Commonly to Stroke Patients	11
Figure 2: Toe and Heel Raising Task	12
Figure 3: Foot and Ankle Circling Task	12
Figure 4: Lower Extremity Rehabilitation Robot: A: Patient Shoe; B: Force Sensor; C: 3DOF Platform; D: Omni-Directional Drive Base	19
Figure 5: Functional six-DOF Lower Extremity Rehabilitation Robot Prototype	19
Figure 6: Three-DOF Omni-Directional Drive Base	23
Figure 7: Finite Element Analysis of Three-DOF Omni-Directional Drive Base	23
Figure 8: a) Three-DOF Parallel Platform; b) Finite Element Analysis of the Linear Actuation Lead Screw	25
Figure 9: Robot Coordinate System: a) A top view of the robot, showing the joint-space parameters of the drive base and the platform coordinate system “P”. b) A back view of the robot, showing the platform link parameters, and the coordinate system of the drive base “B” and platform.....	27
Figure 10: Algorithm used for solving the platform forward kinematics.	31
Figure 11: Tekscan FlexiForce Sensor Specifications. Image Courtesy of Tekscan https://www.tekscan.com/products-solutions/force-sensors/a201	32
Figure 12: Tekscan Pressure Sensor Calibration Curves, from FlexiForce Datasheet	33
Figure 13: Six-DOF force/torque sensor displaying the location of the installed pressure sensors. Sensors 2, 9, 12 & 15 are located between the footplate and the platform base plate. The other sensors are placed between the side panels and the footplate. The Z axis comes out of the page and intersects the X and Y axes.	33

Figure 14: Custom Force Sensor Calibration Setup: A: Handle; B: ATI Gamma Force/Torque Sensor; C: Custom Force/Torque Sensor	37
Figure 15: Relation between the pressure sensor values multiplied by the conversion matrix and the readings from the Gamma Force/Torque sensor in a) X; b) Y; c) Z; d) α ; e) β ; f) γ ; and the associated line of best fit used for the calibration matrix.	38
Figure 16: ATI and custom sensor force readings when the user applied forces in the X direction.	40
Figure 17: ATI and custom sensor torque readings when the user applied torque about γ	41
Figure 18: Magnitude of error in force measurement for forces and torques applied in the Y, Z, β and α directions individually.	41
Figure 19: Communication Flow Diagram.	43
Figure 20: Simplified Operational Amplifier Circuit.	45
Figure 21: Actuator velocity signal a) before and b) after observer tuning.	47
Figure 22: Frequency response of low-pass filter implemented in C.	47
Figure 23: Motor Velocity Tracking Control Method	49
Figure 24: Motor Velocity Tracking Control Performance	49
Figure 25: Motor Velocity Tracking Control Step Response	50
Figure 26: PCB design for Manufacturing and Assembly	52
Figure 27: Signal Processing & Control Board	52
Figure 28: Experimental Setup: A: Optical Tracker; B: Game Interface; C: Micron Tracker Display; E: Robot	53

Figure 29: The trajectory of the robot in a) X and Y when commanded to track a circular trajectory; and b) γ , β , and α when each was commanded to follow a sinusoidal trajectory	54
Figure 30: Real-time Trajectory Control Setup using an HD ² haptic device and the six-DOF lower-limb rehabilitation robot.	55
Figure 31: a) The force and motion of the individual's foot in the X and Y direction during assisted motion along Y; b) the force and rotation of the ankle about Y as the robot assisted in maintaining a neutral ankle position.	57
Figure 32: Side View of Three-DOF Robot for In-Home Lower-Limb Rehabilitation ...	60
Figure 33 Top View of Three-DOF Robot for In-Home Lower-Limb Rehabilitation	60
Figure 34: Commercial Design of Lower-Limb Rehabilitation Robot.....	63
Figure 35: Mechanical and Electrical Layout of Rehabilitation Robot A) Omni-Wheel; B) Flexible Coupling Housing; C) Battery, CPU & Circuit Board Holder; D) Actuator; E) EPOS Motor Controller	63
Figure 36: Standard Flexible Coupling: A) Hub; b) Spider.....	65
Figure 37: Custom Flexible Coupling Rapid Prototyped Mold and Spider Material	66
Figure 38: Experimental Setup to Calibrate and Evaluate Coupling Stiffness and Sensor Performance	68
Figure 39: Linear Shaft Rotation vs. Torque for Initial Flexible Coupling Prototype	68
Figure 40: Validation of the Flexible Torque Sensor using an ATI Gamma Sensor.....	69
Figure 41: Rise and Fall Time of the Flexible and Gamma Torque Sensors.....	69
Figure 42: Hytrel Coupling Calibration and Validation against an ATI Gamma Sensor .	70
Figure 43: left: Intermediate; and right: Final Custom Flexible Coupling	72

Figure 44: Modular Flexible Actuation and Torque Sensing Assembly	73
Figure 45: The Set of Parts and Tools Required to Assemble the Module.....	73
Figure 46: Three Step Assembly for Assembling Actuation Modules	74
Figure 47: Coordinate System of the Omni-Directional Drive Base	77
Figure 48: Modified Canfield Mechanism Designed to be Mounted to a Mobile Base ...	83

List of Appendices

Appendix A: Custom Circuit Board Schematics	90
Appendix B: Costs Associated with Circuit Board and Six-DOF Lower-Limb Robot....	94

List of Symbols

Six-DOF Robot Modeling

$\theta_1, \theta_2, \theta_3, \theta_4$	Angular position of each wheel
$x_{base}, y_{base}, \alpha_{base}$	Translational and rotational components of the robot base
r_w	Wheel radius
r	Ratio of the base radius to wheel radius
\vec{L}_i	Vector of platform link i
L_{ix}, L_{iy}, L_{iz}	Cartesian components of each link length vector
r_s	Ratio of lead screw pitch to gear ratio
\vec{Z}_p	Vector from the base frame to the platform frame
γ, β	Rotational components of the robot platform with respect to base
\vec{B}_i	Vector from the base frame to the universal joint COR of link i attached to the base
\vec{P}_i	Vector from the platform frame to the universal joint COR of link i attached to the platform
R_{xy}	Rotation matrix from platform to base coordinate system
$\theta_5, \theta_6, \theta_7$	Angular position of each platform motor
$\dot{\theta}_1, \dot{\theta}_2, \dot{\theta}_3, \dot{\theta}_4$	Angular velocity of each wheel
$\dot{x}_{base}, \dot{y}_{base}, \dot{\alpha}_{base}$	Translational and rotational velocities of the robot base
$\dot{\gamma}, \dot{\beta}, \dot{Z}_p$	Translational and rotational platform velocities

Six-DOF Force and Torque Sensing

$F_x, F_y, F_z, T_x, T_y, T_z$	Six-DOF force and torque sensing components
R_{FSR}	One-DOF force sensor resistance
R_s	Feedback resistance
V_{reg}	Output voltage from voltage regulator
V_{out}	Output voltage to microcontroller

Wheel Velocity Measurement

f	Encoder sampling frequency
CPR	Encoder counts per revolution
V_{max}	Maximum wheel velocity
D_{wheel}	Wheel diameter
$\dot{\theta}_n$	Current velocity estimate
$\dot{\theta}_{n-1}$	Previous velocity estimate
μ	Current update parameter
μ_{n-1}	Previous update parameter
$\dot{\theta}_{avg_n}$	Filtered average velocity
$\dot{\theta}_{avg_{n-1}}$	Previous filtered average velocity
p	Kalman filter pole
ε	Error estimate

lpg	Low-pass gain
K	Kalman Gain
P	Prediction Error
ρ	System noise
m	Measurement noise

Admittance Control

\vec{V}	Robot velocity
\vec{F}_a	Force applied by the patient
\vec{T}_{act}	Robot trajectory
\vec{T}_{des}	Desired trajectory
K_F, K_T	Stiffness gains

Impedance Control

M, C	Dynamic parameters of the robot
q	Angular position of the wheel
τ	Torque applied by the robot
τ_{ext}	Torque applied by the patient
θ	Angular position of the motor shaft
B	Actuator inertia

B_θ	Reduced actuator inertia
K_θ	Desired stiffness parameter
D_θ	Desired damping parameter
u	Control input

Additional Variables used in Three-DOF Robot Modeling

δ	Angle between the X axis and the vector from the wheel centre of contact to the origin
φ	Tilt angle of each wheel
r_b	Radius of the circle created from the contact point of the wheels

Chapter 1

1 Introduction

Worldwide, 15 million individuals experience a stroke each year, and 50,000 of these cases occur in Canada [1]. Approximately two-thirds of these individuals will suffer neurological deficit and over half will never fully regain motor skills essential for everyday tasks, diminishing their independence in daily living [2, 3, 4]. Ideally, therapists are physically involved in the patient rehabilitation process; however, the number of therapists is limited [5]; and many patients must perform their rehabilitation exercises independently. In these cases, how correctly the patient performs therapy cannot be monitored, and the qualitative assessment scales used during patient check-ups (e.g. Fugl-Meyer Assessment, Berg Balance Scale) lack sensitivity to small changes in recovery that can be useful in adapting therapy. Robotic devices can be incorporated into rehabilitation regimens to provide greater access to guided therapy, measure patient-specific variables important to assessing on-going recovery [6] and improve motion control and coordination for both the upper [3, 7] and lower limbs [8]. Through continued support from the research, industrial and medical communities, novel devices and applications will be conceived and the use of these devices for diagnosis, therapy, and assessment throughout recovery will be accepted.

1.1 Effects of Stroke on Neuromuscular Deficit

A stroke event can have quite varied effects on neuromuscular functionality based on the severity and location of the injury, and as a result, the effectiveness of traditional rehabilitative programs on recovering motor skills and somatosensory pathways varies greatly among patients. To more fully understand the effects of stroke on reacting to a stimulus and completing a desired motion response the sequence of sensory and actuation events can be categorized as: sensing, signal interpretation, decision making, signal generation, and actuation. In the sensing stage the individual takes in stimuli from his or her environment and converts the stimuli to electrical impulses. These impulses travel to specialized areas in the brain, such as the visual, auditory and sensory areas and are

processed to provide appropriate information to the frontal lobe to decide how best to react to the stimulus. The frontal lobe then communicates with the motor cortex to determine the appropriate movement response and the motor cortex generates an electrical impulse that travels to the muscle fibers. This signal excites the muscle fibers to actuate, causing a physical response [9, 10, 11]. In the event of a stroke, in which there is a lack of blood flow to an area of the brain, by blockage (ischemic stroke), vessel rupture (hemorrhagic stroke) or trauma, cells along the brain's blood vessel paths die from lack of oxygen, causing local brain failure. The functions of the brain are highly compartmentalized which causes a wide variety of post-stroke symptoms between patients, especially when cell death is localized in the sensory interpretation, cognitive or motor control centers. Kolb & Wishaw [12] reference the frontal lobe in that,

“There is no other part of the brain where lesions can cause such a wide variety of symptoms. The frontal lobes are involved in motor function, problem solving, spontaneity, memory, language, initiation, judgement, impulse control, and social and sexual behavior”.

The typical neuromuscular symptoms of stroke are muscle rigidity, motor control deficit, coordination loss, weakness and pain [13]. In many cases muscle rigidity is caused by under-regulation of the motor cortex, causing pain and constant stimulation of muscles. The ensuing joint inactivity causes tendons to shorten and joints to stiffen, resulting in a low range of motion. Motor control deficit and weakness can be caused by many areas of the brain as it can be affected by loss of proprioception and tactile feedback, an inability to decide upon movement commands and a reduction in the number of muscles fibers that can be recruited to perform the command. The effects of these neuromuscular deficits are felt most by the limb contralateral to the side of the brain that experienced the injury [14]. Coordination tasks are most affected by damage to the cerebellum, having greatest effect on walking gait, reaching tasks and hand motion. Although neurological damage is usually localized, it can affect many areas of neuromuscular control, requiring a specialized therapy plan for each patient.

1.2 Clinical Therapy & Rehabilitative Impact

Prescribed rehabilitation regimens vary between patients, but a common practice is to combine therapist-directed joint movement and self-directed muscle actuation immediately after stroke diagnosis to prevent joint stiffening and pain [15]. This therapy can also vitalize damaged or unused areas of the brain to change physiologically and functionally in order to regain motor skills lost due to stroke [16, 17].

During the first six months of traditional therapy patients usually recover a portion of their motor control skills, but these gains plateau and individuals are left with limited motor functionality [18]. From analysis of patients in traditional and novel rehabilitation programs, it has been shown that the time to initiation of guided-limb actuation has the greatest effect on patient recovery [19, 20], and focus on functionally-oriented rehabilitation (e.g. walking, grasping, and reaching) can provide therapy that helps patients develop more fully in the short-term and can provide rehabilitative benefits far after the initial six months [21].

In order to understand why these rehabilitative effects are observed neurological studies have been performed. These studies have shown that after a stroke, patients have higher than normal neural activity, due to accelerated synaptogenesis and dendrite remodeling, but this higher than normal activity diminishes over time as the lesion heals. To accelerate recovery it is important for patients to activate sensing and actuation pathways to form connections between the motor cortex and muscles, and between the sensory pathways and the brain. After the initial healing phase brain activity subsides to normal levels, and memory, learning and neuroplasticity pathways are relied upon to train the brain to use its current resources in functional coordination tasks [22]. As such, guided movement immediately after stroke, and continued functional training in the later stages of recovery are essential to obtaining a maximal improvement in neuromuscular function.

Occupational and physical therapists are the most involved in patient neuromuscular rehabilitation, and their focus is on expanding range of motion, improving motor control and developing coordinated movement. Therapists assist patients in stretching exercises

to regain range of motion, guide patients in controlled movement of individual joints and coordination tasks, and teach patients movement strategies that will increase their success rate in performing daily tasks. The progression in rehabilitation exercising starts with positioning the patient in an orientation that is safe, either sitting or lying down, and applying force to their limb to move a single joint along one DOF. The second stage is to have the patient focus on actuating the joint to perform motion tasks and the third stage is to have the patient perform similar tasks under the weight of the limb and with a weight applied. These three stages allow the patient to recover proprioceptive connections on what the motion should feel like, followed by creating connections between the motor cortex and muscle fibers to actuate and strengthen muscles [23]. Once these three stages are complete the patient can then focus on performing functional tasks that require coordination between joints.

The exercises for the upper limb focus on reaching and holding objects, and the exercises for the lower-limb are geared toward helping patients walk, sit, stand and lie down. For the shoulder and elbow these exercises include raising and lowering the arm from various orientations, and moving the arm toward and away from the body, concentrating on moving the arm in a controlled motion without twisting the arm. For the wrist these exercises include flexion, extension, pronation and supination, with the greatest focus on increasing range of motion. The typical issue with the hand is that the muscles tend to contract, causing cramping and making it difficult to grasp large objects. The initial therapy is to stretch the hand flat and move it along a flat surface, followed by practicing picking up and placing objects and performing arm exercises with an open palm. The initial hip and knee exercises are similar to the shoulder and elbow exercises, followed by practicing transferring body weight between the legs. In ankle rehabilitation the exercises are similar to wrist exercises, where the main focus is on flexion and extension to protect against drop-foot gait and internal rotation to maintain balance and a symmetric gait while walking.

Patient progress during stroke recovery is heavily dependent on the location and severity of the stroke, the timing and quality of rehabilitation training and surgical interventions administered to the patient, and the patient's attitudes. Of the fifty-percent of stroke

survivors that are not independent and require special care due to moderate to severe motor impairment [24], the most likely candidates to suffer this disability are those who have suffered a stroke to the anterior cerebral artery impacting the frontal lobe, and the individual with greatest chance of regaining motor skills are those with impairment to the deep brain.

1.3 Limitations & Challenges of Current Therapy

Worldwide, the demand for physiotherapy-intensive treatment is growing due to higher rates of disability linked to aging populations, and stable rates of stroke incidence per capita [25, 26]. As a result, it will become increasingly difficult to provide early initiation to stroke therapy, provide sufficient daily therapy to produce the maximal rehabilitative effect for each patient, and continue functional therapy long-term. In Canada, sixty-three percent of stroke victims already do not have access to rehabilitation therapy due to insufficient supply of physicians and facilities [5] and the cost of funding these rehabilitation programs is substantial [27]. As a result, many candidates that are projected to have low potential for recovery are not accepted into or motivated to continue rehabilitation programs, causing emotional issues and significantly impacting their personal budget if a caregiver is required [5, 28].

Current estimates state that it takes an average of 11 days, in Ontario, Canada, between the time of stroke and the start of acute therapy, a delay that is proven to significantly impact final recovery as this is when neural activity and the rate of spontaneous rehabilitative gain are highest. This can be attributed to a lack of rehabilitation equipment and staff within hospitals, and is pronounced in rural communities where delay times are on average 6 days above the average [5, 27, 29, 30].

For lower-limb therapy in particular, the force the therapist needs to exert and the workspace they need to cover is large as the lower-limb is powerful, rigid and heavy. Also, certain functional training motions such as walking motions incorporate too many joints to be controlled by a single therapist. As a result, therapists need to take breaks often as the therapy is physically exhausting and requires the assistance of other therapists to offer gait training. At times such therapy is not offered due to the number of

patients that need therapy. In addition, such powerful motion can be unsafe to the therapist and patient, and the amount of control the therapist has on the patient's limb is low, so treatment may not be ideal. To compensate for the weight of the patient's limb and body, and keep the patient stable throughout therapy, exercise plans have been developed that allow the patient to sit or lie down and use braces and standard exercise equipment to train movements similar to everyday activities. This type of therapy has shown to have value in the recovery process, although some studies show that training the patient in the position used in daily tasks yields faster results [31].

In current rehabilitation programs, the therapist makes decisions on patient recovery based on feel and experience. However, this type of therapy does not identify small changes in patient improvement, and is heavily reliant on therapist judgment, leading to non-optimal adaptation of the patient's rehabilitation program. Assessments are performed on a regular basis and can be used to assess patient improvement and adapt therapy as well; however these scales are qualitative and have similar disadvantages. The data generated by these assessments is non-specific to the type of stroke experienced by each patient and requires intuition to interpret in order to adapt therapy. Typical assessment scales used in therapy include the Fugl-Meyer Assessment, Berg Balance Scale, Functional Independence Measure, Wolf Motor Function Test, Late Life Function and Disability Instrument, Functional Ambulation Category, Rivermead Mobility Index, Modified Ashworth Scale, and the Barthel Index [32]. Of these scales, the Fugl-Meyer assessment is most used clinically as it is comprehensive, and gives a reliable measurement of impairment with respect to independence [33]. This scale evaluates the patient in 61 tests and ranks the patient on a scale from 0-2 based on muscle activity, flexibility, reflexes, sensing, and coordination. From a therapy optimization point-of-view, however, this data is difficult to work with as it lacks the detail of information required to adapt therapy daily or in real-time. Also, the metrics are not patient-based and can give meaningless correlations between patients as stroke survivors have quite varied capabilities. Further, patients cannot be transferred easily between therapists without sacrificing recovery gains as designing a therapy program requires intuition and knowledge about each patient's recovery trends.

1.4 Motivation

Rehabilitation robots have been used in therapy for over twenty years and have proven to be more useful than receiving no additional rehabilitative support in many cases, and have shown to give rehabilitative gains equal to or better than training with experienced therapists in some cases. However, the use of these robots is still limited to engineering research settings, especially in the case of lower-limb devices, due to their current size, weight and cost. As a result, patients must rely on current therapy protocols in which they have limited access to therapy, and are only provided therapy opportunities in the first few months after stroke. This significantly deteriorates recovery outcomes leaving patients unable to walk or get out of bed, and fully reliant on others. By focusing on portability, compactness, affordability, safety and specific therapy procedures for lower-limb therapy in the robot design stage an innovative device that maximally impacts the independence of stroke survivors and is suitable for at-home patient rehabilitation can be conceived and developed.

1.4.1 Socio-Economic Impact of Robotic Stroke Therapy

Over 60% of Canadian stroke survivors do not have access to stroke therapy, which is draining to the Canadian budget, and does not provide adequate recovery results for performing daily tasks. Health care for stroke survivors needs to improve in order for these patients to gain independence and participate in society. Through decentralized access to neuromuscular rehabilitation therapy and improved techniques in therapy a greater number of older adults will recover to a level where they can live independently.

Developing portable, affordable and safe robotic systems for lower-limb stroke rehabilitation therapy will allow each patient to own their own system and use it in their home and in the clinic. This will assist them in completing exercises properly and daily. The creation of connections from the motor cortex to neuromuscular junctions is most active directly after stroke, but decreases to normal levels within the first three months as healing slows. For this reason, it is important to begin therapy within the first few days after stroke diagnosis. In this time the patient is assessed for their amount of neuromuscular deficit and the clinician must make a diagnosis of whether rehabilitative

therapy will help the patient. This process can take two-to-three weeks, and over half of patients that need therapy are not even admitted. During this time it would be useful to have a portable system for patients to use for simple and safe guided therapy. Participating in preselected movement and range of motion exercises daily would give patients the opportunity to establish a greater number of functioning muscle activation sites to recover greater muscular strength and control, and prevent tendon shortening and pain. In addition to increasing muscle activity through initial-stage therapy, a device that can train patients to make compound muscle movements with a task-based focus could provide rehabilitative benefit to patients throughout their life. The gains from this type of therapy are much slower as the brain has to learn how to activate the proper muscles using the limited neuromuscular connections the patient has, but the recovery from this therapy benefits from frequency and duration. Since current rehabilitation programs are in short supply they are less accessible to these patients, but would be suitable for an accessible device. In addition to the accessibility issues related to rehabilitation, 40% of patients that are admitted to rehabilitation programs drop-out [5], and these drop-outs have been linked to emotional causes such as anxiety, depression, lack of control over their illness and therapist de-motivation. Through independent therapy patients have the opportunity to take control of their rehabilitation, solving many of these issues.

Apart from the direct costs of rehabilitation programs, patient independence will ease the workload of family members, and these family members will not need to take as much time off work. A hands-free method of therapy would also allow therapists to monitor the therapy of multiple patients at once, like in a typical workout class. The therapist could then take an observatory role from which to critique patient form, focus on modifying therapy strategies to speed recovery, and identify unsafe scenarios caused by erratic patient movement. This would also minimize therapist fatigue and pain due to physical exertion in awkward stances. Safe, accessible care is essential to improving the lives of patients and those who care for them, and would also lower the health care costs of rehabilitation per patient if these devices are made affordable.

1.4.2 Therapy Techniques

Therapy-oriented design is essential to developing devices with significant improvement over current practice that can be commercialized for social, economic and/or social impact in the near future. Current technologies (i.e. actuators, controllers, sensors) are advanced enough to be used in useful ways to provide therapy. By gaining the transdisciplinary expertise necessary to identify deficiencies in elderly care therapy and combining this knowledge with technological integration more complete solutions to therapy needs can be generated. Once the initial device is developed and evaluated clinical trials can be held, following Ethics Review Board approval, to determine the recovery benefits of the device.

From a commercialization perspective, these devices will allow greater access to affordable therapy and adherence to therapy programs, as well as allow patients to recover more fully than with current therapy techniques alone. This will reduce governmental health care costs as therapists will be able to provide therapy to multiple patients simultaneously, and reduce the number of long-term care facilities as patients' recover more fully and will be able to perform daily tasks individually and participate socially in the community. The rehabilitation devices developed during this Masters' thesis have the potential to significantly change the way rehabilitation therapy is performed and deepen our understanding of stroke recovery. This level of impact in combination with the knowledge, partnerships and funding within the AGE-WELL NCE community will provide ample opportunities for the commercialization of these devices.

Innovation is essential to economic and social growth as it expands the possibilities of what can be accomplished, injects new ideas into the society, and spurs new research questions. AGE-WELL's goal is to provide transdisciplinary innovation, by building on knowledge and experience in health sciences, engineering, social sciences, and public policy. By involving therapists, patients and industry in the generation of constraints, specifications and concept generation, a set of therapy tasks and robot requirements can be developed that require a novel robot design and lead to an effective rehabilitation solution. To summarize the generated requirements the device should be affordable, lightweight, easy to use, portable, and able to perform task-specific movements and

measure relevant stroke recovery information. From the completion of the mechanical and electrical design it will be important to design a control algorithm that is safe and robust when used by various patients with varying neuromuscular disorders.

1.4.3 Rehabilitation Tasks for Clinical & At-Home Therapy

The lower-limb rehabilitation robot presented in this thesis was developed to provide the following three rehabilitative therapies to stroke patients during recovery.

1.4.3.1 Early-Stage Motion Assistance

In the initial months following stroke it is important to assist patients with lower-limb deficit to repeatedly actuate their hip, knee and ankle in order to recover neuromuscular pathways essential for movement. By actuating each DOF of each joint there is a greater potential for each muscle group of the lower-limb to be established in the patient's neuromuscular architecture. In this type of dexterous rehabilitation it is also important to actuate over a large range of motion in order to alleviate pain and increase proprioception, flexibility and circulation. To provide such dexterous and high range of motion manipulation this rehabilitation robot is comprised of a three DOF omni-directional drive base and a three DOF actuation platform that controls the trajectory of the patient's foot. Since the lower-limb is a redundant mechanism, joints can be braced to provide therapy to specific joints as is customary in traditional therapy [34]. Figure 1, provided by Stroke-Rehab.com, gives a demonstration of a recommended exercise for stroke survivors in which the patient extends and relaxes the knee in a sitting position.



Figure 1: Sitting Knee Extension Task Prescribed Commonly to Stroke Patients

Image Courtesy of www.stroke-rehab.com

1.4.3.2 Ankle Training & Exercise in Dynamic Environments

The second task involves training the ankle under dynamic knee motion and external forces. From this therapy the patient can experience the sensations of dynamic loading in everyday activities while being assisted in controlling ankle rotation. In addition, the robot's parallel mechanism provides sufficient torque to be used in ankle strength training before beginning demanding exercises in an upright position. Figure 2 and 3, also provided by Stroke-Rehab.com, show two ankle exercises recommended for stroke survivors.



Figure 2: Toe and Heel Raising Task

Image Courtesy of www.stroke-rehab.com

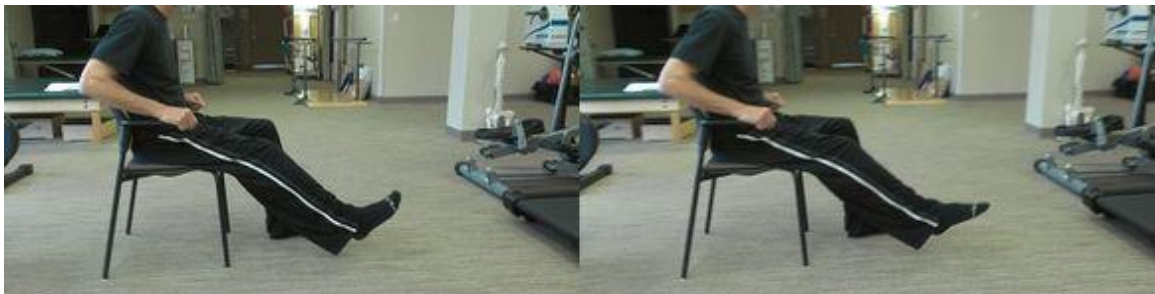


Figure 3: Foot and Ankle Circling Task

Image Courtesy of www.stroke-rehab.com

1.4.3.3 Functional Motion Therapy

Providing joint actuation assistance is important in early stage stroke therapy, but prolonged therapy should focus more on functional tasks (e.g. walking, turning, sitting and standing, climbing stairs). To train a desired foot trajectory personalized for each patient, the therapist manipulates the patient's foot while the robot is actively backdriven. Since this robot is attached only at the foot, trajectory personalization is possible for patients of varying body proportions without changing the geometry of the robot. As patients are seated for this therapy their body weight is supported and they do not have to focus on balancing. As a result, they can focus on developing muscle-memory, learning and memorizing coordination skills from following task-like trajectories before performing functional rehabilitation from an upright position.

1.5 Robotic Therapy for Lower-Limb Rehabilitation

To overcome current issues with access to sufficient therapy, and quantitative assessment of recovery, a number of mechatronic rehabilitation devices have been created that are specialized for the upper and lower limb, and can provide recovery with similar or better results than traditional therapy [25, 35, 36, 37]. These robots can also adapt therapy in real-time based on patient success, provide a scalable medium for therapy as multiple patients can perform therapy at the same time, and motivate patients to execute their therapy plan more frequently through the creation of interactive gaming environments.

Robotic devices for upper and lower limb therapy have been developed and clinically tested, but the current ankle, balance and gait rehabilitation robots show lower efficacy than upper-limb robots. Only one gait trainer has shown recovery results similar to that of traditional therapy [38]. Other lower-limb systems have been commercialized and have been incorporated into rehabilitation regimens [39, 40, 41, 42]; however, many of these devices have a high cost-to-performance ratio and do not allow for personalized therapy [25]. The power and workspace required for these robots make them more difficult and costly to design, manufacture and control, the patient neuromuscular activation must be much stronger to actuate the lower-limb as the limb's weight greater, and patients lose

vision-based feedback (as they cannot see their legs while walking). Further, due to therapist fatigue and the complexity of functional therapy there is a great need for these devices in rehabilitation clinics. The current systems do not provide active hip abduction/adduction therapy, which is critical for changing direction while walking, balancing on uneven surfaces, and stretching. To improve performance and personalization, it will be important to create devices that patients can access directly after a stroke for joint and muscle actuation and continue to use afterward for functional training.

Devices with multiple DOFs and a large workspace provide greater flexibility in hip, knee and ankle therapy, and portability is essential for accessibility in clinics and homes. For the ankle, which is highly dexterous, Girone *et al.* [43] designed a Stewart platform actuation system with force feedback, to provide resistive forces during orthopedic rehabilitation. The workspace of the system was too limited to be extended to hip and knee rehabilitation. To expand the workspace of upper-limb rehabilitation devices without compromising portability or compactness, Luo *et al.* [44] developed a mobile omni-directional robot that encompassed the planar workspace of the upper-limb, and a compliant force-sensing structure was recently added to a similar system [45].

To control robots to perform stroke therapy many control implementations have been proposed and the most commonly implemented forms are trajectory control, impedance control, electromyographic (EMG) assistance, and active-resistance [46, 47, 48, 49]. In trajectory control applications the robot is in full control of the patient's motion, teaching the patient what a movement will feel like, with the goal of energizing the somatosensory system and having the patient actively replay the exercise. However, the joints of stroke patients can be very rigid and may lack the range of motion necessary to perform the task, in which case the robot could injure the patient. An impedance controlling algorithm was then proposed by Hogan for upper limb rehabilitation, where by the robot applies guiding forces to the patient while the patient is cued to move along a desired trajectory [50]. A desired velocity, final position and system impedance are decided initially, and a real-time minimum jerk trajectory calculation was performed to update the real-time desired trajectory. From clinical testing and patient recovery data, improvements to this

general control strategy have been implemented to increase the rate of patient recovery by assisting patients only when force-guidance is required. Common methods for applying this assist-as-needed therapy are to establish a region around the desired trajectory where the patient will receive no assistance, or to activate this assistance only if the patient has not moved for a certain period of time [51, 52, 53]. Impedance parameters were also tuned automatically using adaptive and performance-based methods during a task or between tasks to challenge patients more as they recover [54]. Patients can be quite strong and rigid, especially in the case of the lower-limb deficit, and this has forced many robot designs to select powerful motors that are heavy and costly or opt for higher gearing that creates backdrivability issues. This lack of passive backdrivability can diminish the performance of impedance control algorithms, motivating researchers to use admittance control algorithms [55] and/or EMG feedback [56] to capture the patient's movement intent through force feedback and provide motion accordingly. It is still unclear which methods of control are most useful in establishing therapy regimens for patients with neuromuscular deficit, and through iterative design, control, and clinical experimentation, further knowledge will be generated on how to perform rehabilitative therapy, both robotically and traditionally, for maximal patient recovery.

Robotic technology is starting to be incorporated into rehabilitation therapy regimens, and as robotic rehabilitation therapy develops, novel techniques to improve therapy will be incorporated into existing regimens for improved recovery results, patient screening and evaluation, and accident (i.e. fall) prevention training. One interesting research area is mirror therapy, where the therapist and the patient hold separate robots and the therapist's movements are used to guide the patient in completing functional therapy tasks [57]. This can be extended to tele-robotic applications as well, where the patient can be in a rural community and still gain access to the most experienced therapists. In this case, with the aid of adaptive control algorithms most of this assistance to patient movement can then be controlled by the patient's robot alone and the therapist can tune adaptive parameters or modify exercises intermittently based on experience. This therapy can then be extended to at-home use where outpatients can perform effective rehabilitation regimens, and further, be used by patients during their everyday life to train the tasks that are most useful to them personally. Another interesting area of research is

in applying a stimulus to an unaffected area of the body that is proportional to the proprioceptive feeling the patient should feel when moving an affected joint. In many patients that have severe stroke, there is a low chance that they will recover the proprioceptive channels necessary to create smooth or effective motion, but with visual, auditory or tactile feedback [58], these patients may regain the ability to perform tasks independently. These are just some of the many avenues in rehabilitation robotics to explore further, and through continued development in rehabilitation robotics research and clinical experimentation, continued improvements in the recovery rate of stroke patients will be achieved.

1.6 Thesis Outline and Organization

In this thesis, novel robotic systems have been developed to provide feasible solutions to motion assistance for in-home lower-limb stroke rehabilitation therapy. Specific requirements on workspace, power, safety, cost, and application have motivated the incorporation of mobile omni-directional drive bases and cost effective force and torque sensors into the robotic systems.

From here onwards, the robot described in Chapter 2 will be referred to as the six-DOF robot and the robot described in Chapter 3 will be referred to as the three-DOF robot.

Chapter 2 presents a six-DOF motion assistance system, in which a parallel platform is mounted onto a mobile base for end-effector style rehabilitation of the hip, knee and ankle. A novel embedded low-cost sensor was designed, manufactured and tested for its performance in measuring the six-DOF force/torque generated by the user's foot while the robot was in use. The performance of the system in providing motion assistance was evaluated through in-lab experiments with a healthy individual's foot attached to the robot's footplate.

Chapter 3 proposes modifications to the drive base structure and control strategy developed in Chapter 2, aimed at improving the usability and performance of the system for assist-as-needed training and neuromuscular skills assessment. The modular three-

DOF drive base developed can be used as a stand-alone system for knee and ankle therapy, is lightweight, compact and wireless for portability, adds an easy to don/doff ergonomic quick-release foot attachment system for safety and reduces the number of actuators to reduce cost and complexity. A novel rotary series elastic joint with high resolution and high sampling rate torque-sensing has been designed, manufactured and validated for its linear elasticity and torque-sensing performance. The joint and sensing module is embedded into the mobile omni-directional drive base and the novel system developed provides backdrivable three-DOF actuation with fast and accurate three-DOF force/torque feedback for assist-as-needed control algorithms, and patient skills assessment. The design concept has been validated via modelling and impedance control simulations, and the system's construction and preliminary testing show improvements in backdrivability and portability.

Chapter 4 gives concluding remarks on the knowledge developed during this thesis work, and presents ideas for future directions of this work.

Chapter 2

2 Six-Degree-of-Freedom Robotic System for Lower-Limb Stroke Rehabilitation

Chapter 2 presents the design and implementation of a novel six-degree-of-freedom (DOF) rehabilitation robot for post-stroke patients with lower-limb neuromuscular deficit¹. The robot combines a mobile drive base and a three-DOF platform to create a portable system for use in homes and clinics, encompasses the dexterity, workspace and power of a typical person, and is inherently safe as the maximum force applied is related to the robot weight and wheel frictional coefficient. The goal of this device is to provide physicians and therapists with a tool for assisting patients in knee, ankle and certain hip movements by tuning initial therapy parameters and providing intermittent adaptation to these parameters based on patient improvement. Patients are seated and the foot of their affected lower-limb is placed on the platform of the robot shown in Figure 4. In this position the patient is safely oriented and can focus fully on developing specific motor control skills. A motion or force cue is then portrayed to the patient and the patient interacts with the device to meet the final goal. When performing assistive therapy the patient's shoe is adhered to the platform using a hook and loop fastener attached to the sole of the shoe so that under high frequency force variations the patient's foot will detach from the device. The robot and its custom circuitry were designed, manufactured and assembled and the robot is displayed in Figure 5.

The kinematics and Jacobian of the robot were developed and these models have been validated experimentally through optical tracking of the robot end-effector in position and velocity control modes. A custom force/torque sensor was designed and implemented as a low cost solution to measuring patient forces and torques during therapy and was

¹ The work described in Chapter 2 was presented and published in the International Conference on Robotic Rehabilitation (ICORR) [59].

evaluated using a commercial force/torque sensor. Using this information an admittance controller was implemented to assist patients with neuromuscular deficit in moving their affected lower-limb along a prescribed path.

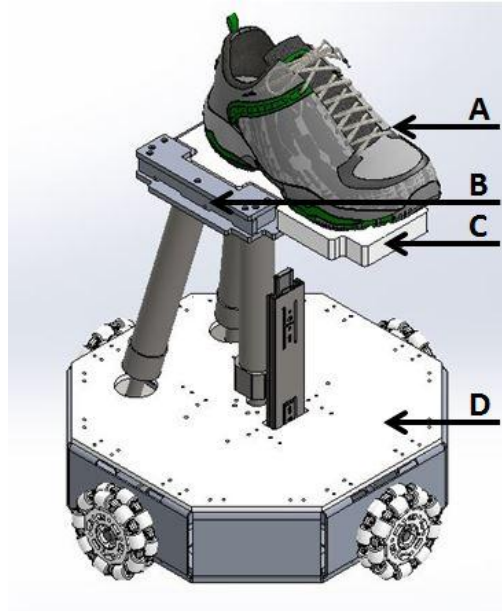


Figure 4: Lower Extremity Rehabilitation Robot: A: Patient Shoe; B: Force Sensor; C: 3DOF Platform; D: Omni-Directional Drive Base



Figure 5: Functional six-DOF Lower Extremity Rehabilitation Robot Prototype

2.1 Mechanical Design & Manufacturing

Robotic solutions for lower-limb rehabilitation therapy present interesting mechatronic challenges as the lower-limb has many DOF and a large workspace, can generate high forces and torques and in the case of post-stroke patients, can be extremely rigid. In response, the robot must provide sufficient dexterity to train the desired muscle groups, move at reasonable speeds to train individuals for everyday motion, and apply forces similar to those of the natural environment. As well, minimizing the number of bulky and costly components, and providing the ability to disengage the robot from applying force to the patient in the case of an unpredicted event is essential to making the device portable, affordable and safe for in-home use. From biomechanical data on the typical range of motion [60], joint velocities and forces required for walking [61], cost reports on the affordability of the HAL lower-limb rehabilitation system [62], and the general guidelines above, a specifications list was generated as shown in Table 1. Conceptual designs were then generated through research on current robotic upper and lower limb devices, as well as functional decomposition, morphological analysis and group brainstorming sessions. Through initial concept development and analysis a list of key requirements was formulated and a decision matrix was used to quantitatively select the appropriate mechanism, as shown in Table 2. This table ranks the robotic system requirements on a 1 to 5 scale, with 5 as most important in terms of overall usefulness to stroke patients. Engineering complexity and implementation aspects were also considered in this table, but given less importance as these challenges are the strengths of the device designer and would be met through time and effort in the detailed design stage.

Table 1: Robot Specifications List

	Range of Motion	Force Capacity	Speed	Sensor Accuracy
Planar Translation	1m	400N	60 cm/s	1mm
Vertical Translation	30cm	400N	30cm/s	0.1mm
Three Rotations	45 ⁰	10Nm	20 ⁰ /s	0.1 ⁰
Overall Robot Specifications				
Maximum Weight	20kg	Max Prototype Cost		\$4000
Max Diameter	40cm	Max Height		60cm
Other Needs: Supports 1000N vertical load, Mounting not required, 100Hz control frequency				

To accommodate the therapy tasks and device specifications, and following from the quantitative mechanism selection process, a three-DOF omni-directional drive base was selected. The drive base provides large-workspace planar motion and rotation for hip and knee flexion/extension, hip adduction/abduction and internal/external rotation. A three-DOF parallel platform was then selected to provide vertical motion for hip and knee flexion/extension, and roll and pitch rotation for plantarflexion/dorsiflexion and supination/pronation of the ankle. This mechanism provides high force and torque as well as structural rigidity and is similar to Stewart platforms which have shown effectiveness in musculoskeletal rehabilitation. For ease of use and transportation in clinical and home environments, the robot was designed to be lightweight, and communicate wirelessly with a host computer.

Table 2: Planar Motion Mechanism Decision Matrix

Concepts/ Customer Requirements	Rank (1-5) 5=Best	Omni-Directional Mobile System	Linear Serial Manipulator	Rotary Serial Manipulator
Lightweight Structure	5	5	2	4
Inexpensive	5	5	1	3
Easy to Disengage System	5	5	3	3
Similarity to Existing in-Home Devices	4	5	1	1
Control Simplicity	3	2	5	4
Backdrivability	3	3	2	4
High Workspace-to-Size Ratio	3	5	1	3
Low Foot Height	3	2	5	5
Ease of Manufacture	2	3	4	2
Compact Structure	2	4	4	2
Patient View of System Complexity	2	5	3	2
Structural Rigidity	1	4	3	2
Total		159	98	116

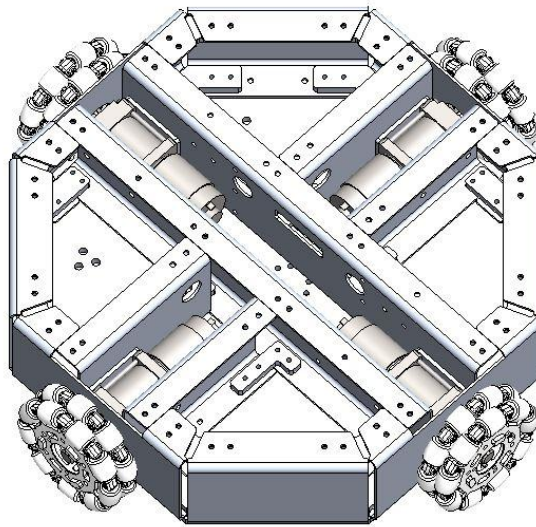
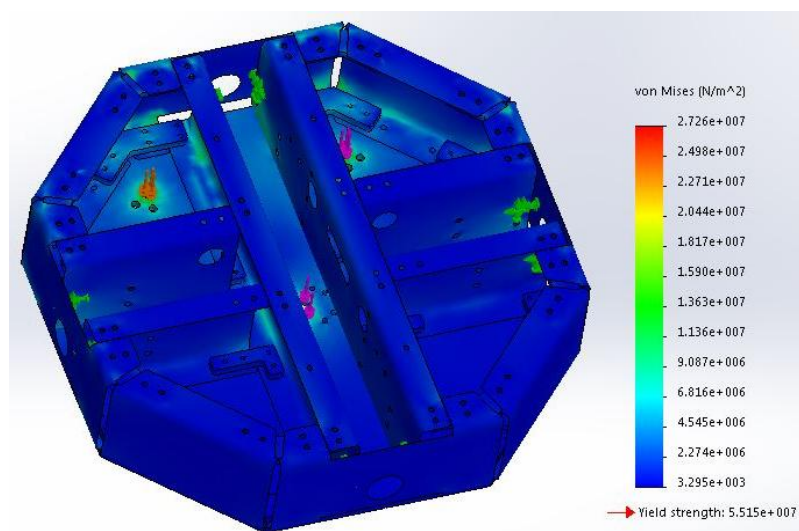
To meet the demanding specifications of lower-limb robotic therapy a custom drive base was developed and is shown in Figure 6. Wheels with a high radial dynamic friction coefficient (0.9 on carpet) were selected to apply sufficient forces while keeping the robot at a reasonable weight of 18.6kg for transporting up stairs. The robot could also be transported along flat ground by actively backdriving the motors. A four-wheel

configuration was chosen as opposed to a three-wheel alternative to provide greater resistance to tipping, more accurate control of one-DOF ground plane movements, and greater force output for the same motor power. A base diameter of 380mm was selected to avoid tipping due to transverse patient loads. The drive base was constructed from sheet aluminum for a high strength to weight ratio, maximal rigidity and space savings for embedding electrical components and wiring. To power the wheels inexpensive high-power brushed DC motors (BaneBots LLC, RS550, 180 Watt, 12V) and planetary gearboxes (BaneBots LLC, P60, 132:1) were selected from a list of suitable actuators in Table 3, and incremental encoders (US Digital, E6, 1024 CPR) were chosen for odometry measurement, with a translational and rotational resolution of 0.31mm and 0.087° , respectively.

In the detailed design stage of the robot base, factors to consider included the compactness of the robot, orientation of the wheels for maximum rotational torque, machinability of the robot frame, ease of assembly and the weight the robot could support. To meet these demands the wheels were positioned at 90° angles to one another, and tangent to the robot circumference. The frame was then designed around the actuator placement, and was designed for laser cutting and 1DOF bending which was a cost-effective method for manufacturing. The robot geometry was then optimized iteratively using SolidWorks to create a compact base that allowed space for embedding the motor controllers and wiring. To optimize the weight of the frame and assure its rigidity a SolidWorks Finite Element Analysis study was performed to iterate the design and select the thickness of material used for the walls and base of the robot. A 1000N load, equal to a typical patient's weight if they were to stand on the robot, was applied to the robot through the three support links to the parallel platform designed and explained below. From this study 12 gauge aluminum sheet metal was used for the robot walls and a $1/8''$ aluminum sheet was used for the base frame. The finite element study showed the robot base would not yield with a safety factor of 2 (maximum von Mises stress of 27 MPa versus yield strength of 55MPa), and the deformation was small, as shown in Figure 7.

Table 3: Drive Base Actuator Selection Chart

Motor + Gearbox / Specification	BaneBots RS550/ BaneBots P60	Maxon 353295/ Maxon 110412	Harmonic Drive LLC FHA-14C
Power (W)	250	250	250
Gearbox Ratio	132:1	93:1	50:1
Motor + Gearbox Efficiency (%)	35	58	70
Actuator Cost (CAD)	65	1325	2890

**Figure 6: Three-DOF Omni-Directional Drive Base****Figure 7: Finite Element Analysis of Three-DOF Omni-Directional Drive Base**

To provide sufficient rigidity, force and torque a lead screw actuated platform was designed and integrated into the drive base to minimize robot height, lower the centre of gravity, and enclose the motors and gears for safety. Using precision lead screws for actuation, rotary and angular contact bearings, and universal joints the motion of the platform was constrained to the three DOF stated above. To drive the 1/8" per turn lead screw a motor was attached to a pinion that meshed with the gear on the lead screw for a 3:1 gear reduction and isolating the motor from loads applied at the footplate. The same motors were selected to drive the lead screws as the drive base, and optical encoders (US Digital, E4P) were used to sense motor rotation for end effector resolutions of 0.0071mm, 0.0035° (pitch), 0.0052° (yaw) at a neutral platform position, respectively. Lead screw actuation was used as opposed to pneumatic actuation in order to avoid the noise and expense of a compressor, as well as for ease of force, and velocity control. Ball screws or series elastic mechanisms could also be used but these could increase the device cost and/or weight considerably. The universal joint placement was then chosen to maximize the ratio of vertical translation to total robot height while ensuring lead screw shear to be below the yield strength limit with a safety factor of 2, from a 1000N vertical load and full-torque lead screw actuation, as analyzed through Finite Element Analysis. The designed structure and associative stress analysis were displayed in Figure 8a and b, respectively. To minimize the height of the robot further and keep the lead screw motors and gearing concealed from the patient the platform was then embedded into the drive base. A lead screw length sufficient for vertical translation was selected and the patient can optimally use the robot from a meter-high seated position. From the robot capabilities presented in Table 4, this robot exceeds the initial design specifications for providing proper foot manipulation and actuation for the predefined rehabilitation tasks.

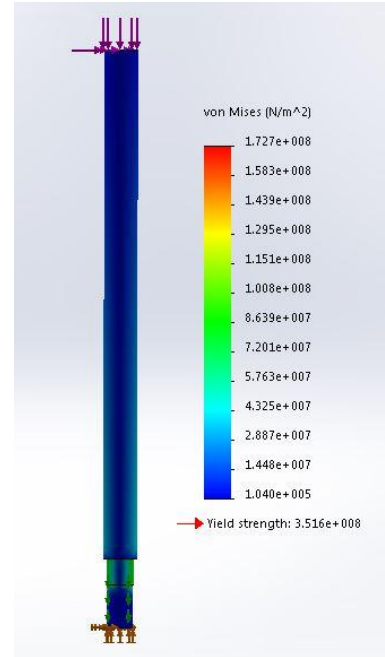
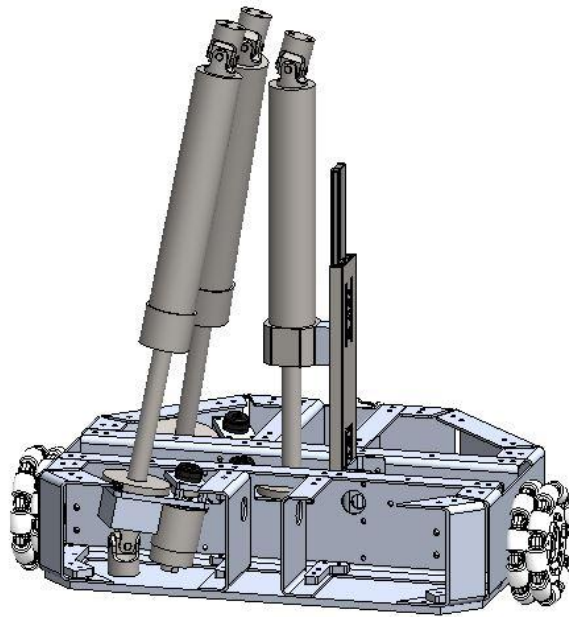


Figure 8: a) Three-DOF Parallel Platform; b) Finite Element Analysis of the Linear Actuation Lead Screw

Table 4: Translation & Rotation Robot Specifications

	Direction of Motion/Force				
	X, Y	Z	γ	β	α
Range of Motion	∞	200 mm	60°	45°	360°
Speed	816 mm/s	373 mm/s	21.4 °/s*	21.4 °/s*	240.8 °/s
Maximum Force	498 N	436 N	16.84 Nm*	16.84 Nm*	125.6 Nm

* values calculated from neutral platform position

2.2 Mathematical Modeling

To assist patients in moving their lower-limb along a prescribed path, an admittance control scheme was developed to control the velocity of the robot, requiring the current and desired position and orientation of the end effector, as well as patient forces and torques, as inputs. To control the robot in the velocity domain, the robot's inverse Jacobian was derived. To determine the current position of the robot end effector, an

iterative method was implemented to solve the forward kinematics. As the motion of the omni-directional base and three-DOF platform are decoupled, in static analysis, the models for each are discussed separately.

2.2.1 Inverse Kinematic Model

The inverse kinematic model of the robot was derived by adapting the model of an omni-directional drive system [63] and a three-DOF parallel platform [64]. The base and platform coordinate systems are shown in Figure 9a and b. The yellow dots in Figure 9b signify the centre of rotation (COR) of the base universal joints. The intersection of the axis connecting these two points and the YZ plane of the base gives the vertical height of the base coordinate system. The vertical height of the platform coordinate system is defined by the COR of the central universal joint. Assuming an ideal case where all wheels maintain full contact with the ground, the frictional coefficient between the wheels and the ground is sufficient to eliminate wheel slippage, and all wheels move synchronously so the least-squares solution of the kinematics is the exact solution, the four-wheel omni-directional drive has a linear relationship between the angular position of each wheel, $\theta_1, \theta_2, \theta_3, \theta_4$, and the translational and rotational components of the robot base, $x_{base}, y_{base}, \alpha_{base}$. The angular position of each wheel is a real number (i.e. not restrained between 0 and 360°), and these assumptions stated above are used throughout system modeling and evaluation. The translational relationship is inversely proportional to the wheel radius, r_w and the rotational component is proportional to the ratio of the base radius to wheel radius, r . In order to maintain isotropic manipulability in the X and Y direction the steering angle of each wheel is fixed and the system becomes redundantly actuated. Given the desired $x_{base}, y_{base}, \alpha_{base}$ of the robot the desired angular position of each motor can be calculated as in Eq. 1.

$$\begin{bmatrix} \theta_1 \\ \theta_2 \\ \theta_3 \\ \theta_4 \end{bmatrix} = \begin{bmatrix} 0 & 1/r_w & r \\ -1/r_w & 0 & r \\ 0 & -1/r_w & r \\ 1/r_w & 0 & r \end{bmatrix} \begin{bmatrix} x_{base} \\ y_{base} \\ \alpha_{base} \end{bmatrix} \quad (1)$$

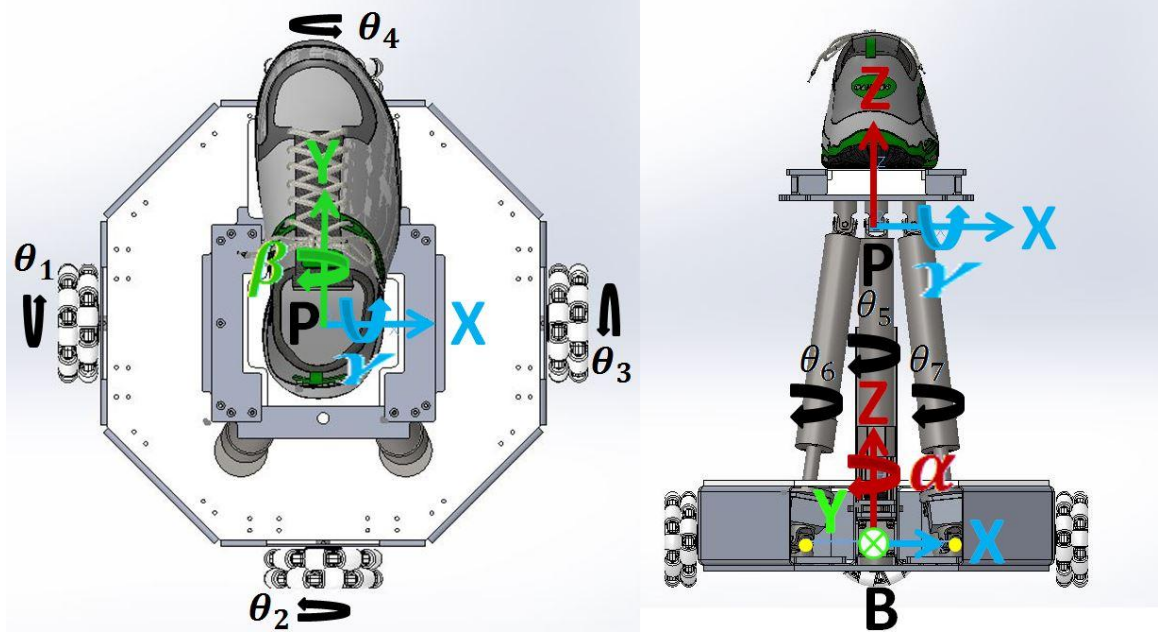


Figure 9: Robot Coordinate System: a) A top view of the robot, showing the joint-space parameters of the drive base and the platform coordinate system “P”. b) A back view of the robot, showing the platform link parameters, and the coordinate system of the drive base “B” and platform.

For parallel mechanisms, as opposed to serial manipulators, the inverse kinematics model is more straightforward and the kinematics model is usually solved iteratively [65]. The inverse kinematics model is solved using vector analysis to find the vector of link i , \vec{L}_i , from the base universal joint COR to the platform universal joint COR, then taking the norm of the resultant vector, $\|\vec{L}_i\|$. The ratio of lead screw pitch to gear ratio, r_s , then converts the link length to the angular position of each motor. \vec{Z}_p is the vector from the base frame to the platform frame and \vec{B}_i is the vector from the base frame to the universal joint COR of link i attached to the base, with respect to the base coordinate system. \vec{P}_i is the vector from the platform frame to the universal joint COR of link i attached to the platform, with respect to the platform coordinate system. R_{xy} is the rotation matrix transforming the platform coordinate system to the base coordinate system, requiring the orientations γ and β .

The calculation for the vector \vec{L}_i is given in Eq. 2, and the rotation matrix is defined in

Eq. 3.

$$\vec{Z}_p + R_{xy}\vec{P}_i - \vec{B}_i = \vec{L}_i \quad (2)$$

$$R_{xy} = \begin{bmatrix} c\beta & s\beta s\gamma & s\beta c\gamma \\ 0 & c\gamma & -s\gamma \\ -s\beta & c\beta s\gamma & c\beta c\gamma \end{bmatrix} \quad (3)$$

Given the desired platform parameters \vec{Z}_p , γ , and β in relation to the base frame, the desired angular position of each motor, $\theta_5, \theta_6, \theta_7$ can be obtained by calculating the norm of each link vector and scaling by r_s , as in Eq. 4. In the designed link configuration, the link length of the central link can be simplified to \vec{Z}_p , as \vec{P}_1 and \vec{B}_1 are zero, which added to the vertical accuracy of the system as a single actuator fully defines the vertical DOF.

$$\begin{bmatrix} \theta_5 \\ \theta_6 \\ \theta_7 \end{bmatrix} = r_s \begin{bmatrix} \|\vec{Z}_p + R_{xy} * \vec{P}_5 - \vec{B}_5\| \\ \|\vec{Z}_p + R_{xy} * \vec{P}_6 - \vec{B}_6\| \\ \|\vec{Z}_p + R_{xy} * \vec{P}_7 - \vec{B}_7\| \end{bmatrix} \quad (4)$$

2.2.2 Inverse Jacobian Formulation

In order to control the velocity of the robot, which is necessary for flexibility exercises as well as rehabilitative therapy using admittance control, the inverse Jacobian is required. The omni-directional drive has a linear relationship between the position of the drive base and the orientation of the wheels, so the desired wheel velocities $\dot{\theta}_1, \dot{\theta}_2, \dot{\theta}_3, \dot{\theta}_4$ can be obtained directly from the translational and rotational velocities $\dot{x}_{base}, \dot{y}_{base}, \dot{\alpha}_{base}$ by taking the time-derivative of the inverse kinematics.

$$\begin{bmatrix} \dot{\theta}_1 \\ \dot{\theta}_2 \\ \dot{\theta}_3 \\ \dot{\theta}_4 \end{bmatrix} = \begin{bmatrix} 0 & 1/r_w & r \\ -1/r_w & 0 & r \\ 0 & -1/r_w & r \\ 1/r_w & 0 & r \end{bmatrix} * \begin{bmatrix} \dot{x}_{base} \\ \dot{y}_{base} \\ \dot{\alpha} \end{bmatrix} \quad (5)$$

By taking the pseudo-inverse of the inverse Jacobian the least squares approximation of the robot Jacobian can be obtained.

To calculate the length of each link in the parallel platform, first the Cartesian components of each link length vector (L_{ix}, L_{iy}, L_{iz}) are calculated from Eq. 6, where P_{ix}, P_{iy}, P_{iz} and B_{ix}, B_{iy}, B_{iz} are the Cartesian components of the vectors from platform

and base origins to their respective COR. The length of each link is then calculated by taking the norm of the link length vector as in Eq. 7. The inverse Jacobian of the parallel platform is then obtained by using the chain rule to take the time-derivative of each link length as in Eq. 8.

$$\begin{bmatrix} L_{ix} \\ L_{iy} \\ L_{iz} \end{bmatrix} = \begin{bmatrix} 0 \\ 0 \\ Z_p \end{bmatrix} + \begin{bmatrix} c\beta & s\beta s\gamma & s\beta c\gamma \\ 0 & c\gamma & -s\gamma \\ -s\beta & c\beta s\gamma & c\beta c\gamma \end{bmatrix} * \begin{bmatrix} P_{ix} \\ P_{iy} \\ P_{iz} \end{bmatrix} - \begin{bmatrix} B_{ix} \\ B_{iy} \\ B_{iz} \end{bmatrix} \quad (6)$$

$$\|L_i\| = \sqrt{(L_{ix}^2 + L_{iy}^2 + L_{iz}^2)} \quad (7)$$

$$\frac{d(\|L_i\|)}{dt} = \left(\frac{1}{\|L_i\|}\right) * (L_{ix} * \frac{dL_{ix}}{dt} + L_{iy} * \frac{dL_{iy}}{dt} + L_{iz} * \frac{dL_{iz}}{dt}) \quad (8)$$

By taking the partial derivatives of each Cartesian component of each link and multiplying the link velocity by the scaling factor r_s the relationship between the platform velocities $\dot{\gamma}, \dot{\beta}, \dot{z}_p$ and each motor velocity $\dot{\theta}_i$ is obtained, and the result is displayed in Eq. 9, with C_i, D_i, E_i, F_i, G_i as intermediate joint variables.

$$\dot{\theta}_i = \frac{r_s}{\|L_i\|} \begin{bmatrix} L_{ix}C_i + L_{iy}D_i + L_{iz}E_i \\ L_{ix}F_i + L_{iz}G_i \\ L_{iz} \end{bmatrix}^T \begin{bmatrix} \dot{\gamma} \\ \dot{\beta} \\ \dot{z}_p \end{bmatrix} \quad (9)$$

$$\begin{bmatrix} C_i \\ D_i \\ E_i \\ F_i \\ G_i \end{bmatrix} = \begin{bmatrix} s\beta c\gamma * P_{iy} - s\beta s\gamma * P_{iz} \\ -s\gamma * P_{iy} - c\gamma * P_{iz} \\ c\beta c\gamma * P_{iy} - c\beta s\gamma * P_{iz} \\ -s\beta * P_{ix} + c\beta s\gamma * P_{iy} + c\beta c\gamma * P_{iz} \\ -c\beta * P_{ix} - s\beta s\gamma * P_{iy} - s\beta c\gamma * P_{iz} \end{bmatrix}$$

From the intermediate variables in Eq. 9, it can be seen that γ and β must be obtained in order to calculate the inverse Jacobian of the parallel platform. However, there is not a direct method for calculating γ and β as the platform orientation has many solutions for the same set of link lengths. As discussed in the following section, a numerical method was used to iteratively find the nearest γ and β solution, and the link orientations in the solution were assessed for validity.

3.2.3 Forward Kinematics

Due to the difficulty in determining end effector orientation, Tsai *et al.* [66] developed two methods for forward kinematic analysis of a specific three-DOF platform, and Li *et al.* [67] extended this theory for generalized three-DOF platforms. The first method in [66] employed polynomial transformation, elimination and analysis of multiple solutions, while the second method employed an iterative approach that was more computationally efficient. Since only one exact solution gives a feasible orientation of each link, as explained by the six rules outlined in [66], the solution from the iterative method can be validated before being used for robot control calculations. As the forward kinematics are required for real-time control of this lower-limb robot, the latter method was chosen. In the current implementation, a Jacobi-based algorithm was selected for iteratively solving the forward kinematics from the inverse kinematics, K_{inv} , and the algorithm is shown in Figure 10. This algorithm was selected because the Jacobian could be readily obtained by inversion of the inverse Jacobian, and the previous γ and β values would be good approximations as the sampling rate was high. Using this method, a maximum of five iterations was used; however, the convergence to a value within 0.1% was reached within the first three iterations throughout velocity profile tracking and control experimentation. Using Matlab/Simulink software on a desktop computer (Intel® Core™ i7 4790 CPU 3.60GHz processor) the time per iteration was 1ms.

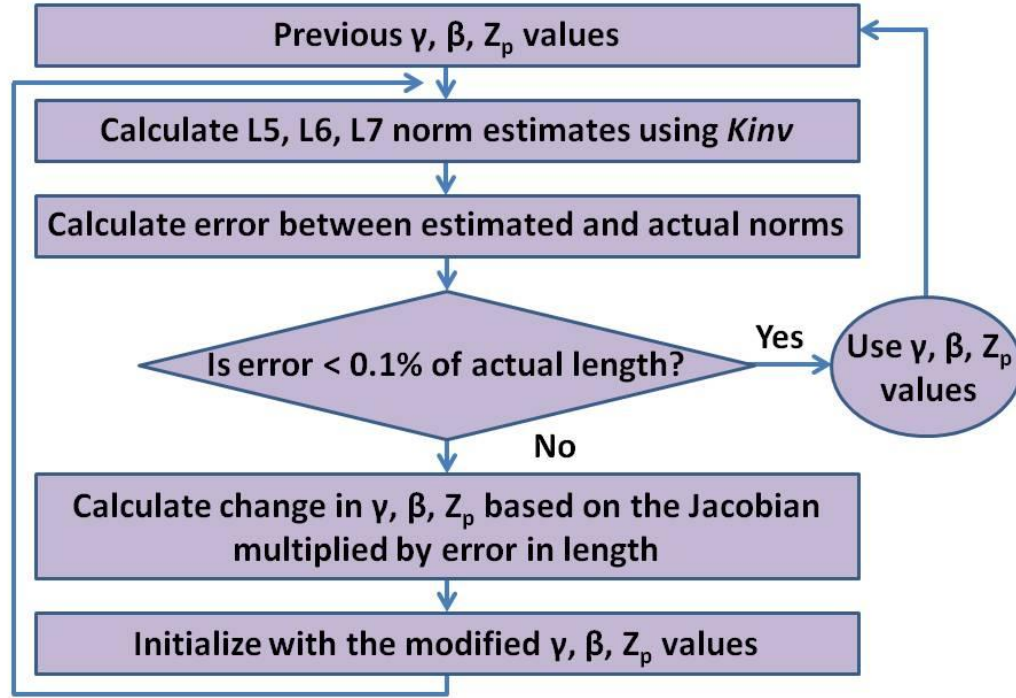


Figure 10: Algorithm used for solving the platform forward kinematics.

2.3 Custom Designed Six-DOF Force Sensor

2.3.1 Sensor Design

To assist patients in moving their lower-limb along a desired trajectory, it is important to measure the force and torque applied by the patient's foot on the robot. For this purpose, a custom six-DOF force/torque sensor comprised of sixteen one-DOF high load capacity resistive force sensors (Tekscan[®], FlexiForce A201) was designed and developed, and the pressure sensor specifications are shown in Figure 11. These sensors were selected because they had a linear relationship between electrical conductance and force applied, as shown in Figure 12, and were of low cost in comparison to force or strain sensing alternatives. The design minimized footplate inertia and robot height, provided high-force/torque measurement and wireless capability, and was of much lower cost than commercially available force/torque sensors of comparable maximum loading, such as the ATI Delta-NET shown in Table 5. The one-DOF sensors were fixed to the outer aluminum walls, and rubber cylinders (McMasterCarr, 60A Durometer) were placed between the sensors and the footplate to direct the force uniformly to the sensors

and add pre-stress. The sensors were positioned in a symmetric configuration, as shown in Figure 13, to cancel loading and unloading non-linearity, allowing the six-DOF sensor to maintain its performance without a decoupling matrix, under simultaneous loading in multiple directions. Figure 13 also shows the coordinate frame of the six-DOF sensor, which is constant in relation to the patient's foot. As the orientation of the patient's foot changes in relation to the robot base frame (e.g. during motion therapy), the force can be transformed from the coordinate frame of the foot to the coordinate frame of the robot base using the platform β and γ values.

Typical Performance		Evaluation Conditions
Linearity (Error)	< $\pm 3\%$	Line drawn from 0 to 50% load
Repeatability	< $\pm 2.5\%$ of full scale	Conditioned sensor, 80% of full force applied
Hysteresis	< 4.5 % of full scale	Conditioned sensor, 80% of full force applied
Drift	< 5% per logarithmic time scale	Constant load of 111 N (25 lb)
Response Time	< 5 μsec	Impact load, output recorded on oscilloscope
Operating Temperature	-40°C - 60°C (-40°F - 140°F)	Time required for the sensor to respond to an input force

Typical Performance

Linearity (Error): < $\pm 3\%$ (Line drawn from 0 to 50% load)

Repeatability: < $\pm 2.5\%$ of Full Scale (Conditioned Sensor, 80% of Full Force Applied)

Hysteresis: < 4.5 % of Full Scale (Conditioned Sensor, 80% of Full Force Applied)

Drift: <5% / logarithmic time (Constant Load of 25lb (111 N))

Response Time: < 5 μsec (Time required for the sensor to respond to an input force; Impact load - recorded on Oscilloscope)

Operating Temperature: -40°C - 60°C (-40°F - 140°F)*

* Force reading change per degree of temperature change = 0.36%/°C ($\pm 0.2\%$ /°F)

Figure 11: Tekscan FlexiForce Sensor Specifications. Image Courtesy of Tekscan
<https://www.tekscan.com/products-solutions/force-sensors/a201>

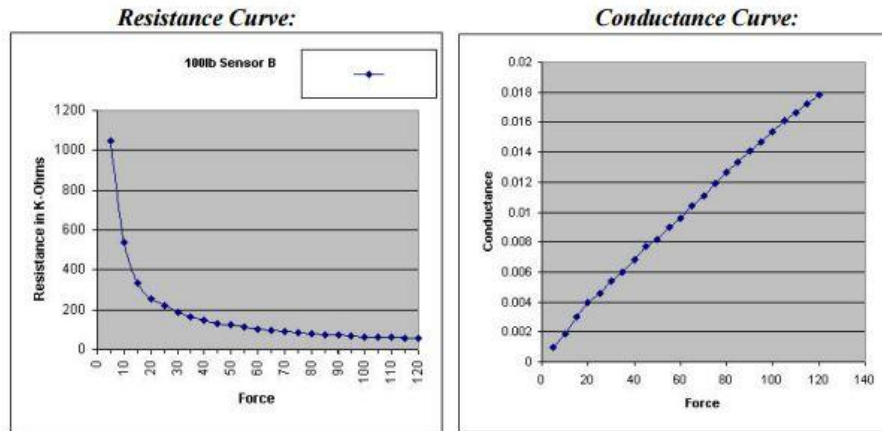


Figure 12: Tekscan Pressure Sensor Calibration Curves, from FlexiForce Datasheet

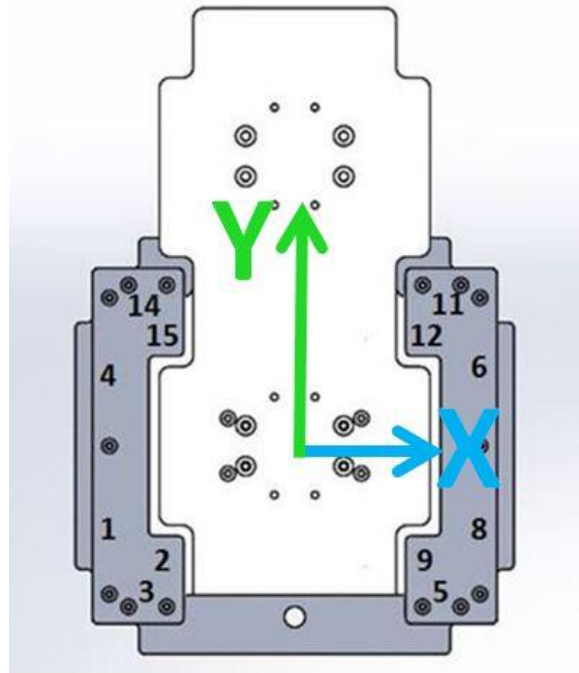


Figure 13: Six-DOF force/torque sensor displaying the location of the installed pressure sensors. Sensors 2, 9, 12 & 15 are located between the footplate and the platform base plate. The other sensors are placed between the side panels and the footplate. The Z axis comes out of the page and intersects the X and Y axes.

2.3.2 Sensor Optimization

Theoretically this force sensing structure should provide six-DOF force readings using just six pressure sensors placed at specific locations, but through past experimentation with the Tekscan sensor, and other pressure sensing pads of lower force ranges, it was found that sensor noise, drift and hysteresis may be of concern [68]. To accommodate these sensor deficiencies, ten more sensors we added to the design and ordered. Four of the ordered sensors were defective; however, this did not significantly affect the performance of the force-torque sensor as the twelve remaining sensors were installed to maintain symmetry, and the vertical preload was sufficient. Using this fabricated system, the six-DOF force/torque that the patient exerted on the footplate was calculated from the linear calibration matrix (6x6), conversion matrix (6x16), and pressure sensor vector (16x1) as shown in Eq. 10.

$$\begin{bmatrix} Fx \\ Fy \\ Fz \\ Tx \\ Ty \\ Tz \end{bmatrix} = (Calibration\ Matrix) * (Conversion\ Matrix) * (Pressure\ Sensor\ Vector) \quad (10)$$

$$Calibration = \begin{bmatrix} 0.0045 & 0 & 0 & 0 & 0 & 0 \\ 0 & 0.0045 & 0 & 0 & 0 & 0 \\ 0 & 0 & 0.00225 & 0 & 0 & 0 \\ 0 & 0 & 0 & 0.0025 & 0 & 0 \\ 0 & 0 & 0 & 0 & 0.0025 & 0 \\ 0 & 0 & 0 & 0 & 0 & 0.0025 \end{bmatrix}$$

$$Conversion = \begin{bmatrix} -1 & 0 & 0 & -1 & 0 & 1 & 0 & 1 & 0 & 0 & 0 & 0 & 0 & 0 & 0 \\ 0 & 0 & -1 & 0 & -1 & 0 & 0 & 0 & 0 & 0 & 1 & 0 & 0 & 1 & 0 \\ 0 & -1 & 0 & 0 & 0 & 0 & 0 & 0 & -1 & 0 & 0 & -1 & 0 & 0 & -1 \\ 0 & 1 & 0 & 0 & 0 & 0 & 0 & 0 & 1 & 0 & 0 & -1 & 0 & 0 & -1 \\ 0 & -1 & 0 & 0 & 0 & 0 & 0 & 0 & 1 & 0 & 0 & 1 & 0 & 0 & -1 \\ 1 & 0 & -1 & -1 & 1 & 1 & 0 & -1 & 0 & 0 & -1 & 0 & 0 & 1 & 0 \end{bmatrix}$$

In sensor design, it is important to analyze the condition number of the conversion (compliance) matrix from the sensor values to the force/torque values as the 2-norm condition number gives a bound on the sensitivity of the force/torque values calculated in

relation to the error in each sensor [69, 70, 71, 72]. More specifically, the maximum sensor error multiplied by the condition number (or the reciprocal of the condition number if less than 1) gives a bound of system error that can be created by sensor errors. In some cases the system may operate in an error region much smaller than the bound. Scaling can reduce the condition number further but should be done with knowledge of the scaling relation between forces and torques for the specific application, otherwise the scaling will be negated through calculations using the force and torque information (e.g. in robot control). The best possible condition number for a system is 1, meaning that the scaling of the sensor readings to the force/torque calculated is equal in all directions. By optimizing the orientation of the sensors to decouple X, Y, and Z forces, and developing custom circuitry that measured the pressure sensor conductance, the conversion matrix condition number was 1.414 for force sensing, which is very close to optimal. Further iterative optimization of the distance of each sensor from the neutral ankle position gave similar force and torque scaling and a low theoretical condition number for the system of 2.0. The scaling units for force and torque used to calculate this condition number are N and (Nm/10) since the amount of effort a healthy individual must exert to produce a 100N force is similar to the amount of effort to produce a 10Nm torque. It is assumed, although not validated, that this effort comparison is similar for stroke patients. After calibration of the system as presented in section 3.3.3 below, the overall condition number was 2.6, which was much closer to one than other six-DOF force/torque sensors [73]. Possible causes for the change in the compliance matrix (and the associate condition number) between the experimental setup and theoretical calculations were the unequal responses to force between sensors and unequal preloading of between sensors.

2.3.3 Sensor Calibration and Evaluation

The calibration setup in Figure 14 used a commercial six-DOF force/torque sensor (ATI Gamma SI-32-2.5), as the gold standard from which to calibrate the newly designed sensor using human forces applied through a handle. The Gamma sensor was positioned at a height where the tool end was at the same height as the median ankle height so the torque read from the Gamma sensor would be the same as those applied by a patients ankle torque centre. The commercial sensor's resolution and sampling frequency was

suitable for calibrating the custom sensor up to the commercial sensor's force limit, as shown in Table 7. The Gamma sensor was connected to the host computer by a PCI-6224 DAQ card and was read by a MATLAB/Simulink/Quarc at a 0.25kHz rate. The pressure sensor values were converted to digital signals within the microcontroller and output through UART to Serial USB communication to the host computer. A C++ UDP code was then implemented to send the serial values into the same MATLAB/Simulink/Quarc program. The one-way communication delay was 4ms for the custom sensor and is why a 0.25kHz update rate was chosen. By applying approximately-sinusoidal forces through the handle, the custom sensor was calibrated and a linear relationship was used to fit the one-DOF sensor values captured by the robot's microprocessor multiplied by the conversion matrix to the ATI force/torque values. Both sensors were biased before starting experiments each day, and the custom sensor did not need to be recalibrated even after months of extensive testing. Figure 15a through f show the relationship between the sensor values and the Gamma force readings used to make the linear calibration matrix. Some sensors show a decreasing trend of force/torque to pressure value due to the way the signals were communicated from the microcontroller to the host, so the sign of these slopes was flipped before the calibration matrix. Calibration sign flips did not affect the condition number of the sensor so this was a valid solution. From the calibration slopes shown divided by the scaling factor in the y-axis label the calibration matrix used during sensor and robot validation was calculated and is shown in Eq. 11. From the graphs below the sensor shows repeatability over multiple loading and unloading cycles, and follows the actual force measured linearly. The X and Y forces and α torque show the greatest hysteresis and backlash of the six-DOF, in the range of 1 N and 0.05 N.m. This is mostly due to difficulties in accurately tuning the pre-stress in the X and Y directions, and the response time of the thermosetting elastomer used between the sensor and the footplate. This creates larger inaccuracy at higher frequencies of force application and could be improved through further design iterations, such as using an easier to adjust pre-stress technique and switching to more linear elastic material such as the silicone rubber Rebound 25 (discussed in Chapter 3). However, the forces and torques that are assumed to be applied to the robot during usual therapy routines can be 100 times greater so these resolutions should be acceptable. A summary of the results of the custom developed six-

DOF force torque sensor are shown in Table 6, including the prototype material cost of the pressure sensors (\$230), material (\$100), and custom sensing circuitry (\$70).

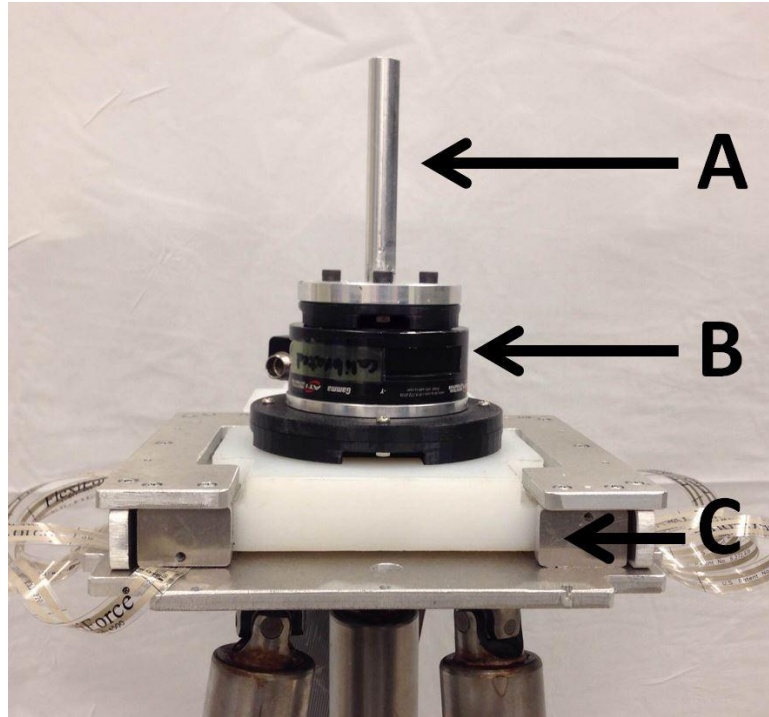
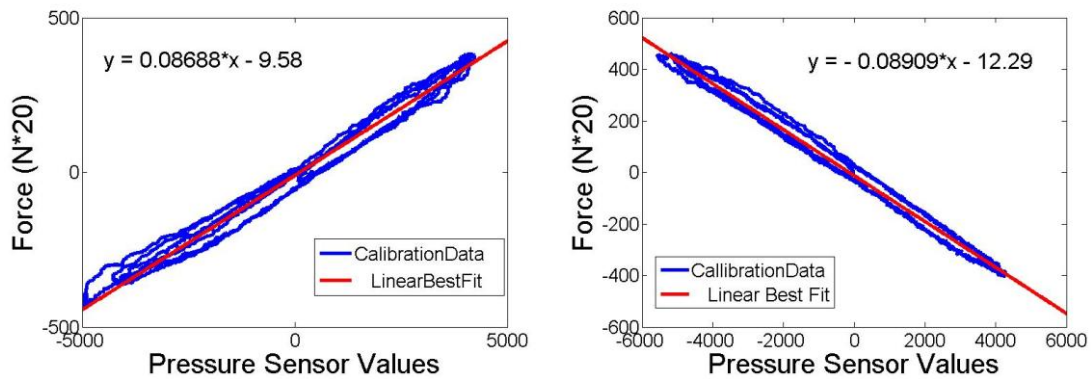


Figure 14: Custom Force Sensor Calibration Setup: A: Handle; B: ATI Gamma Force/Torque Sensor; C: Custom Force/Torque Sensor



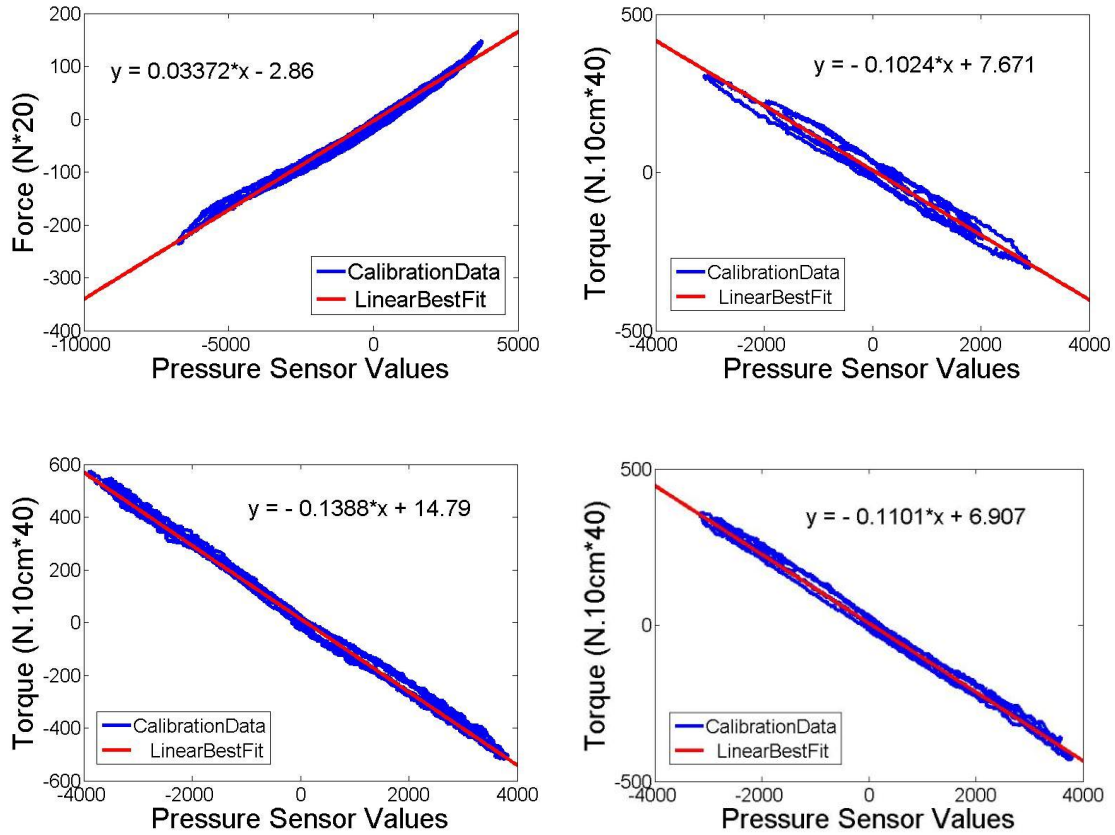


Figure 15: Relation between the pressure sensor values multiplied by the conversion matrix and the readings from the Gamma Force/Torque sensor in a) X; b) Y; c) Z; d) α ; e) β ; f) γ ; and the associated line of best fit used for the calibration matrix.

$$\text{Experimental Calibration} = \begin{bmatrix} 0.0434 & 0 & 0 & 0 & 0 & 0 \\ 0 & 0.00445 & 0 & 0 & 0 & 0 \\ 0 & 0 & 0.00169 & 0 & 0 & 0 \\ 0 & 0 & 0 & 0.00256 & 0 & 0 \\ 0 & 0 & 0 & 0 & 0.00347 & 0 \\ 0 & 0 & 0 & 0 & 0 & 0.00275 \end{bmatrix} \quad (11)$$

After calibration, the handle was manipulated in each direction separately at varying frequencies and the sensor showed a mean accuracy within 2% of the ATI readings at frequencies below 0.5Hz, and was able to follow the force profiles at frequencies under

2Hz. This data was used to develop the resolution characteristics in Table 7. Figure 16 and 17 show the force profile of the ATI and custom sensor in the X and γ directions, respectively, during experimentation. Figure 18 shows the error magnitude in the other four DOF as force/torque amplitudes and profiles similar to those in the X and γ directions were applied. The handle was then manipulated along non-specific trajectories to provide force and torque in many DOF at once. The sensor maintained its performance with a mean error of 3% of the ATI readings for all DOF. As validated by these results, this custom force sensor provides good accuracy and responds quickly. It is expected that the sensor readings will be suitable for controlling the robot to provide early-stage assisted movement therapy to stroke patients.

Table 5: ATI Delta-NET Force/Torque Sensor Specifications, Sensor Comparison

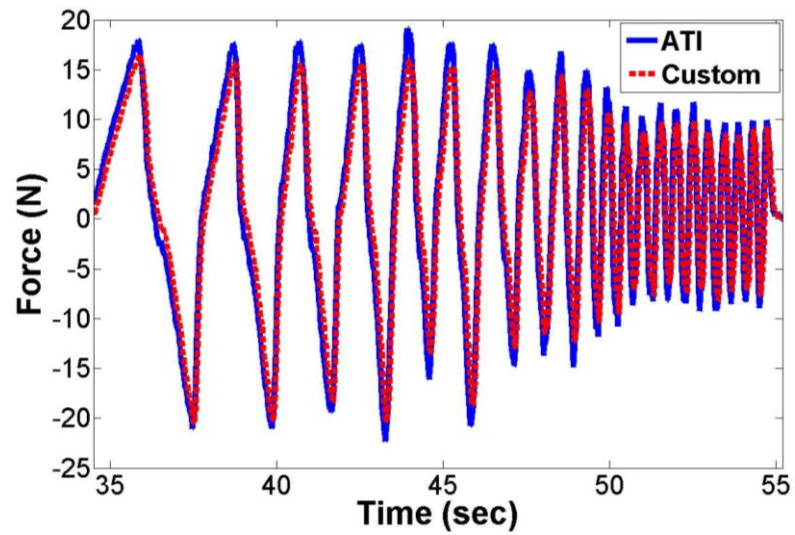
	Direction of Force/Torque			
	Fx, Fy	Fz	Tx, Ty	Tz
Maximum Load	330 N	495 N	15 Nm	15 Nm
Resolution	1/32 N	1/16 N	1/528 Nm	1/528 Nm
Cost	\$7900			

Table 6: Custom Force/Torque Sensor Specifications

	Direction of Force/Torque			
	Fx, Fy	Fz	Tx, Ty	Tz
Maximum Load	222 N	444 N	25 Nm	50 Nm
Resolution	1/2 N	1/2 N	1/20Nm	1/10 Nm
Cost	\$400			

Table 7: ATI Gamma Force/Torque Sensor Specifications, Used for Calibration

	Direction of Force/Torque			
	Fx, Fy	Fz	Tx, Ty	Tz
Maximum Load	32 N	100 N	2.5 Nm	2.5 Nm
Resolution	1/160N	1/80N	1/2000Nm	1/2000Nm

**Figure 16: ATI and custom sensor force readings when the user applied forces in the X direction.**

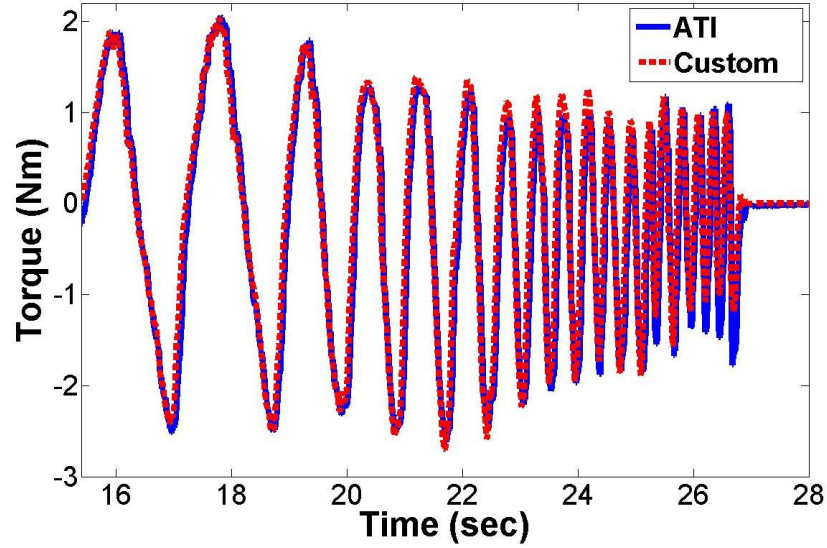


Figure 17: ATI and custom sensor torque readings when the user applied torque about γ .

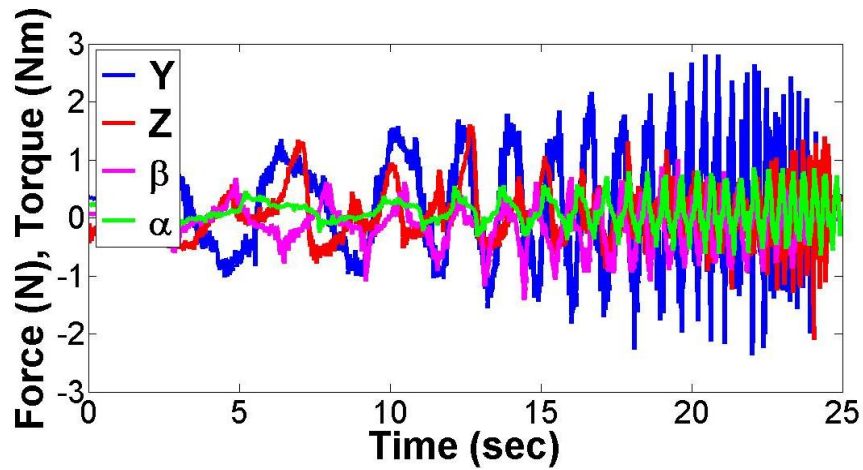


Figure 18: Magnitude of error in force measurement for forces and torques applied in the Y , Z , β and α directions individually.

2.4 Electrical Design

The robot was designed to be used in the early recovery of stroke patients for in-home environments. The main motion control issues these patients have are related to range of motion, initiating motion, coordinating joint, and to a lesser extent spasticity. In designing a robot that is usable by stroke survivors the device had to be portable and

compact, communicate wirelessly with off-board devices as many patients have very limited hand motion for plugging in devices, and operate at a fast enough frequency to gain accurate force and velocity information and control the robot to move smoothly and perform well in admittance control mode.

3.4.1 Overview of Communication Flow

To accommodate these specifications a distributed network of computing devices was used to process sensor signals and provide real-time control at a frequency that met the controller pulse-width modulation frequency (200Hz) as shown in Figure 19. To define a desired trajectory profile or update the desired trajectory in real-time various joysticks can be used. In this setup the Quanser HD² six-DOF robot was used as the joystick as it was easily backdrivable and encompassed the DOF of the rehabilitation robot designed. The joystick communicated with a host computer which could be stationed at the therapist's office and was not needed to be easily transportable. The host computer then performed admittance control mathematical operations and sent the resulting velocity commands to the mobile computer (Raspberry Pi) mounted to the robot through User Datagram Protocol (UDP). The Raspberry Pi was connected to the wireless network through a wireless to USB adapter (Edimax EW7811UN) for receiving these commands and sending position, velocity, patient force and patient torque sensor information back to the host computer. As the Raspberry Pi is a standalone computer future developments of coding architecture could see implementing the control algorithm on the Raspberry Pi, and receiving only velocity profiles or trajectories from the host computer wirelessly for a stand-alone solution. To capture and process sensor data, control the robot velocity, and perform software safety limits a compact control board was designed, manufactured and programmed in C. The control board communicated via Universal Asynchronous Receiver/Transmitter (UART) to serial USB with the Raspberry Pi and provided the option to directly connect to a host computer easily for testing the system and debugging in at-home environments. Also, an SPI communication interface was built into the custom circuit board for high frequency synchronous communication with the Raspberry Pi. The asynchronous serial communication method did create a bottleneck in data transfer due to its low communication rate and delay with the host computer and

Raspberry PI due to the maximum recommended baud rate of 38400bps in QT software used to transfer serial data to MATLAB/Simulink/Quarc and in the Raspberry PI's Linux operating system as well. In all, the wireless and compact communication platform developed met the system specifications, provided easy interfacing to program each computing device, and added functionality for stand-alone therapy and faster more-reliable communication.

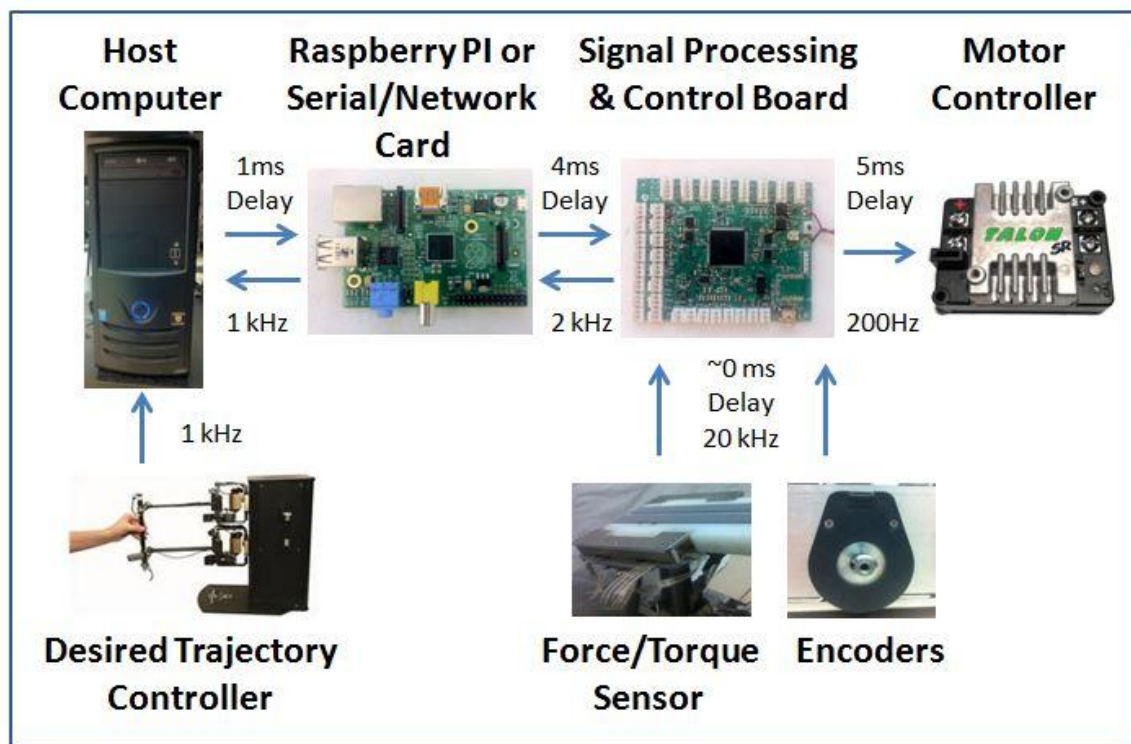


Figure 19: Communication Flow Diagram.

2.4.1 Custom Circuitry Design & Module Implementation

In creating a stand-alone at-home mobile therapy robot on-board distributed processing was necessary because of possible wireless communication delays to a host computer, and size and weight constraints within the robot. Mobile computing devices provide the flexibility and power to run software programs that make updating programs easier and calculating matrices more efficient; however their lack of high-frequency I/O, specialized registers, and analog circuitry affect their performance in sensor processing and motor control. For these purposes it was necessary to design and program compact on-board

circuitry using a high-performance microcontroller and other specialized microchips to perform linearized analog signal capture, signal processing of position, velocity and pressure data, and low-level motor control. Interrupt-generated software architecture was used to create a high-frequency processing system that was robust to system stalls or crashes as no internal programming loops were necessary. A list of registers required was generated from the tasks described below and were used to select the microcontroller. The schematics used to design the final circuit board were produced using CadSoft Eagle PCB Design Software and are displayed in Appendix A.

Sensor Capture & Signal Processing

The relation between the FlexiForce pressure sensor conductance and the force applied to the sensors was linearly related, so by creating a circuit that measured the sensor conductance the force sensing system condition number would remain low and the conversion matrix would remain linear. Within the FlexiForce datasheet [74] a simple circuit diagram was displayed showing an inverting op-amp configuration to perform this conductance measurement. However, this system required excess circuitry to apply negative voltages to the pressure. Instead, a modified circuit for using this sensor at the full microcontroller ADC resolution was design. Minimal components were used in the circuit design, which incorporated a voltage regulator (LinearTechnology, LT3021ES) and an operational amplifier (STMicroelectronics, TSV914A). The output voltage, V_{out} , was linearly related to the sensor conductance ($\frac{1}{R_{FSR}}$) as shown by Eq. 12, with R_s as the feedback resistance and V_{reg} as the regulator's output voltage. A simplified version of the circuit is shown in Figure 20, for sensing a linear change in voltage based on the force applied to the sensor. Connecting the Voltage Reference Low pin of the microcontroller to the regulator voltage (0.4V) gives maximum resolution for 50 lb forces when $R_s=1M\Omega$, and R_s can be swapped with a potentiometer to tune this resolution.

$$V_{out} = V_{reg} * (1 + \frac{R_s}{R_{FSR}}) \quad (12)$$

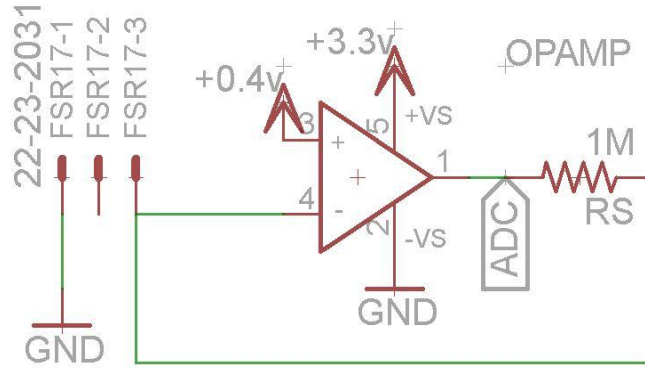


Figure 20: Simplified Operational Amplifier Circuit.

The analog pressure sensor signals showed significant noise and hysteresis at the 5kHz sampling rate that each sensor was sampled by the microcontroller ADC converter, and sufficient cancellation of noise was seen using a 100Hz low-pass filter. This low frequency filter affected the dynamic response of the sensor, but significantly helped in signal stabilization which kept the robot motion smooth during admittance controlled therapy. One analog input channel was required per pressure sensor for a total of sixteen channels and an interrupt was generated at the end of each conversion to signal the automatic conversion of the next channel to begin.

To detect each rising or falling edge from the quadrature encoders a pull-up resistor connected to a 5V regulator was applied to the A, B and I encoding channels. These output signals were then connected to the input capture channels on the microcontroller to give interrupt driven position calculation. Since the encoders were placed on the wheel side of the gearboxes any backlash from the low-cost gearboxes was detected and could be used for more accurate position and velocity control. As well, the encoder sampling rate necessary was decreased proportionally to the gearbox ratio. Using this interrupt based approach the position values were directly accessible for velocity calculation and the only criteria was that the microcontroller clock frequency had to be faster than the necessary encoder frequency of 2kHz as shown in Eq. 13, where f , CPR , V_{max} , D_{wheel} are the encoder frequency in Hz, encoder counts per revolution, maximum velocity and wheel diameter, respectively.

$$f = CPR * V_{max} / D_{wheel} \quad (13)$$

An external oscillator was added to the circuit to give a 40MHz clock frequency to easily meet this condition.

From a position control standpoint the encoder placement was ideal as the gearbox backlash was large (3^0), but did create some difficulties in velocity control as the backlash, friction and inertia non-linearity of the gearbox, and a reduction in resolution by the gearbox resolution had an effect on the simplicity of the motor velocity control. To test the wheel encoders' ability to read the wheel velocity an actuator was swept through an open-loop velocity sequence. The encoder position was sampled at a high frequency (20 kHz) and an observer [75] was used to calculate the wheel velocity. Initially the observer calculation gave very noisy results as shown in Figure 21a, but through careful tuning of the system poles and the addition of a first-order low pass filter the velocity calculated became much smoother as shown in Figure 21b. Eq. 14 and 15 show the observer and low pass filter calculations implemented in C to give a smooth velocity output, and Figure 22 shows the low-pass filter frequency response. The sampling frequency of the encoder position, current wheel position, current velocity estimate, previous velocity estimate, current update parameter, previous update parameter, filtered average velocity, and previous filtered average velocity average are denoted $f, \theta, \dot{\theta}_n, \dot{\theta}_{n-1}, \mu, \mu_{n-1}, \dot{\theta}_{avg_n}, \dot{\theta}_{avg_{n-1}}$, respectively. The tunable parameters are the pole, p , the error estimate, ε , and the low-pass gain, lpg . Values of 25, 0.4, and 0.8, respectively, were chosen from observational testing to give a smooth response with a 0.1sec time-lag. The low-pass filter was later substituted by a Kalman filter as it attained a similar smoothness with less phase lag. The Kalman filter implemented is shown in Eq. 16, where continuing from the previous notation, the Kalman Gain, Prediction Error are denoted K, P and the tunable parameters are the system noise, ρ and the measurement noise, m . In controlling the linear actuators the resolution of the encoders to vertical height and angular resolution was much higher so only a properly tuned observer was required to calculate smooth motion accurately.

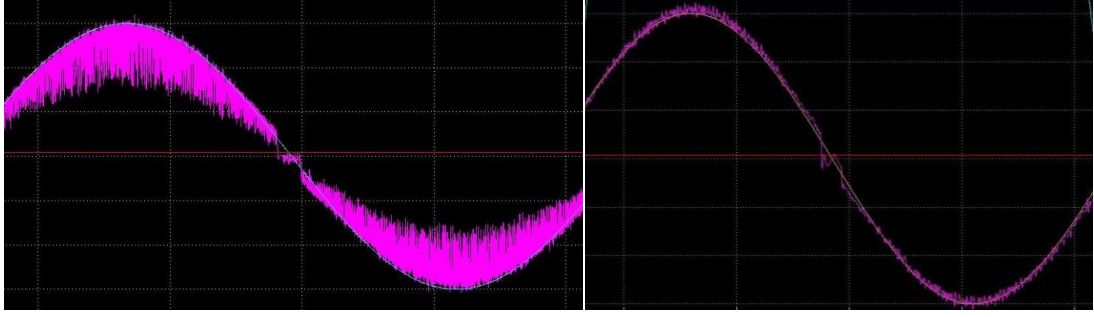


Figure 21: Actuator velocity signal a) before and b) after observer tuning.

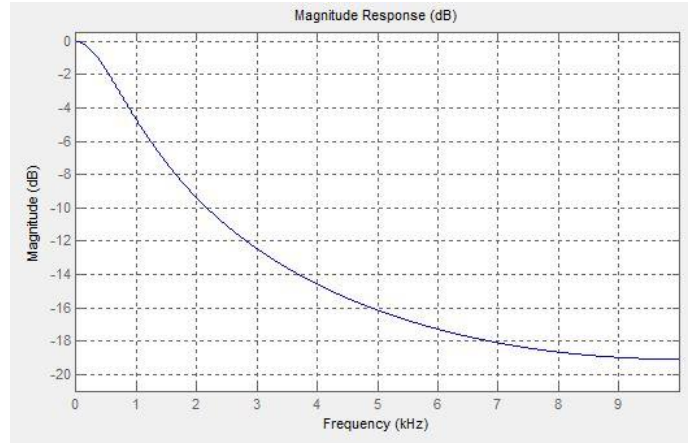


Figure 22: Frequency response of low-pass filter implemented in C.

$$\mu = \frac{\varepsilon * \mu_{n-1} * f + \varepsilon * \dot{\theta}_{n-1} + p * 2 * \theta}{\varepsilon * f + p * 2} \quad (14)$$

$$\dot{\theta} = \dot{\theta}_{n-1} + \left(\frac{p^2}{\varepsilon * f} \right) * (\theta - \mu)$$

$$\dot{\theta}_{avg_n} = \dot{\theta} * (1 - lpg) + \dot{\theta}_{avg_{n-1}} * lpg \quad (15)$$

$$K = \frac{P + \rho}{P + \rho + m} \quad (16)$$

$$\dot{\theta} = \dot{\theta}_{n-1} + K * (\dot{\theta} - \dot{\theta}_{n-1})$$

$$P = (1.0 - K) * (P + \rho)$$

Motor Control

To meet the robot power and cost specifications and isolate high current from the control circuit a Talon SR speed controller from Cross The Road Electronics was selected. Since lower voltage devices (under 30V) are easier to gain CSA approval for the robot was designed for 12V operation and 85A of peak current was specified. The controller specified met these capabilities and its PWM communication method was ideal for interfacing with the output compare module of a microcontroller for automatic duty-cycle implementation through digital output pins. The custom circuit would relay PWM commands directly to the low current ($<1\text{mA}$) PWM interface on the controller and the controller would regulate the voltage in relation to the input battery voltage. As the motor input voltage is proportional to speed, voltage regulation was suitable for admittance control.

A PID controller was then used with encoder velocity feedback to accurately control the actuator velocity in the range of speeds required for therapy. The battery voltage was also required as input to the controller as the speed controller regulated the voltage in relation to the input voltage. A compact, lightweight, high current draw, and high storage capacity lithium polymer battery (ZIPPER Traxxas compatible 6400mAh 3S1P 30C Lipo Pack) was selected to power the robot, did not cause significant voltage drops during operation and allowed the system to run for an hour of consistent use before recharging. As opposed to purchasing expensive and bulky circuitry to regulate the high current input voltage, a simple low-current voltage divider provided high resolution battery voltage measurement by the microcontroller ADC. Due to the effects of motor cogging (400mA required starting torque) as well as gearbox inertia and friction, and encoder resolution the initial PID controller implemented required was very sensitive to the gain values. Also a very large integral term was needed to track the current velocity and the derivative term to increase the frequency response caused instability. For this reason, a simple actuator velocity to duty cycle model was developed for feed-forward control of the PWM duty cycle through experimental modeling. This model significantly benefitted the velocity tracking controller, especially at low speeds ($<5\text{ rpm}$ at the gearbox output shaft) and considerably reduced the gain values of the PID controller that followed. The PID

controller was then tuned experimentally to give accurate velocity tracking in free space and under applied loads and the resulting control structure is shown in Figure 23. The system response was analyzed and Figure 24 and 25 show the tracking performance for a 0.1Hz sine wave at a 60rpm output shaft amplitude, and the step response for a 30rpm amplitude. The under-damped nature of the step response was necessary to provide good control performance at higher-frequencies as high current pulses were required to overcome motor cogging and the gearbox inertia then maintained the higher speed. Through a more sophisticated velocity to duty cycle model this step response could be improved in the future, but the current system functioned well enough for in-lab experimentation.

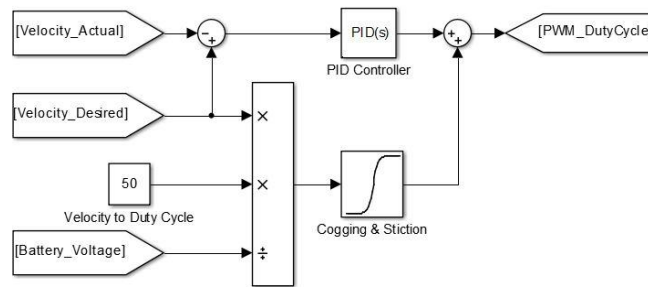


Figure 23: Motor Velocity Tracking Control Method

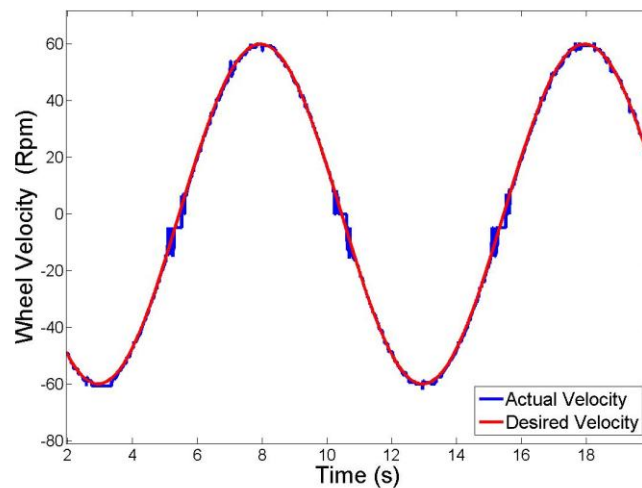


Figure 24: Motor Velocity Tracking Control Performance

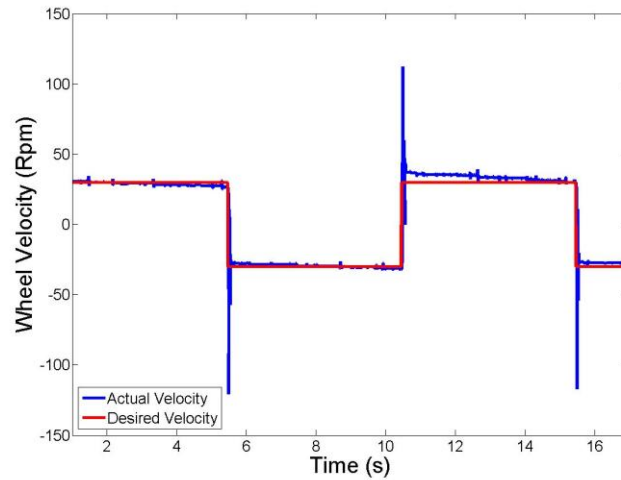


Figure 25: Motor Velocity Tracking Control Step Response

This feed-forward control strategy was then implemented for the upper platform as well and performed better than the wheel velocity tracking control as the lead screw friction was less than the gearbox friction and the encoder resolution was much higher. Safety limits on maximum velocity and maximum velocity error were added to the control circuit to stop the robot automatically in potential unpredicted situations. An on-off switch, a circuit breaker, and additional LEDs were added to the circuit and robot so users and developers could easily shut-down the robot in case of emergency and to save power, and monitor the system from afar. Accelerometer circuitry was also implemented and communicated to the microcontroller through I²C communication for monitoring the global acceleration, velocity and position of the robot for safety and to potentially account for wheel slippage in odometry measurements.

Communication

Distributed processing was used to acquire sensor data and send motor commands at a high frequency. The post processed data then needed to be transferred between devices so a combination of serial, UART, SPI, Bluetooth, I²C and wireless methods were used. To transfer data between on-board computing devices the circuit board included UART to serial USB communication for easy setup, with SPI functionality for higher frequency data transfer through unallocated test pins or available PWM or encoder ports. Bluetooth

communication was added for communication with mobile devices, and in areas with weak wireless signals. I²C was then used to communicate with the in-circuit accelerometer for global reference frame information.

Microcontroller Selection

The modules listed above required a select microcontroller with high functionality and detailed specifications as listed in Table 8. To meet these specifications, and because the Microchip PIC family had a large selection of devices the dsPIC33EP512MU814 was chosen [76].

Table 8: Required Specifications for Microcontroller

Processing Speed	40MHz, 10MIPS
Input Capture	14
Output Compare	7
ADC	17
Timers	2 @ 32-bit
Communication	2-UART, SPI, I ² C

A chart listing the circuit board components selected and the associative cost of the board is presented in Appendix B.

Circuit Board Design

From the schematic the board layout was created using CadSoft Eagle PCB Design Software, with the specifications that the board have a maximum of 4in by 4in for compactness on the robot, and meet the further specifications of MyRO PCB's standard board designs for easy manufacture and cost-savings. From these specifications the PCB board in Figure 26 was designed and manufactured. The PCB was then hand soldered in-house and the microcontroller was programmed for the signal processing, motor control and communication needs specified above. Figure 27 shows the final circuit board product, labeled to show as summary its functionality.

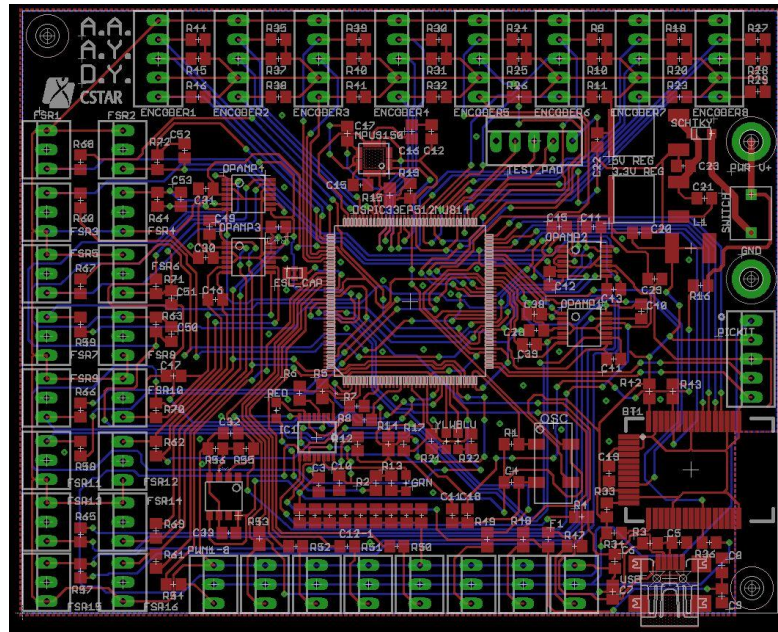


Figure 26: PCB design for Manufacturing and Assembly

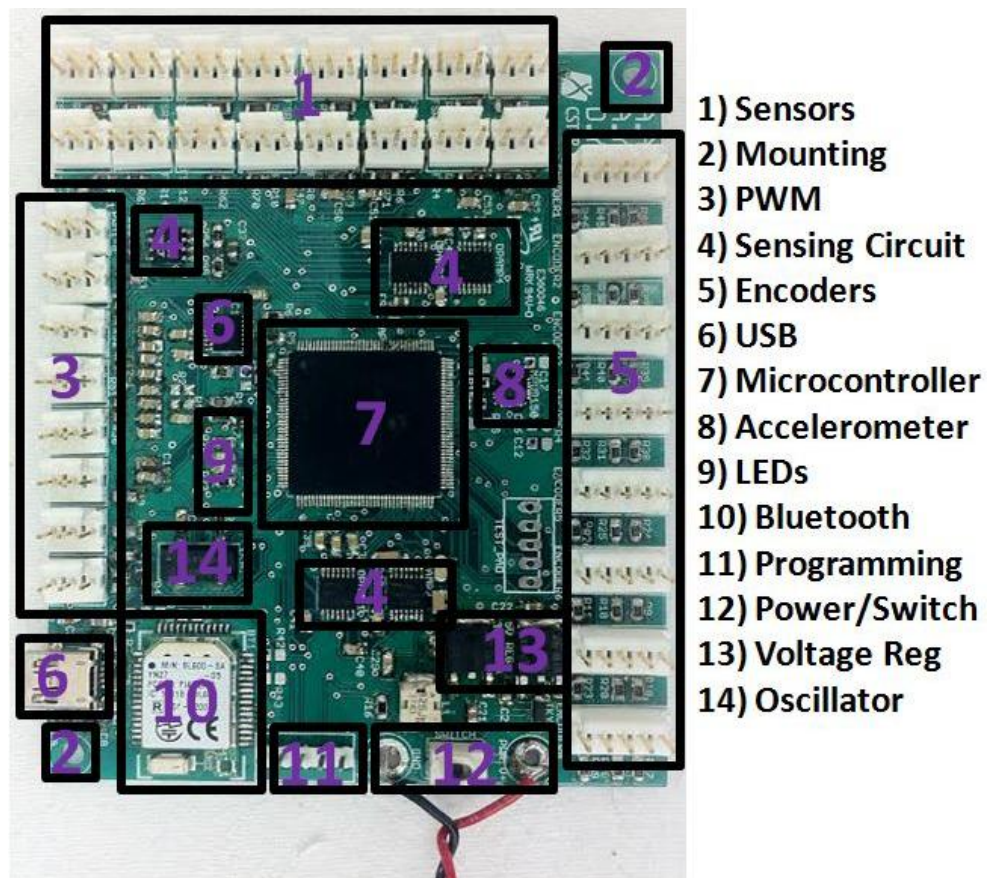


Figure 27: Signal Processing & Control Board

2.5 Robot Control

The rehabilitative tasks stated previously require the robot to assist patients in moving along desired trajectories. To analyze the robot's functionality, a free-space trajectory controller was implemented to evaluate the robot's tracking performance, and an admittance controller was developed to validate the robot's ability to perform motion assistance. For each of these evaluations an optical tracking system (Micron Tracker 2, Claron Technology) was used to validate the position and orientation of the platform using the experimental setup shown in Figure 28.

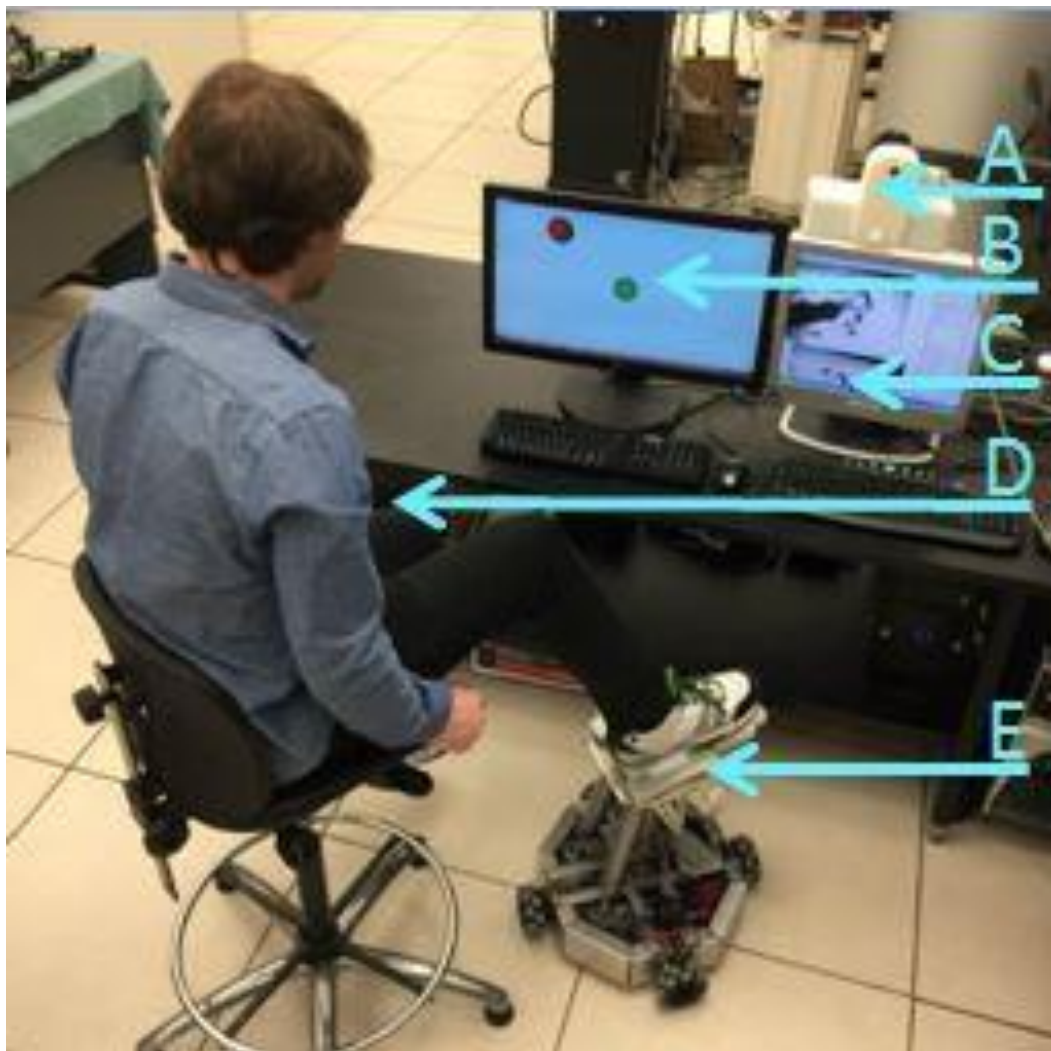


Figure 28: Experimental Setup: A: Optical Tracker; B: Game Interface; C: Micron Tracker Display; E: Robot

2.5.1 Trajectory Control

To evaluate the robot's ability to track planar motion the robot drive base was commanded to follow a 0.1Hz, 140mm amplitude sinusoidal trajectory in both the x and y directions for 50 seconds, forming five circular trajectories. As shown in Figure 29a, the robot's mean error in tracking was less than 1mm per rotation and the accumulated maximum error was 4mm due to wheel slippage. The robot was then commanded to follow a 0.1Hz sinusoidal trajectory along all rotation axes, and the results in Figure 29b show a mean error of 0.2° .

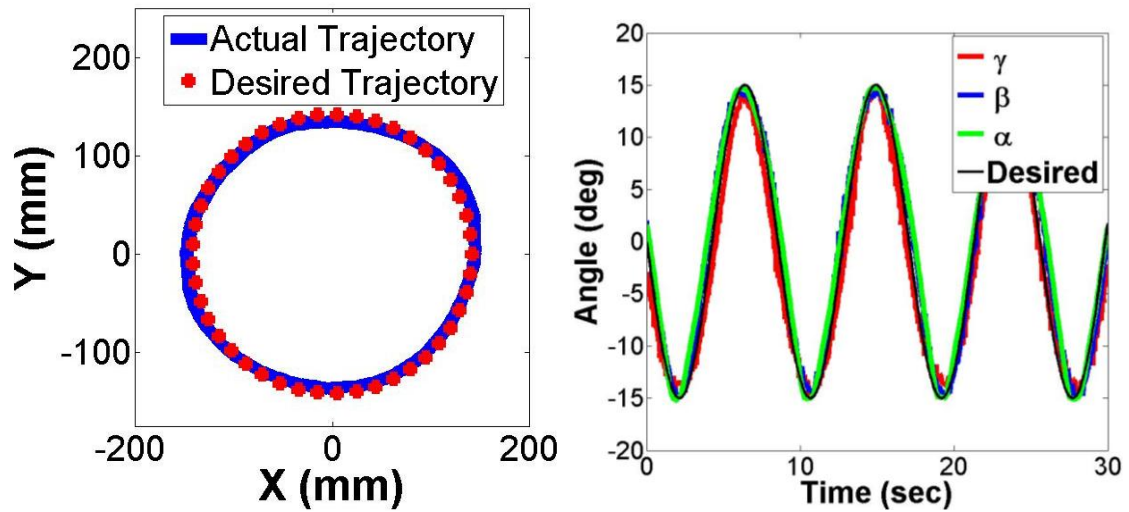


Figure 29: The trajectory of the robot in a) X and Y when commanded to track a circular trajectory; and b) γ , β , and α when each was commanded to follow a sinusoidal trajectory

The host computer was then connected to a Quanser HD² haptics-enabled device, and the robot was commanded to follow joystick directed movement as shown in Figure 30. The robot showed good qualitative results in tracking performance but lagged the joystick due to a low communication rate between the computer and robot. This experiment was a proof of concept that the robot could be used by a therapist to control the motion of a patient's limb. This would reduce the therapist's fatigue during procedures and allow them to attain quantitative data on patient performance during the task from the footplate force/torque sensor. As an extension to this method of therapy, the patient could use the

joystick with his or her unaffected arm or leg to train their affected limb. This may create a more natural experience for the patient, and allow the patient to recover proprioceptive and neuromuscular connections faster or more completely as was recently demonstrated in [77]. Within this real-time trajectory modification framework there are still many robotics and medical questions to be explored and is provided here as a motivation to future work. For individuals without neurological injury, there is some evidence to suggest that upper limb activities can enhance lower-limb muscle activity during locomotor-like tasks. In participants with stroke, however, despite a correlation between paretic upper limb function and independent ambulation, there is insufficient data indicating that differences in upper limb activity alter lower-limb activity and/or recovery [78].

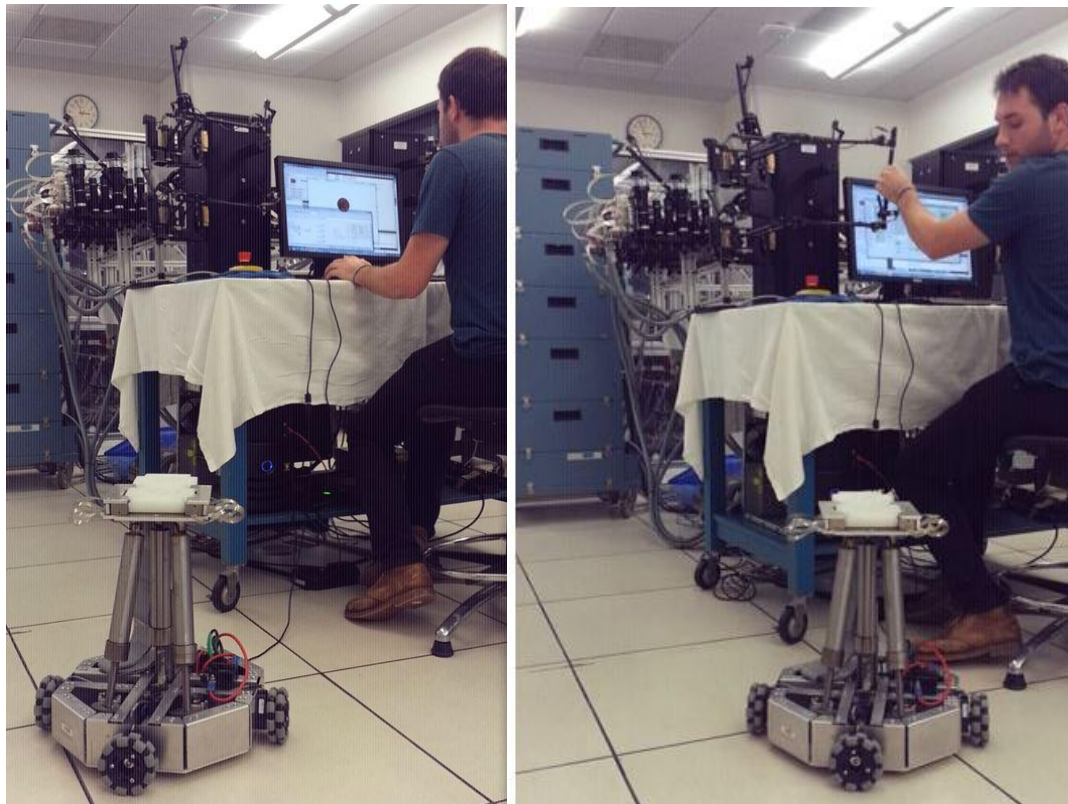


Figure 30: Real-time Trajectory Control Setup using an HD² haptic device and the six-DOF lower-limb rehabilitation robot.

2.5.2 Admittance Control

In lower-limb rehabilitation robots, the forces and torques required to provide motion assistance to stroke patients is large. To meet these requirements high gearing is used which introduces non-backdrivability into the system and creates a non-linear relationship between input current and output torque. Without the use of torque sensors it is difficult to control the torque applied to the system, while using encoder feedback it is more straightforward to control the motor velocity. Also, as these systems are not easily backdrivable, the patient cannot dictate the robot velocity. By adding a patient force sensor to the system an admittance controller could be developed, with the added benefit that if the patient's foot releases from the robot or the robot slides the robot would be less likely to go unstable than if an impedance controller was use.

A zero-order admittance controller was developed to control the robot velocity \vec{V} based on the force applied by the patient, \vec{F}_a , the deviation of the robot trajectory \vec{T}_{act} from the desired trajectory \vec{T}_{des} , and gains, K_F, K_T , as in Eq. 17, to validate the robot's performance in assisting movement.

$$\vec{F}_a \cdot K_F - (\vec{T}_{act} - \vec{T}_{des}) \cdot K_T = \vec{V} \quad (17)$$

For evaluation, a healthy individual was asked to place his foot on the robot and attempt to track the desired position portrayed by the red circle on the computer display in Figure 28. The desired trajectory was along the y axis, and to test the performance of the system the individual applied deviating forces in the X direction as shown in Figure 31a. As the deviation from the desired trajectory grew, the robot velocity was modulated to apply steering forces toward the desired trajectory. In the next task the individual applied torques about γ and the robot applied restraining forces to keep a neutral foot angle as shown in Figure 31b.

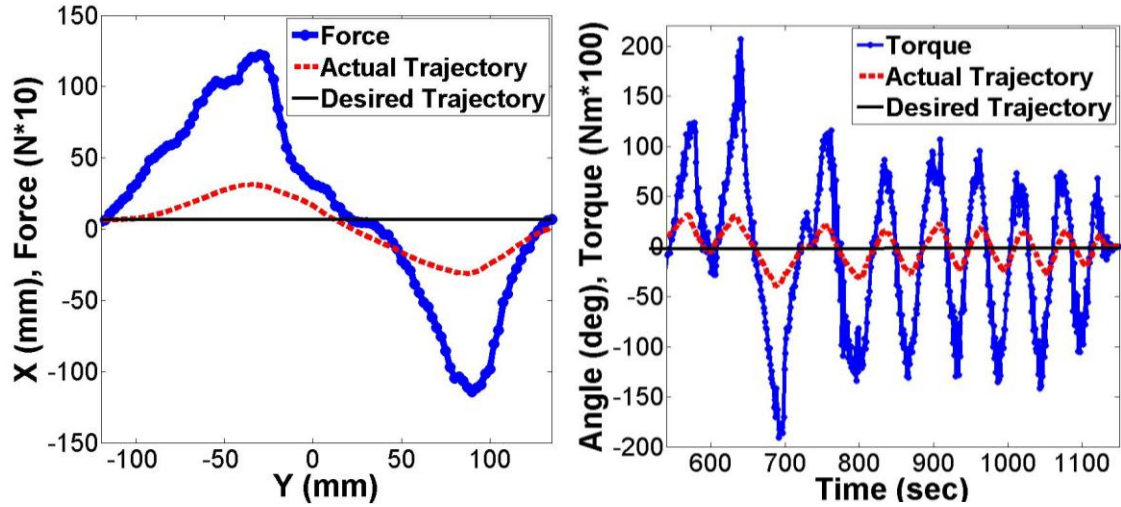


Figure 31: a) The force and motion of the individual's foot in the X and Y direction during assisted motion along Y; b) the force and rotation of the ankle about Y as the robot assisted in maintaining a neutral ankle position.

2.6 Summary of Six-DOF Rehabilitation System

To provide assisted lower-limb rehabilitation to post-stroke patients a safe and portable six-DOF robot has been designed that encompasses the power and workspace of the lower-limb. A low-cost force/torque sensor was designed and utilized in controlling the robot's admittance for a total robot cost of \$3,536, which is summarized in Appendix B. Experimental results show the reliability of this device in performing motion assistance to a healthy individual, and extensive testing will be completed in the future on healthy individuals with varying physical characteristics, and on post-stroke patients with a specific level of impairment.

Chapter 3

3 Flexible Mobile Robotic System for In-Home Stroke Rehabilitation Motion Assistance and Assessment

From the design, implementation and validation of the six-DOF system presented in Chapter 2 technical and experiential knowledge was gained, from which an improved system can be developed that is ready for clinical testing, is useful for in-home therapy and has potential for commercialization. The design, mathematical models and control strategy of the improved system are presented here in Chapter 3, and the focus of this system is to provide stroke survivors with neuromuscular rehabilitation therapy in their home within the first six months following a stroke. As stated in Chapter 1, the regeneration of neuromuscular pathways occurs mostly in the first six-months and the time to initiation of rehabilitation therapy and participation rate in daily therapy play a large role in the patient's final recovery. To target this time-period after stroke a device that is inherently safe, easy-to-use and allows patients to exercise from a safe posture is required. It is less important to be oriented in a task-like position during this stage in recovery as dendrite remodeling and synaptogenesis are the two main mediums for recovery in this time-period, as opposed to muscle memory or neuroplasticity. As such, devices that patients could interact with while seated would have value over gait-training devices, and by reducing system complexity the cost could be reduced to affordable levels and the system could be made less bulky for better performance during assistance tasks.

In designing a useful and commercializable solution for lower-limb therapy, rehabilitation systems that have been proven to be successful for patient recovery and commercialization were analyzed to discover prevailing themes. In the past many lower-limb solutions have focused on complexity over modularity [80], [81], but their success in showing recovery results has been limited. Modularity, on the other hand, provides either bulk movement for heavy or muscular limb segments, or dexterous therapy for the ankle, as opposed to one complex system that provides therapy for all joints. This allows the weight and back-driving torque of ankle modules to be significantly reduced due to

their lesser workspace and power requirements, and provides better performance in impedance controlled therapy.

As patients generally need to dedicate their focus to one or a few movements at a time to recover effectively not all modules need to be incorporated in all therapy regimens, so the modular design can provide more affordable and portable therapy. Presently many groups have begun to take a modularity approach, developing successful ankle therapy systems [6], [43], [82], [83], [84], [85]. The next step for providing robotic lower-limb therapy is to develop a system for bulk movement of the knee and/or hip.

To provide a solution to this need, a novel mobile omni-directional drive system was developed, following from the advantages of such a system explained in Chapter 2, for the motions discussed in Section 2.1. A novel joint flexibility and torque sensing coupling was designed, validated and incorporated into the system for smooth human-robot interaction during impedance control. The mechanical and electrical design overcomes the limitations imposed by the robot presented in Chapter 2, reduces the number of actuators for a more portable and affordable solution, and incorporates an ergonomic foot attachment method that makes donning and doffing simple and comfortable. The manufactured robot is shown in Figure 32 and Figure 33. An impedance algorithm was selected from the literature to provide assist-as-needed control and the mathematical models of the robot have been derived for use with this algorithm. Through the design, modeling and control algorithms developed, the robot can provide assist-as-needed training, as well as skill assessment using the robot in a fully-passive declutched state, and static resistance tests to measure the amount of force the patient can generate.

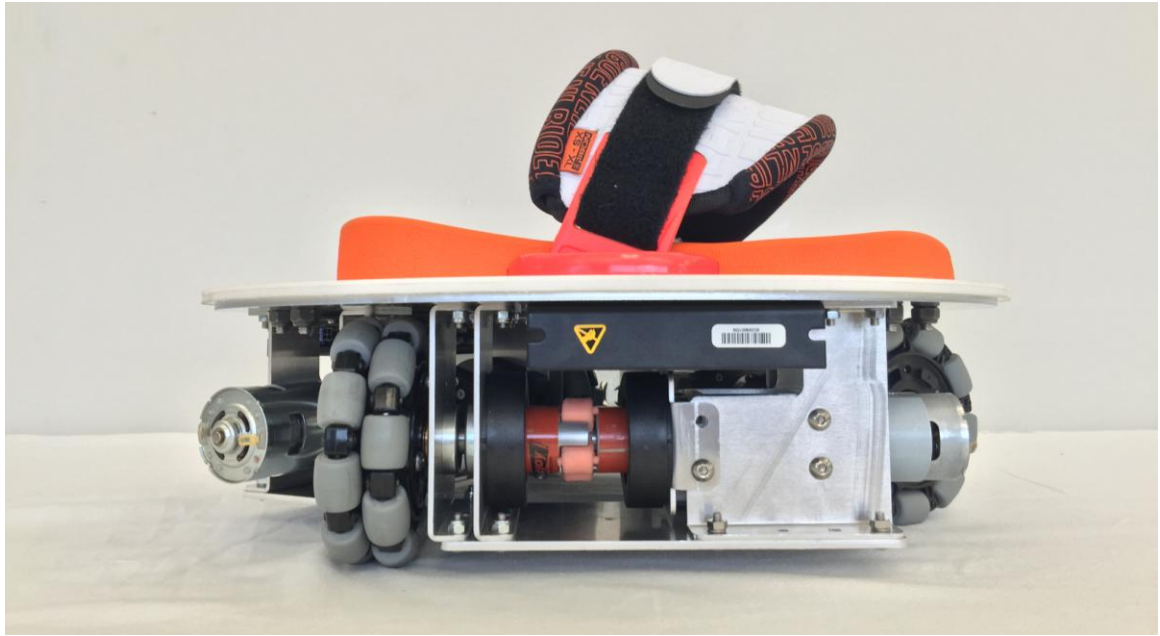


Figure 32: Side View of Three-DOF Robot for In-Home Lower-Limb Rehabilitation

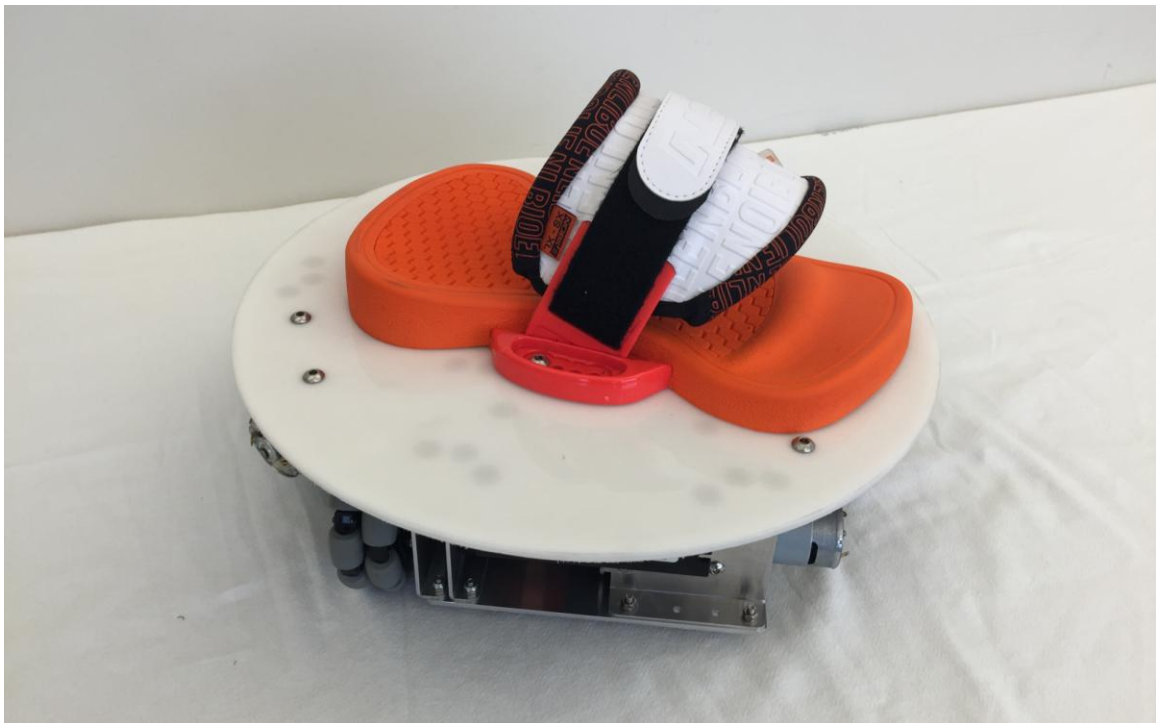


Figure 33 Top View of Three-DOF Robot for In-Home Lower-Limb Rehabilitation

3.1 Mechanical Design

The lower-limb rehabilitation robot presented here is an affordable solution to in-home lower-limb rehabilitation. Building on the design methodology and lessons learned from designing and controlling the robot presented in Chapter 2, the novel patient-safe, compact, lightweight, backdrivable, affordable, and easy to assemble design in Chapter 3 is capable of providing assist-as-needed training for specific rehabilitation tasks.

To create an easy to use robot suitable for in-home therapy the robot needed to have only the DOF required for therapy and be patient-safe, compact, and lightweight. These features allow the robot to be used in unsupervised therapy and portable for use throughout a home or clinic. The actuators are fully isolated from the patient and a cover can be placed around the robot as shown in Figure 34 for further protection during patient use. An ergonomic one-size-fits-all kiteboard binding is mounted on the robot using quick-release screws and the patient slides their foot into the binding for use. For intensive exercise a single strap can be tightened to affix the patient's foot. The mobile drive system mechanically limits the maximum force that can be applied to the patient as the wheels will slip at large forces, and a simple frame can be placed around the desired robot workspace if mechanical motion stops are required. To minimize the robot diameter to 380mm, decrease the system weight, and reduce the robot cost a three-wheel design was selected. Although the four-wheel design made control of linear motions simpler, the wheel slippage experienced due to over-constrained movement of the wheel during fast motion was significant, and the need for a suspension system to apply an equal pressure distribution across all wheels is needed which can significantly increase the chance of system failures, weight, and cost. A tilted wheel configuration was used to minimize the robot diameter further and increase the pushing force. The robot frame was then designed around the wheels, flexible torque sensor, motor and gearbox to minimize the length of each actuating mechanism and the robot height, and the mechanical and electrical layout is shown in Figure 35. This design allows the patient to be seated in a standard chair and use the robot with their foot at a comfortable height. The three-DOF mobile system designed minimizes robot height and weight, and is patient-safe and ergonomic for use in in-home therapy.

In creating an affordable robot many factors need to be considered that can be assumed to be negligible if cost is not of great concern. An aluminum sheet metal frame with only 1-DOF bending was selected to reduce weight and cost of manufacture while providing a rigid robot structure as in Chapter 2.1. The machining tolerance of 0.1mm for hole alignment and 0.3mm for bend lengths was sufficient for assembling the robot as the sheet metal is flexible and care was taken to specify the critical tolerance dimensions. As was experienced while controlling the six-DOF robot in Chapter 2, low-cost motors and gearboxes reduce actuation efficiency, and the cogging effect of these motors cause difficulties in motor control. The link between efficiency and cost is associated with the manufacturing processes required. In low cost gearboxes gear teeth are not post-processed after the broaching process, and the gears ride on a metal surface for axial retention and are placed on a metal shaft for radial retention, adding friction and backlash. Motor cogging occurs when the permanent magnets on the stator of the brushed DC motor align with the slotted ferromagnetic core on the rotor where the copper wire is wound [86]. Special designs that skew the core slots or permanent magnets, change the core construction or eliminate the need for a core can reduce the effects of cogging, but also reduce efficiency or power output and incur large manufacturing costs. As cogging affected both the motor control and backdrivability of the system significantly, and the gear ratio amplified the effect of cogging on backdrivability, a low-cost motor with a lower no load RPM and a greater stall torque was selected (BaneBots LLC, RS775, 360 Watt, 18V), and a gear ratio of 64:1 was used (BaneBots LLC, P60, 64:1). As the robot does not require gravity compensation, and the 120g change in weight per actuator should not affect the robot performance in dynamic applications much as the robot was 10kg. Experiments were performed using the low-cost motors (Banebots RS775, Banebots RS550) as well as a Maxon motor (Maxon 305007) to validate their rated no load RPM and backdrivability. A Maxon EPOS controller and a current sensing power supply (BK Precision, 30V/1A) were used to drive each actuator. From these experiments it was shown that the rated no load current was quite accurate for the RS550 (1.4A) and Maxon (80mA) motors and the no load current was lower than specified (800mA) for the RS775 motor. Through further experimentation with the RS775 motor in this setup, the EPOS

controller was able to control the motor velocity, current and position well under no load and loaded conditions, with the gearbox attached.

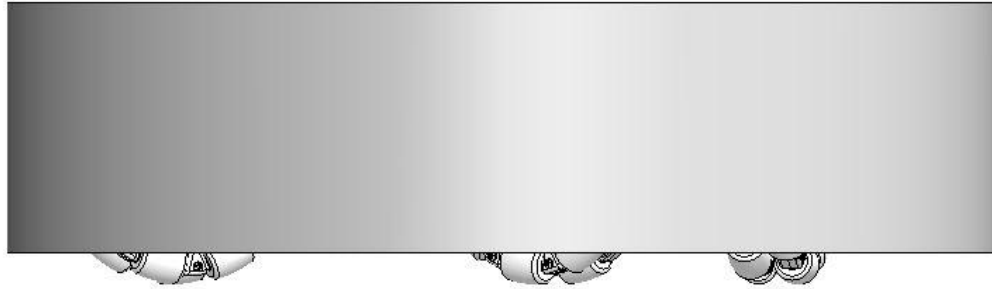


Figure 34: Commercial Design of Lower-Limb Rehabilitation Robot

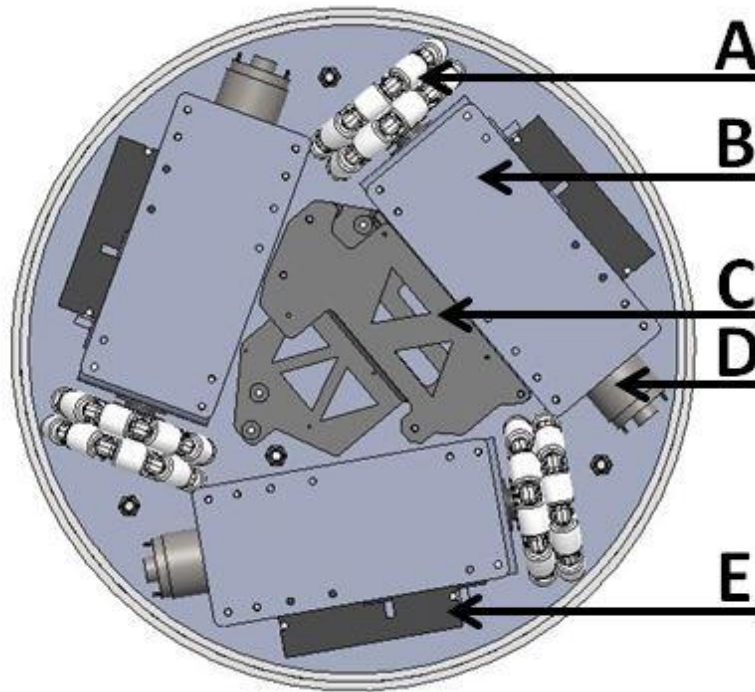


Figure 35: Mechanical and Electrical Layout of Rehabilitation Robot A) Omni-Wheel; B) Flexible Coupling Housing; C) Battery, CPU & Circuit Board Holder; D) Actuator; E) EPOS Motor Controller

3.2 Custom Flexible Sensor for Joint Torque Sensing and Three-DOF Force Sensing

3.2.1 Sensor Design

There is a common issue in lower-limb rehabilitation robots that, due to the power and torque required for motion assistance, the speed reduction (gearing or ball-screw pitch) and inertia required for the patient to easily backdrive the system is too large, even when high-quality high-cost components are used. As a solution to this issue, many systems incorporate joint flexibility in the form of series elastic actuators [6], [87]. This joint flexibility allows the patient to move smoothly without requiring the robot system to operate at a lower bandwidth, avoiding high dynamics [88]. The tradeoff is that it is difficult to control the system to feel very rigid as controlling the robot to feel stiffer than the joint flexibility can cause non-passivity, which is especially an issue in non-minimum phase systems. Recently, several researchers have focused on creating a rotary series elastic actuator that has a constant spring stiffness in the range of 100Nm/rad to 300Nm/rad for knee rehabilitation [88], [89]. Current issues with these flexible mechanisms are that under high rehabilitative loading, the force-to-deformation profile is nonlinear and the material stress is exceeded. For a typical knee-to-ankle length of 0.45m, a 100Nm/rad stiffness gives $\sim 217\text{N/rad}$ stiffness at the ankle, and a stiffness of 10 Nm/rad for flexible series elastic actuation in mobile platforms with 4in wheels. From these initial specifications a range of custom rotary series elastic joints were then developed. The flexible joints designed, manufactured and validated experimentally gave a uniform stress during actuation, linear elasticity throughout its desired torque range and low backlash and hysteresis.

The flexible coupling developed is required to provide backdrivability and passive assistance to patients with high frequency motion, and allow the robot to be controlled in impedance control mode in situations where the output torque of the actuator is not reliably modeled by the motor current. After researching previous flexible joint designs, it was found that many flexible couplings for industrial applications had been developed for joint alignment and over load protection. However, in these applications, the desired joint flexibility is much too stiff, typically over 3000 Nm/rad. Due to the flexibility

specifications driven by mobile lower-limb rehabilitation, a custom design was required to adapt commercial couplings to a useful rehabilitation solution.

From an analysis of commercial devices, it was shown that spider-type couplings gave the most linear force displacement response of all flexible couplings as governed by Eq. 18. They are used in start and stop applications and can be adapted for zero-backlash solutions [90]. Eq. 19 then gives the formula for specifying coupling parameters and Figure 36 shows the typical design of a commercial flexible coupling.

$$\text{Angular Displacement} = \frac{\text{Force} * \text{Length Between Teeth}}{\text{Elastic Modulus} * \text{Area} * \text{Coupling Radius}} \quad (18)$$

$$\text{Torque/Angular Displacement} = \frac{\text{Elastic Modulus} * \text{Area} * \text{Coupling Radius}^2}{\text{Length Between Teeth}} \quad (19)$$

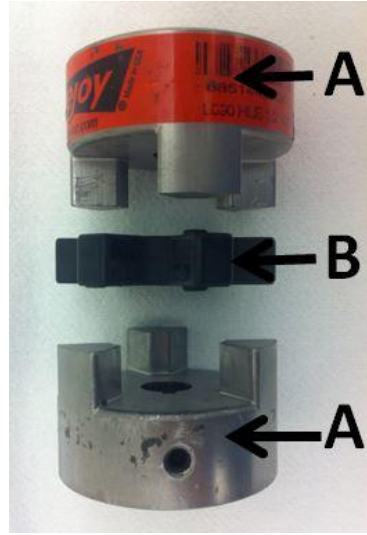


Figure 36: Standard Flexible Coupling: A) Hub; b) Spider

Using a commercial spider coupling hub as the exterior for strength and ease of manufacture, a custom spider was then designed that provided linear elasticity at the desired stiffness throughout the range of torques applied during therapy. To design a spider that met the above specifications, an ideal material was selected, a spider shape was conceived and modeled in finite element analysis to attain a low-backlash linear elastic structure, and a digital torque sensing enclosure was added for high-resolution

torque measurements. Following from Eq. 19, a spider material was selected to reduce the elastic modulus of standard spiders (roughly 6.2GPa for Hytrel spiders) for added flexibility while maintaining linear elasticity. As smaller spacing between hub teeth would give a more linear application of force, a superelastic material (elongation >10%) was required to give the deformation required, while having low hysteresis. From these specifications and preliminary material testing against other materials, a silicone rubber Rebound 25A was selected as it gave the lowest elastic modulus, with a fast response and low hysteresis. As elastomers are rated by hardness instead of elastic modulus the conversion below gives the elastic modulus of the chosen material, which is 0.947 GPa.

$$\text{Elastic Modulus (MPa)} = \text{EXP}((\text{Shore A}) * 0.0235 - 0.6403) \quad (20)$$

The custom elastomeric spider was created by mixing and pouring a two-part Rebound 25A compound into the 3D-printed and sealed mold shown in Figure 37. The spider was designed using the basic shape of the standard spider and adding material at the edges to reduce backlash and give pre-stress to the coupling for faster response.



Figure 37: Custom Flexible Coupling Rapid Prototyped Mold and Spider Material

To select an appropriate coupling, the 100Nm/rad specification for previous knee series elastic actuators was used. As these actuators were used as exoskeletons attached at the knee joint, the stiffness needed to be scaled based on the length from the knee joint to the ankle joint, and the mobile base wheel diameter. Assuming a typical length of 0.45m and a wheel radius of 0.0508m (2in) the actuator joint stiffness should be about 10 Nm/rad for this mobile base. This calculation approximated the joint stiffness to robot stiffness ratio as one because this is the average stiffness for all directions of motion although the

stiffness is not isotropic and varies depending on the force direction. This relation is shown in more detail in Chapter 3.3. Eq. 19 was then used to select a stock 54mm diameter spider coupling (McMasterCarr, 6408K14), as the area (13mm x 12mm), length (9mm) and contact radius (25mm) parameters of this coupling gave a theoretical joint stiffness of 10.83Nm.

To validate the stiffness of the selected coupling and custom spider an experimental setup was designed that allowed isolated torques to be applied to the coupling as in Figure 38. The experimental setup is composed of a handle for applying torque by hand, an ATI Gamma SI 32.5 – 2.5 commercial force/torque sensor for measuring 1-DOF torque, a 1024 count per revolution encoder (US Digital, E6), a bearing for restraining lateral movement, and the custom flexible coupling. The encoder specified was then changed to a 10,000 count per revolution encoder (from US Digital) for implementation in the robot, as this increased the sensor resolution ten-fold. The resulting torque to angular displacement plot is shown in Figure 39 showing linear elasticity throughout the torque range limited by the Gamma sensor. The slope of the plot showed an actual stiffness of 13 Nm/rad with this coupling which is within 10% of the theoretical value and is most probably caused by the retaining force of the central material and friction between the spider and hub. From this experimental setup, it was also shown that a digital encoder would be able to measure torque accurately, and would allow for impedance control of less efficient, less backdrivable actuators where the motor current to actuator torque relation is complex. The digital measurement would also eliminate drift, provide an update rate above 1kHz, be reliable in long-term use and give an affordable solution compared to commercial torque sensors which cost about \$5000. This digital encoder was then used to sense torque when oscillating frequencies between 0.2Hz to 5Hz were applied, as limited by the speed of the hand in applying torque. The resulting plot in Figure 40 shows that the sensed torque was accurate to within 10% of the full scale value for all frequencies tested using this linear fit, and the resolution was 0.05Nm with the 1024 CPR encoder as shown by the step size in the sensed values. Impulse torques were then applied to the sensor to observe the settling time of the coupling although the flexibility was quite low for oscillations to be identified. The sensor tracked the impulse torque well at a 1kHz sampling rate as shown in Figure 41 with low settling time;

however it was identified from this plot that the sensor experienced backlash of 0.2Nm, which could be detrimental to torque control at low torques. This proof-of-concept highly-flexible coupling sensor showed that a linear elastic response could be achieved through material selection and the sensor was able to attain high resolution at a high sampling rate.

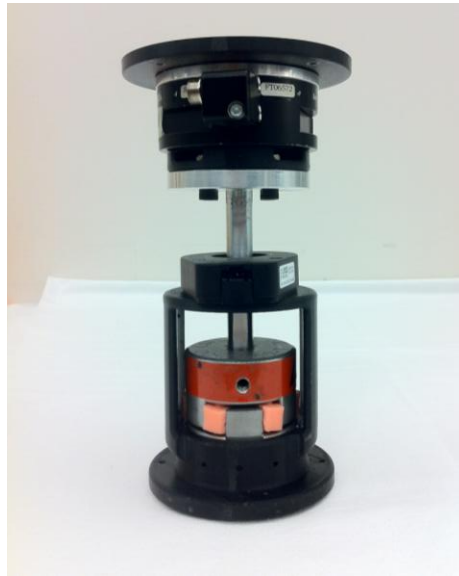


Figure 38: Experimental Setup to Calibrate and Evaluate Coupling Stiffness and Sensor Performance

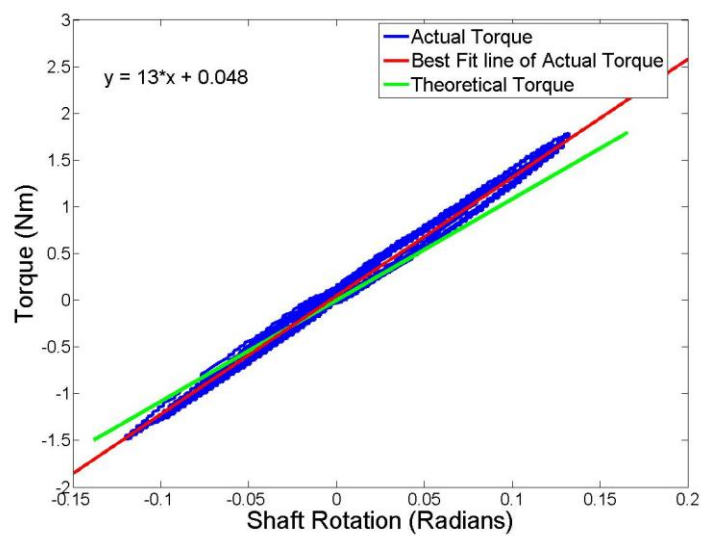


Figure 39: Linear Shaft Rotation vs. Torque for Initial Flexible Coupling Prototype

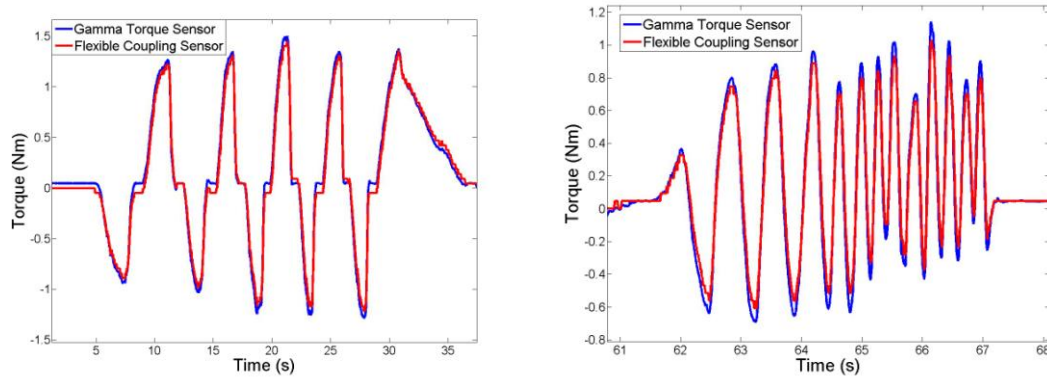


Figure 40: Validation of the Flexible Torque Sensor using an ATI Gamma Sensor

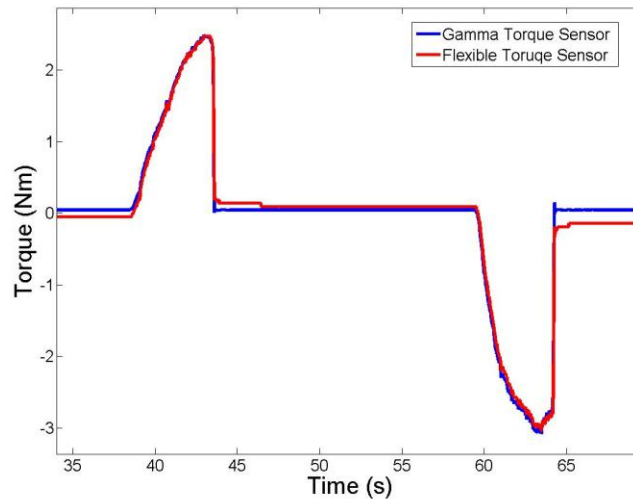


Figure 41: Rise and Fall Time of the Flexible and Gamma Torque Sensors

The proof-of concept sensor above performed well in flexibility and sensing experiments, but had large inertia and some backlash. To miniaturize the sensor and reduce backlash while maintaining a stiffness of 9 Nm/rad, further research on specialized couplings was conducted and the stiffness model, Eq. 19, was used to select an ideal coupling. As the coupling stiffness is proportional to r^2 miniaturizing the coupling diameter brought a commercial sensor into the stiffness range specified. The components selected were an aluminum coupling hub with a 33.2 mm diameter and a 60g mass (McMasterCarr, 6408K11) and a zero-backlash Hytrel spider (McMasterCarr, 6408K91). The elastic modulus of this material was about 6.2 GPa, the area was 11mm

by 8mm, the length was 9.5mm and the average contact radius was 12.5mm for a theoretical stiffness of 8.974Nm/rad. Using the experimental setup in Figure 38 with the new coupling the evaluated stiffness was 12Nm/rad and was mostly due to differences in the elastic modulus from the modulus specified in the datasheet. The calibration result and sensing performance are shown in Figure 42, which shows linear elasticity and very low backlash. Errors in linearity and torque sensing are attributed to inefficiencies in the experimental setup as at lower flexibility shaft misalignment is a bigger issue. In the future it would be beneficial to create an improved testing apparatus with two bearing supports to hold the shaft vertical.

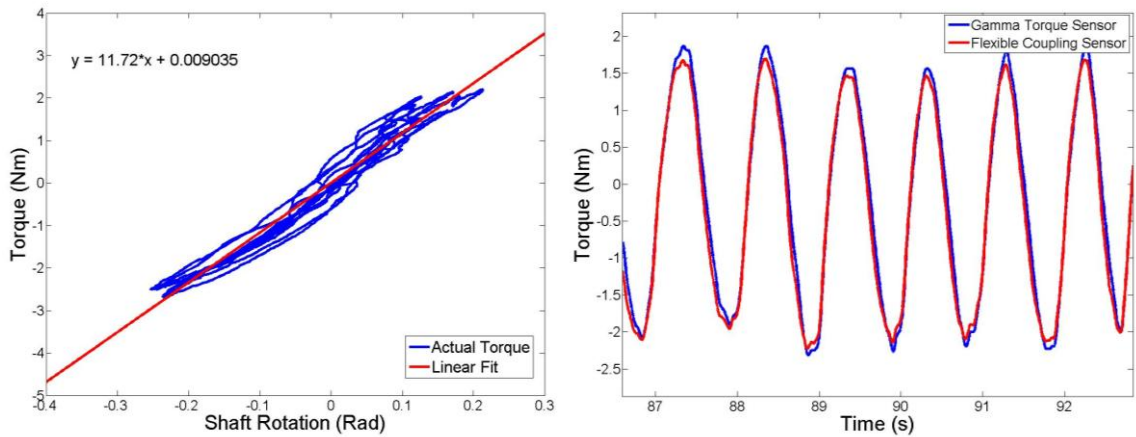


Figure 42: Hytrel Coupling Calibration and Validation against an ATI Gamma Sensor

The robot was assembled once the desired couplings mentioned above were selected, and the system flexibility gave a smooth motion transition into the actuator backdrivability range (2N) through in-lab experimentation. A concern with the system is that the robot feels quite stiff (when unpowered) for early-stage neuromuscular therapy. The joint flexibility initially specified was determined by long-term gait rehabilitation training researchers, but in early-stage therapy, the stiffness of the system should be lower to allow for larger spasticity without requiring highly dynamic robot actuation. This reduces the required system bandwidth and motor current draw, making the system more reliable and safe. To allow the patient to move within their spasticity region with under 10N of force, a joint flexibility of 5mm/N (or 0.4Nm/rad at each joint) was

specified based on clinical spasticity measurements [91]. To reduce the stiffness of the current spider, the material could be changed or the shape could be redesigned. As previous designs incorporated Rebound silicone rubber and showed large deformation while maintaining linear elasticity, this material was selected for the next coupling prototype. The same hubs as for the Hytrel coupling were used for easy modification, and for adapting the robot over time to patient needs. Through experimental calibration, the new spider showed linear behavior and a stiffness of 0.36 Nm/rad as per the specification. The sensor was then tested for its performance in low and higher frequency sensing.

This sensor responded very well in experimental testing and replaced the original couplings in the robot. With these couplings the robot felt much more forgiving to shaky or incorrect movement, providing patients with neuromuscular deficit to train to move in the correct general path without having the robot give too much assistance that the patient would not be given the opportunity to learn. As a final iteration to the spider design, multiple shapes were studied using finite element analysis to reduce backlash, and give linear stress distribution through the coupling. The finite element studies showed that incorporating a ring around the sensor would give an almost constant stress distribution throughout the spider arms and would provide support between arms to reduce backlash. The final design of this coupling was developed; however only slight improvement to backlash and linearity was seen and the stiffness remained similar. The intermediate and final flexible couplings are shown in Figure 43.

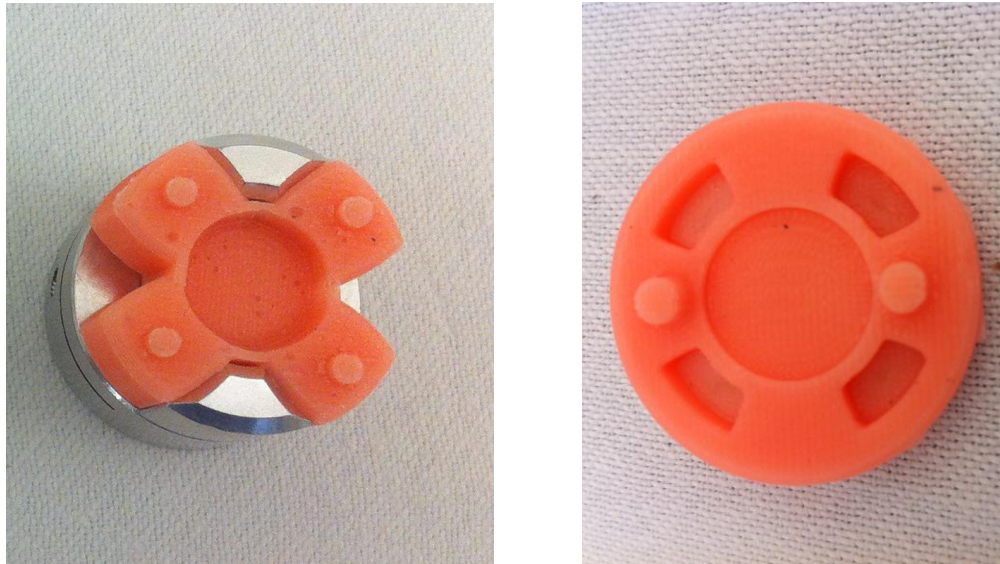


Figure 43: left: Intermediate; and right: Final Custom Flexible Coupling

In conclusion, a flexible commercial coupling was selected to meet the stiffness criteria stated in the literature. As this criterion was determined through gait-training tasks with patients in long-term rehabilitation training programs, the stiffness seemed very high for patients with low neuromuscular control and increased spasticity. The new flexibility specifications required low stiffness not available commercially, or discussed in research, so a custom joint needed to be designed. Using the same coupling hubs as selected above, and adapting the material and spider shape to give a linear torque to rotation profile with low backlash, a modular solution was achieved. In impedance control tasks, it is important not only to add passive structures for soft interaction but also to control joint torque for applying guiding forces to the patient. The relation between motor current and joint torque is nonlinear, and time and temperature varying in high-power, highly-g geared actuators, so torque sensing is required to control the apparent stiffness of the robot with higher accuracy. The joint torque was sensed using encoders (US Digital, E6, 10,000CPR) on the input and output shafts of the couplings, giving 0.005Nm and 0.0005Nm resolutions, respectively, for the stiffer and more flexible coupling. Having the motor, gearbox, encoder, coupling and wheel selected, a final actuator design could be developed. The design goals were to create modular actuation system for easy assembly that was compact and low weight. A sheet metal frame was

chosen to create a rigid housing, and hole placement was selected so there were no hard to reach screw locations and the motors and gearboxes could be easily removed. The system could also be riveted as opposed to using fasteners, but for research systems experience suggest that easy to assemble and disassemble systems are beneficial in future experimentation. Figure 44 shows the design of the flexible actuation and torque sensing module, Figure 45 shows the part and tool layout before assembly and Figure 46 shows the three step assembly of each module. The modules can then be easily installed on the main foot plate as in Figure 32 above.

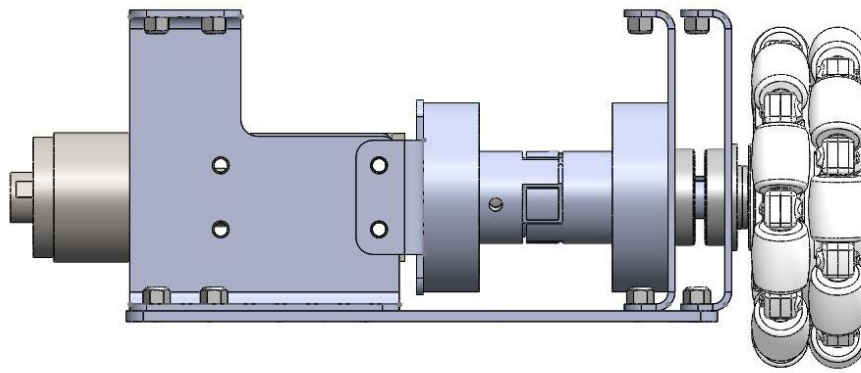


Figure 44: Modular Flexible Actuation and Torque Sensing Assembly

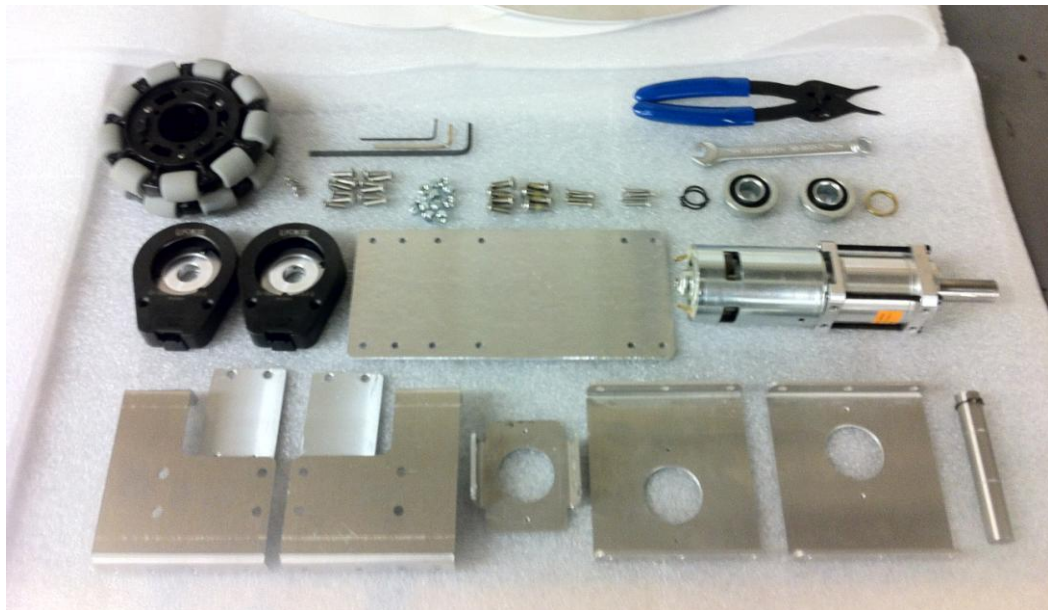


Figure 45: The Set of Parts and Tools Required to Assemble the Module

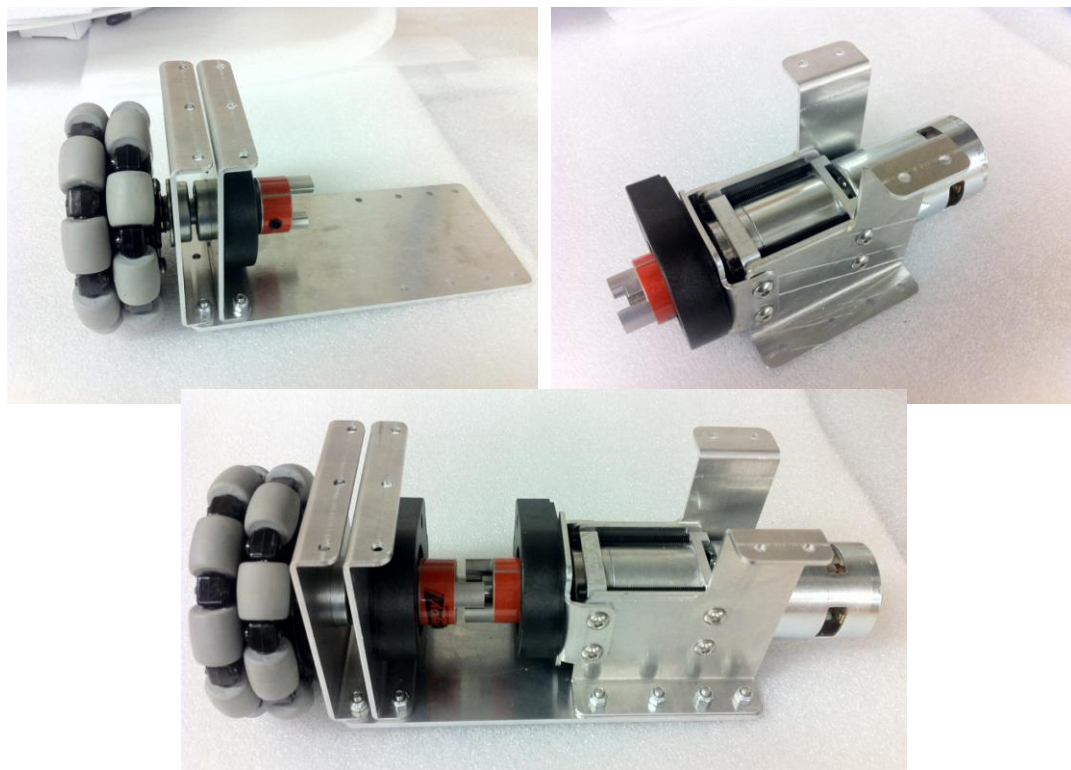


Figure 46: Three Step Assembly for Assembling Actuation Modules

3.3 Robot Control & Mathematical Modeling

The mechanical design of the three wheel robot was completed to overcome issues that hindered the control of the six-DOF robot in Chapter 2. By reducing the number of actuators, the gear reduction, and the degrees of freedom the modified system decreases inertia and increases backdrivability. Further, embedded flexible couplings have been custom designed to provide linear joint flexibility and torque sensing. EPOS 24/5 controllers from Maxon Motors were selected for the research and clinical version of this robot as the documentation and programming community for these controllers would speed code development. These controllers communicate directly with the on-board CPU to reduce communication delays, and function at a 1kHz update rate for high frequency control if needed. Simple current controllers could replace the EPOS controllers for the in-home affordable version of the device once the system is properly tested clinically. An impedance control algorithm was selected to control this robot for assist-as-needed

training, and mathematical models of the kinematics, Jacobian and dynamics models were researched and selected as required for this algorithm. As the flexible couplings can also be declutched from the output shaft, the robot can be used with a simple kinematic model to evaluate the patient's performance in free-space motion. As well, the robot can be used in an unpowered, clutched state to train and evaluate patients in isometric strength training using the passive resistance of the sensorized flexible joints.

To control the robot to act as a spring-mass-damper system with variable impedance parameters that could be tuned by therapists or adapted over time, an impedance control algorithm was selected. This algorithm was chosen over an admittance control algorithm for safety reasons, as an admittance controlled system may respond dangerously when the patient's joint limits or range of motion is reached to maintain a desired velocity [50]. The tradeoff is that if the patient's foot is detached from the system, an impedance controller may not respond safely; but a pressure sensor can be used to detect foot detachment and power down the system to address this issue. As in many rehabilitation systems, flexibility has been incorporated into the system to give the system a softer feel, and a flexible joint impedance controller developed by DLR [92], [93] was selected and is shown below;

$$M(q)\ddot{q} + C(q, \dot{q})\dot{q} + g(q) = \tau + \tau_{ext} \quad (20)$$

$$B\ddot{\theta} + \tau = \tau_m \quad (21)$$

$$\tau_m = BB_\theta^{-1}u + (I - BB_\theta^{-1})\tau \quad (22)$$

$$u = -K_\theta(\theta - \theta_a) - D_\theta\dot{\theta} \quad (23)$$

The dynamics parameters M , and C are the dynamics parameters of the robot as calculated using the equations in [95], q represents the angular position of the wheels (real numbers), τ and τ_{ext} are the torques applied by the robot and the patient, θ is the angular position of the motor shafts (real numbers), B is the actuator inertia, B_θ is the reduced actuator inertia, K_θ and D_θ are the desired stiffness and damping parameters, and u is the control input.

Recently, this control algorithm has been implemented for a knee exoskeleton and has shown good performance [89]. From Eq. 20 to 23, it was identified that the kinematic and

Jacobian model was needed to convert from patient forces F_{ext} to external torques τ_{ext} , and the Lagrangian parameters were needed for the dynamics equations. In addition, as the robot provides planar motion, the gravity compensation term is zero, simplifying the control.

The inverse kinematic model for the three wheel omni-directional drive base was presented in [63], and [94] and shows the manipulability profile of the three wheel system. The three-leaf clover profile gives a general view of the world frame stiffness felt by the flexible joints in each direction. Adapting these equations for the tilted-wheel design developed gives the kinematic model in Eq. 24 and the coordinate system and joint variables are shown in Figure 47, where δ is the angle that the line connecting the origin and the wheel centre of contact make with the X axis, and φ is the tilt angle of the wheel. To transform this equation into world frame coordinates, Eq. 25 can be used, assuming no wheel slippage. The inverse Jacobian can be found by taking the time-derivative of the inverse kinematic model and the kinematic and Jacobian models can be solved by inversion as the matrix is square and of constant value. As these models are being used for force to torque conversion as opposed to position or velocity measurement, the shaft flexibility does not need to be incorporated into this model. For position, velocity and acceleration measurement, the two-encoder system also gives direct measurement of the wheel rotation (not just the motor rotation), and as such the robot position is completely known from the equations below, taking r_w as the wheel radius and r_b as the radius of the circle created from the contact point of the three wheels.

$$\begin{bmatrix} \theta_1 \\ \theta_2 \\ \theta_3 \end{bmatrix} = (1/\pi r_w) \begin{bmatrix} \cos(\varphi) & \sin(\varphi) & r * \cos\varphi \\ -\sin(\delta_2 + \varphi) & \cos(\delta_2 + \varphi) & r * \cos\varphi \\ -\sin(\delta_3 - \varphi) & -\cos(\delta_3 - \varphi) & r * \cos\varphi \end{bmatrix} \begin{bmatrix} x_{base} \\ y_{base} \\ \alpha_{base} \end{bmatrix} \quad (24)$$

$$r_b = 167\text{mm}, \varphi = \frac{\pi}{4}, \delta_2 = \delta_3 = \frac{\pi}{6}$$

$$\begin{bmatrix} x_{base} \\ y_{base} \\ \alpha_{base} \end{bmatrix} = \begin{bmatrix} \cos(\alpha_{base}) & \sin(\alpha_{base}) & 0 \\ -\sin(\alpha_{base}) & \cos(\alpha_{base}) & 0 \\ 0 & 0 & 1 \end{bmatrix} \begin{bmatrix} x_{world} \\ y_{world} \\ \alpha_{world} \end{bmatrix} \quad (25)$$

The dynamic parameters of the robot were then calculated using the equations in [95]. These variables could be experimentally obtained in future work if needed for further precision using the method presented in [96]. The mathematical models and impedance control algorithm were simulated in MATLAB/SIMULINK to validate the system's response for varying apparent stiffness values, and a range of stiffness values that showed stability when considerable noise was injected were observed.

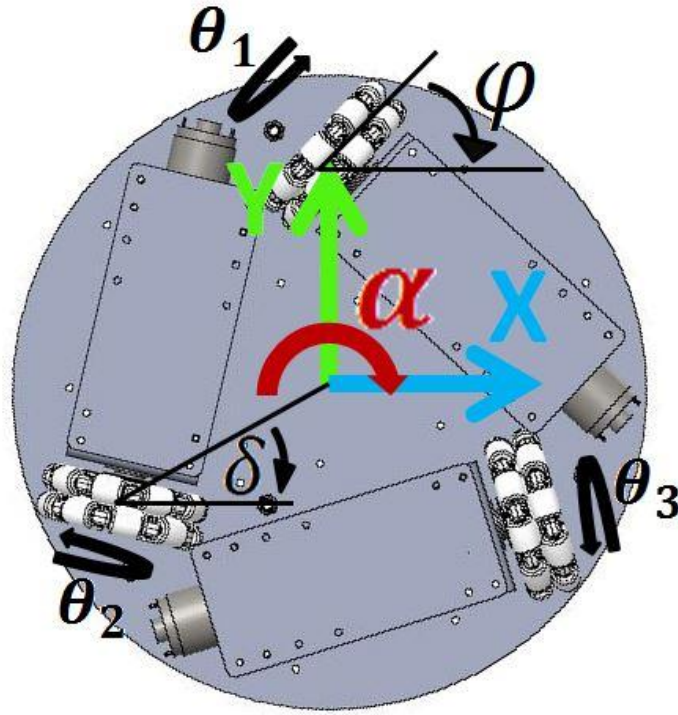


Figure 47: Coordinate System of the Omni-Directional Drive Base

From the experimental results shown in Chapter 2, and the improved design of the mobile base, the three-DOF system should perform equally well or better in velocity control and impedance/admittance control tasks than the six-DOF system. Through the formulation and acceptance of an ethics proposal for evaluating the system's performance in impedance control tasks with healthy individuals, this three-DOF system will be assessed for its clinical readiness and efficacy. From a robotics perspective this research

platform provides a new direction for in-home neuromuscular therapy, and allows for future development of advanced robot control and serious game strategies that can help patients recover faster and more completely, as well as provide an open structure for the development of novel ankle therapy solutions.

Chapter 4

4 Concluding Remarks and Future Work

The knowledge gained on the design and control of rehabilitation robots during this thesis will give guidance in the development of future rehabilitation systems for in-home use. The novel robotic systems developed in this work demonstrate the functionality of mobile drive systems in performing motion guidance and assist-as-needed training and the contributions of the developed systems are outlined in Section 4.1. A discussion on the design and implementation of rehabilitation systems for in-home use is provided in Section 4.2, and future work involves evaluating the rehabilitative efficacy of these robotic systems as explained in Section 4.3.

4.1 Thesis Contributions

The overarching goal of the devices presented in this thesis is to give stroke survivors with lower-limb neuromuscular deficit the opportunity to perform common rehabilitation exercises outside of scheduled occupational therapy hours (e.g. in a therapist's waiting room, at the patient's home). The motivation for this goal is that clinical studies show robotic therapy combined with occupational therapy produces better recovery outcomes than occupational therapy alone. This is due to an increase in the number of exercise repetitions performed while mental and physical exertion is maintained. For usage in clinics and homes these devices need to be portable and affordable so they can be easily incorporated into daily routines without burdening the patient or therapist or using considerable health care resources.

A summary of the major contributions of this thesis are presented below:

- Design of a novel six-DOF robotic system for lower-limb rehabilitation. The device is low-cost (\$3,500 prototype), portable and incorporates an omni-directional drive base and three-DOF platform.

- Design of a novel six-DOF force and torque sensing system. The device consists of low-cost one-DOF force sensors embedded into an optimized structure for high accuracy force and torque measurement.
- Validation of the performance of the six-DOF sensing and actuation system in trajectory guidance and motion assistance therapies with a healthy individual.
- Design of a novel rotary series elastic joint that provides linear elasticity and torque sensing capability. The joint is low-cost and provides high accuracy, resolution and sampling rate torque measurements using two encoders and a custom flexible spider coupling.
- Design of a novel three-DOF robotic system for in-home lower-limb rehabilitation. The design incorporates the rotary series elastic joint discussed above into modular actuation units for use in impedance-controlled motion assistance therapy. This design also has lower inertia than the previous system and is easier to backdrive. This device is low-cost (\$1,500 prototype), portable and easy to use for motion assistance and assessment of recovery after stroke.

4.2 Discussion

When creating systems for end users, it is important to generate detailed and accurate specifications in order to meet their needs, create a useful product, and avoid overdesigning areas of the system. By conducting experiments when the useful data has not already been gathered previously, accurate specifications can be outlined and this information can be used by other researchers as well. In the field of rehabilitation robotics, this requires close collaboration between therapists, patients and researchers to design experiments in a meaningful way, and understand the underlying reasons for difficulties in rehabilitation therapy.

In performing the research described in this thesis, the tradeoff between affordability, complexity, and performance was understood more fully. It is usually possible to attain two of these characteristics but in attaining all three, there may be large delays in design

and presentation of ideas. In simplifying the design and focusing on developing one idea at a time, the attainable outcomes of the product become much clearer, and the system has a higher chance of attaining performance levels that are acceptable for therapy. A common example of this is in the design of modular rehabilitation robotic systems. By focusing on a single joint, or a single therapy task, the device can help the patient perform that task much better than a therapist can. If a complex system, such as a gait training device is developed, it becomes much more difficult to provide clear rehabilitative benefit over standard therapy, whether the reasons are due to the robotic system or the mental and physical learning capabilities of the patient.

4.3 Future Work

In Chapter 2, the six-DOF version of the lower-limb rehabilitation robot was developed. There are some aspects of this work that can be improved or augmented. The robot currently feels fairly stiff due to the low motor control update rate, the non-backdrivability of the actuators, and the slowness of the communication. Also, the system inertia, sensing resolution and difficulty in defining a dynamic model of the parallel mechanism made the control of the robot in start/stop applications somewhat difficult. The direction chosen in Chapter 3 to overcome these issues was to make the system less complex and focus on assistance in important exercising tasks. In continuing with this direction, the next steps would be to:

- 1) Obtain ethics approval to validate the robot's functionality with healthy individuals.
- 2) Observe how well the robot performs when healthy individuals are asked to perform a task that requires learning.
- 3) Validate the safety of the system and test its efficacy in neuromuscular rehabilitation.

From the completion of these three steps the value of mobile systems in lower-limb rehabilitation can be assessed and new ideas to develop this system further can be conceived. Some possible issues that may need to be addressed are:

- 1) Detecting and measuring wheel slippage, with possible solutions being to incorporate accelerometer information or visual tracking information to calculate the motion of the robot in the world frame
- 2) Ensuring that the device is safe for use by patients with neuromuscular and/or cognitive disability, through fault-detection software or adding redundant sensors. The two-encoder system does provide some redundancy, but the addition of safety stop buttons and sound/visual functionality may be useful in case of unexpected issues and for reminding the patient to do their exercises.

From a therapy perspective, new functionalities that could be tested with this device could involve modifying assistance parameters or trajectories in real-time to provide better therapy, analyzing muscle rigidity and reaction time, and training individuals for critical situations such as fall recovery and obstacle avoidance.

As a different approach, one could redesign the parallel structure of the six-DOF system in Chapter 2 for mounting to the drive base presented in Chapter 3, or as a stand-alone unit. It would be important to discuss with therapists before taking on this endeavor however, as the design may affect the system performance or be quite expensive. So it would be important to establish specifications first. One such mechanism that could be developed would be a Canfield mechanism [97] as it provides the three-DOF not applied by the drive base, for a six motor six-DOF solution. A proof-of-concept system was designed in SolidWorks that uses harmonic drive motors to keep the low-profile of the robot, as shown in Figure 48. This mechanism has been studied in detail and several applications for its use have been found. The downside of this mechanism is that it is difficult to create a compact mechanism that would rotate about the patient's ankle joint so the drive wheels may need to be activated even for isolated ankle therapy. In conclusion, the robotic platforms developed in this thesis, for clinical analysis of mobile rehabilitation, provide many opportunities for future work in studying and advancing lower-limb rehabilitation therapy using robots.

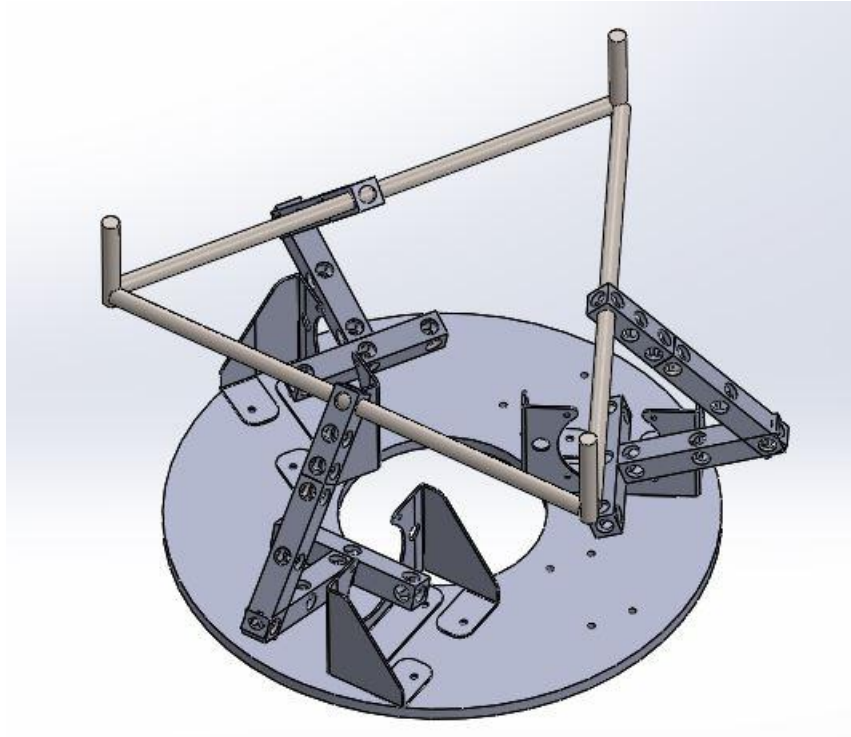


Figure 48: Modified Canfield Mechanism Designed to be Mounted to a Mobile Base

5 References

- [1] D. Mozaffarian, *et al.*, "Heart Disease and Stroke Statistics—2015 Update A Report from the American Heart Association," *Circulation*, 131.4 (2015): e179, 2015.
- [2] G.E. Gresham, *et al.*, "Residual disability in survivors of stroke—the Framingham study," *New England Journal of Medicine*, 293.19 (1975): 954-956.
- [3] A.K. Welmer, *et al.*, "Limited fine hand use after stroke and its association with other disabilities," *Journal of Rehabilitation Medicine*, 40.8 (2008): 603-608.
- [4] S.M. Lai, *et al.*, "Persisting consequences of stroke measured by the Stroke Impact Scale," *Stroke* 33.7 (2002): 1840-1844.
- [5] Heart & Stroke Foundation, "2014 Report on the Health of Canadians," 2014.
- [6] A. Roy, *et al.*, "Measurement of human ankle stiffness using the anklebot," *10th IEEE International Conference on Rehabilitation Robotics (ICORR2007)*, pp. 356-363, 2007.
- [7] P.S. Lum, *et al.*, "Robot-assisted movement training compared with conventional therapy techniques for the rehabilitation of upper-limb motor function after stroke," *Archives of Physical Medicine and Rehabilitation*, 83.7 (2002): 952-959.
- [8] K.P. Westlake, C. Patten, "Pilot study of Lokomat versus manual-assisted treadmill training for locomotor recovery post-stroke," *Journal of Neuroengineering and Rehabilitation*, 6:18, 2009.
- [9] M.R. Schoenberg, *et al.*, "Neuroanatomy primer: Structure and function of the human nervous system. In *The Little Black Book of Neuropsychology*," pp. 59-126. Springer US.
- [10] S. Skoglund, "Joint Receptors and Kinaesthesia," in *Handbook of Sensory Physiology, Somatosensory System*, D. Albe-Fessard, *et al.*, Berlin, Heidelberg: Springer Berlin Heidelberg, 1973, pp. 111–136.
- [11] K. Sukel, *Neuroanatomy-A Primer*. July, 27, 2011. Retrieved April 13, 2015.
- [12] B. Kolb, I. Whishaw, "Fundamentals of Neuropsychology," 1990.
- [13] I. Khan, "Neurological Deficits per Location of a Stroke," Symposium. Lecture conducted from Vanderbilt University Medical Centre for Stroke. Jan. 1, 2013.
- [14] L.M. Carey, T.A. Matyas, "Frequency of discriminative sensory loss in the hand after stroke in a rehabilitation setting," *Journal of rehabilitation medicine*, 2011, 43(3), 257-263.
- [15] G. Kwakkel, *et al.*, "Effects of Augmented Exercise Therapy Time after Stroke," *Stroke*, vol. 35, pp. 2529-2539, October, 2004.
- [16] S. A. Raskin, "Neuronal Organization and Change after Brain Injury," in *Neuroplasticity and Rehabilitation*, New York, USA, Guilford Press, 2011, ch. 2.
- [17] M. A. Dimyan and L.G. Cohen, "Neuroplasticity in the Context of Motor Rehabilitation after Stroke," *Nature Reviews Neurology*, vol. 7, pp. 76-85, February, 2011.
- [18] H. S. Jorgensen, *et al.*, "Recovery of Walking Function in Stroke Patients: The Copenhagen Stroke Study," in *Arch. of Phys. Med. and Rehabil.*, vol. 76, pp. 27–32, January, 1995.
- [19] K. Salter, *et al.*, "Impact of Early vs. Delayed Admission to Rehabilitation on Functional Outcomes in Persons with Stroke," *J. of Rehabil. Med.*, vol. 38, pp. 113-117, 2006.

- [20] P.W. Duncan, *et al.*, "Management of adult stroke rehabilitation care a clinical practice guideline," *Stroke*, 2005, 36(9), e100-e143.
- [21] L. W. Forrester, *et al.*, "Exercise-Mediated Locomotor Recovery and Lower-Limb Neuroplasticity after Stroke," *J. of Rehabil. Research and Development*, vol. 45, pp. 205, 2008.
- [22] M. A. Dimyan and L.G. Cohen, "Neuroplasticity in the Context of Motor Rehabilitation after Stroke," *Nature Reviews Neurology*, vol. 7, pp. 76-85, February, 2011.
- [23] National Stroke Association. "Hope: The stroke recovery guide," Denver Colorado: The National Stroke Association. 2007, Ch. 4.
- [24] Stroke Rehabilitation Information. National Institute of Neurological Disorders and Stroke (NINDS). (2014, March 13). Retrieved July 20, 2015.
- [25] Z. Qian, Z. Bi, "Recent Development of Rehabilitation Robots," *Advances in Mechanical Engineering*. 2014.
- [26] National Institute on Aging. (PDF) "Why Population Aging Matters: A Global Perspective," 2007.
- [27] R. D. Zorowitz, *et al.*, "Costs and Rehabilitation Use of Stroke Survivors: A Retrospective Study of Medicare Beneficiaries," *Topics in Stroke Rehabilitation*, vol. 16, pp. 309-320, 2009.
- [28] "The quality of stroke care in Canada," Canadian Stroke Network, 2011.
- [29] "Ontario Stroke Evaluation Report 2011: Improving System Efficiency by Implementing Stroke Best Practices. Institute for Clinical Evaluative Sciences," 2011.
- [30] "Optimal Onset-to-Admission Interval for Inpatient Stroke Rehabilitation: A Rapid Review," Health Quality Ontario. 2013.
- [31] M.C. Kosak, M.J. Reding, "Comparison of partial body weight-supported treadmill gait training versus aggressive bracing assisted walking post stroke." *Neurorehabilitation and Neural Repair*, 14(1), 13-19, 2000.
- [32] D. Kidd, *et al.*, "The Functional Independence Measure: a comparative validity and reliability study." *Disability and rehabilitation*, 17(1), 10-14, 1995.
- [33] J. Sanford, *et al.*, "Reliability of the Fugl-Meyer assessment for testing motor performance in patients following stroke." *Physical therapy*, 73(7), 447-454, 1993.
- [34] "Stroke Rehab e-book: A Guide for Patients & Their Caregivers," Stroke-Rehab.com. 2015.
- [35] I. Díaz, *et al.*, "Lower-limb robotic rehabilitation: literature review and challenges." *Journal of Robotics*, 2011.
- [36] G. Kwakkel, *et al.* "Effects of robot-assisted therapy on upper limb recovery after stroke: a systematic review." *Neurorehabilitation and neural repair*, 2011.
- [37] H.I. Krebs, *et al.*, "Rehabilitation robotics: pilot trial of a spatial extension for MIT-Manus." *Journal of NeuroEngineering and Rehabilitation*, 2004.
- [38] J. Hidler, *et al.*, "Multicenter randomized clinical trial evaluating the effectiveness of the Lokomat in subacute stroke," *Neurorehabilitation and Neural Repair*, 23(1), 5-13, 2009.
- [39] S. Freivogel, *et al.*, "Improved Walking Ability and Reduced Therapeutic Stress with an Electromechanical Gait Device," *J. of Rehabil. Med.*, vol. 41, pp. 734-739, 2009.

- [40] K. P. Westlake and C. Patten, "Pilot Study of Lokomat versus Manual-Assisted Treadmill Training for Locomotor Recovery Post-Stroke," *J. of NeuroEng. and Rehabil.*, vol. 6, pp. 18, June, 2009.
- [41] S. H. Peurala, *et al.*, "Effects of Intensive Therapy using Gait Trainer or Floor Walking Exercises Early after Stroke," *J. of Rehabil. Med.*, vol. 41, pp. 166-173, February, 2009.
- [42] L.W. Forrester, *et al.*, "Ankle Training with a Robotic Device Improves Hemiparetic Gait after a Stroke," *Neurorehabilitation and Neural Repair*, vol. 25, pp. 369-377, February, 2011.
- [43] M. Girone, *et al.*, "The Rutgers Ankle Orthopedic Rehabilitation Interface," in *Proc. of ASME Dyn. Syst. Control Div. (DSCD)*, vol. 67, pp. 305-312, 2009.
- [44] D. Luo, *et al.*, "Position and Orientation Control of an Omni-Directional Mobile Rehabilitation Robot," in *Proc. of IEEE Int. Conf. on Control Applications (CCA)*, pp. 50-56, 2012.
- [45] M. Sarac, *et al.*, "ASSISTON-MOBILE: A Series Elastic Holonomic Mobile Platform for Upper Extremity Rehabilitation," *Robotica*, vol. 32, pp. 1433-1459, December, 2014.
- [46] K. Anam, A. Al-Jumaily, "Active exoskeleton control systems: State of the art," *Procedia Engineering*, 41, 988-994, 2012.
- [47] L. Marchal-Crespo, D.J. Reinkensmeyer, "Review of control strategies for robotic movement training after neurologic injury," *Journal of neuroengineering and rehabilitation*, 6(1), 20, 2009
- [48] J. Cao, *et al.*, "Control strategies for effective robot assisted gait rehabilitation: The state of art and future prospects," *Medical engineering & physics*, 36(12), 1555-1566, 2014.
- [49] W. Meng, *et al.*, "Recent development of mechanisms and control strategies for robot-assisted lower limb rehabilitation," *Mechatronics*, 2015.
- [50] N. Hogan, "Impedance control: An approach to manipulation: Part II—Implementation," *Journal of dynamic systems, measurement, and control*, 107(1), 8-16, 1985.
- [51] C.D.Takahashi, *et al.*, "A robotic device for hand motor therapy after stroke," *9th IEEE International Conference on Rehabilitation Robotics (ICORR2005)*. pp. 17-20, 2005.
- [52] R.C.V. Loureiro, W.S. Harwin, Reach & grasp therapy: design and control of a 9-DOF robotic neuro-rehabilitation system. *10th IEEE International Conference on Rehabilitation Robotics (ICORR 2007)*:757-763, 2007.
- [53] T.G. Sugar, *et al.*, Design and control of RUPERT: A device for robotic upper extremity repetitive therapy. *IEEE Transactions on Neural Systems and Rehabilitation Engineering*, 2007, 15(3):336-346.
- [54] H.I. Krebs, *et al.*, "Rehabilitation robotics: performancebased progressive robot-assisted therapy," *Autonomous Robots*, 2003, 15:7-20.
- [55] S.K. Banala, *et al.*, "Robot assisted gait training with active leg exoskeleton (ALEX). *IEEE Transactions on Neural Systems and Rehabilitation Engineering*, 17(1), 2-8, 2009.
- [56] S. Lee, Y. Sankai, "Power assist control for walking aid with HAL-3 based on EMG and impedance adjustment around knee joint." *IEEE/RSJ International*

- Conference on Intelligent Robots and Systems (IROS2002)*.vol. 2, pp. 1499-1504. 2002.
- [57] M. Shahbazi, *et al.*, "A novel shared structure for dual user systems with unknown time-delay utilizing adaptive impedance control." *IEEE International Conference on Robotics and Automation (ICRA2011)*, pp. 2124-2129, 2011.
 - [58] D. Zanutto, *et al.*, "Effects of complementary auditory feedback in robot-assisted lower extremity motor adaptation," *IEEE Transactions On Neural Systems and Rehabilitation Engineering*, 21.5: 775-786, 2013.
 - [59] A. Yurkewich, *et al.*, "A Six-Degree-of-Freedom Robotic System for Lower Extremity Rehabilitation." *IEEE International Conference on Rehabilitation Robotics (ICORR2015)*. Singapore. Accepted March 28, 2015. Presented August 13, 2015.
 - [60] C. C. Norkin, D. J. White, "Lower Extremity Testing," in *Measurement of Joint Motion: A Guide to Goniometry*, 2009, ch. 3.
 - [61] J. P. Paul. "Forces Transmitted by Joints in the Human Body," *Institution of Mech. Engineers*, vol. 181, pp. 8-15, 1966.
 - [62] J. Funk, "Robotic Exoskeletons: Becoming economically feasible," 2013.
 - [63] H. P. Oliveira, *et al.*, "Modeling and Assessing of Omni-Directional Robots with Three and Four Wheels," *Contemporary Robotics: Challenges and Solutions*, December, 2009.
 - [64] C. Ng, *et al.*, "Design and Development of 3-DOF Modular Micro Parallel Kinematic Manipulator," *Int. J. of Advanced Manufacturing Technology*, vol. 31, pp. 188-200, November, 2006.
 - [65] X. Huang, *et al.*, "Forward kinematics of the 6-6 Stewart Platform with Planar Base and Platform using Algebraic Elimination," *IEEE Int. Conf. on Automation and Logistics*, pp. 2655-2659, 2007.
 - [66] M. S. Tsai, *et al.*, "Direct Kinematic Analysis of a 3-PRS Parallel Mechanism," *Mechanism and Machine Theory*, vol. 38, pp. 71-83, January, 2003.
 - [67] Y. Li and Q. Xu, "Kinematics and Inverse Dynamics Analysis for a General 3-PRS Spatial Parallel Mechanism," *Robotica*, vol. 23, 219-229, March, 2005.
 - [68] A. Hollinger, M. Wanderley, "Evaluation of commercial force-sensing resistors." *International Conference on New Interfaces for Musical Expression*, 2006.
 - [69] M. Uchiyama, *et al.*, "Evaluation of the robot force sensor structure using singular value decomposition," *Advanced Robotics (International Journal of the Robotics Society of Japan)*, vol. 5, pp. 39-52, 1991.
 - [70] E. Bayo, J. R. Stubbe, "Six-axis force sensor evaluation and a new type of optimal frame truss design for robotic applications," *Journal of Robotic Systems*, vol. 6, pp. 191-208, 1989.
 - [71] Y. Nakamura, *et al.*, "Design and signal processing of six-axis force sensor," *4th International Symposium of Robotics Research*, pp. 75-81, 1988.
 - [72] A. Bicchi, "A criterion for optimal design of multi-axis force sensors," *Journal of Robotics and Autonomous Systems*, vol. 10, no. 4, pp. 269-286, 1992.
 - [73] R. Haslinger, *et al.*, "A fiberoptic force-torque-sensor for minimally invasive robotic surgery," *IEEE International Conference on Robotics and Automation (ICRA2013)*, pp. 4390-4395. 2013
 - [74] FlexiForce User Manual. Tekscan. December, 2013. Retrieved July 20, 2015.

- [75] High Gain Observer (PDF). Clemson University. Lecture Slides.
- [76] DsPIC33EP512MU814. MicroChip Technologies. Retrieved July 20, 2015.
- [77] M. Hoda, *et al.*, "A Novel Study on Natural Robotic Rehabilitation Exergames Using the Unaffected Arm of Stroke Patients," *International Journal of Distributed Sensor Networks*, 2015.
- [78] J. Hidler, *et al.*, "Advances in the understanding and treatment of stroke impairment using robotic devices." *Topics in Stroke Rehabilitation*, 12(2):22-35, 2015.
- [79] A. Lo, *et al.*, "Robot-assisted therapy for long-term upper-limb impairment after stroke." *New England Journal of Medicine*, 362.19: 1772-1783, 2010.
- [80] C. Werner, *et al.*, "Treadmill Training With Partial Body Weight Support and an Electromechanical Gait Trainer for Restoration of Gait in Subacute Stroke Patients A Randomized Crossover Study." *Stroke* 33.12 : 2895-2901, 2002.
- [81] S. Banala, *et al.*, "Robot assisted gait training with active leg exoskeleton (ALEX)," *IEEE Transactions on Neural Systems and Rehabilitation Engineering*, 17.1: 2-8, 2008.
- [82] J.A. Saglia, *et al.*, "A high-performance redundantly actuated parallel mechanism for ankle rehabilitation," *Int J Robot Res*, 28:1216–27, 2009.
- [83] J.A. Saglia, *et al.*, "Control strategies for patient assisted training using the ankle rehabilitation robot (ARBOT)." *IEEE/ASME Trans Mechatron*, 1–10, 2012.
- [84] Y.H. Tsoi *et al.*, "Joint force control of parallel robot for ankle rehabilitation." *IEEE International Conference on Control and Automation (ICCA2009)*, p. 1856–61, 2009.
- [85] S.Q. Xie, "An iterative fuzzy controller for pneumatic muscle driven rehabilitation robot." *Expert Syst Appl*, 38:8128–37, 2011.
- [86] Maxon Motors. Permanent Magnet DC Motor with Coreless Winding. Rep. Maxon Academy, 2012. Web. Feb. 2015.
- [87] J.F. Veneman, *et al.* "Design and evaluation of the LOPES exoskeleton robot for interactive gait rehabilitation," *IEEE Transactions on Neural Systems and Rehabilitation Engineering*, 15.3: 379-386, 2007.
- [88] S. Fabrizio, *et al.*, "Design and characterization of a compact rotary series elastic actuator for knee assistance during overground walking," 4th IEEE RAS & EMBS International Conference on. IEEE Biomedical Robotics and Biomechatronics (BioRob), 2012.
- [89] W. dos Santos, A. Siqueira, "Impedance Control of a Rotary Series Elastic Actuator for Knee Rehabilitation," *World Congress*. vol. 19. no. 1. 2014.
- [90] E. Rivin, "Criteria For Power Transmission Couplings," Rep. SDP/SI, 2015. Web. Feb. 2015.
- [91] N. O'Dwyer, *et al.*, "Spasticity and muscle contracture following stroke." *Brain* 119.5: 1737-1750, 1996.
- [92] A. Albu-Schäffer, *et al.*, "A unified passivity-based control framework for position, torque and impedance control of flexible joint robots." *The International Journal of Robotics Research*, 26.1: 23-39, 2007.
- [93] C. Ott, *et al.*, "A passivity based cartesian impedance controller for flexible joint robots-part I: Torque feedback and gravity compensation." *IEEE International Conference on Robotics and Automation (ICRA2004)*, vol. 3, 2004.

- [94] N. Lynch, "Conceptual Design of a Robot for the RoboCup Competition." Bethlehem, Pennsylvania Final report, 2005.
- [95] M. Velasco-Villa, *et al.*, "Dynamic trajectory-tracking control of an omnidirectional mobile robot based on a passive approach." *INTECH* Open Access Publisher, 2010.
- [96] R. Chao, S. Ma, "Passivity-based model free control of an omnidirectional mobile robot." *IEEE International Conference on Mechatronics (ICM 2015)*, 2015.
- [97] S. Canfield, C. Reinholtz. "Development of the carpal robotic wrist." *Experimental Robotics V.*, 423-434, 1998.

Appendices

Appendix A: Custom Circuit Board Schematics

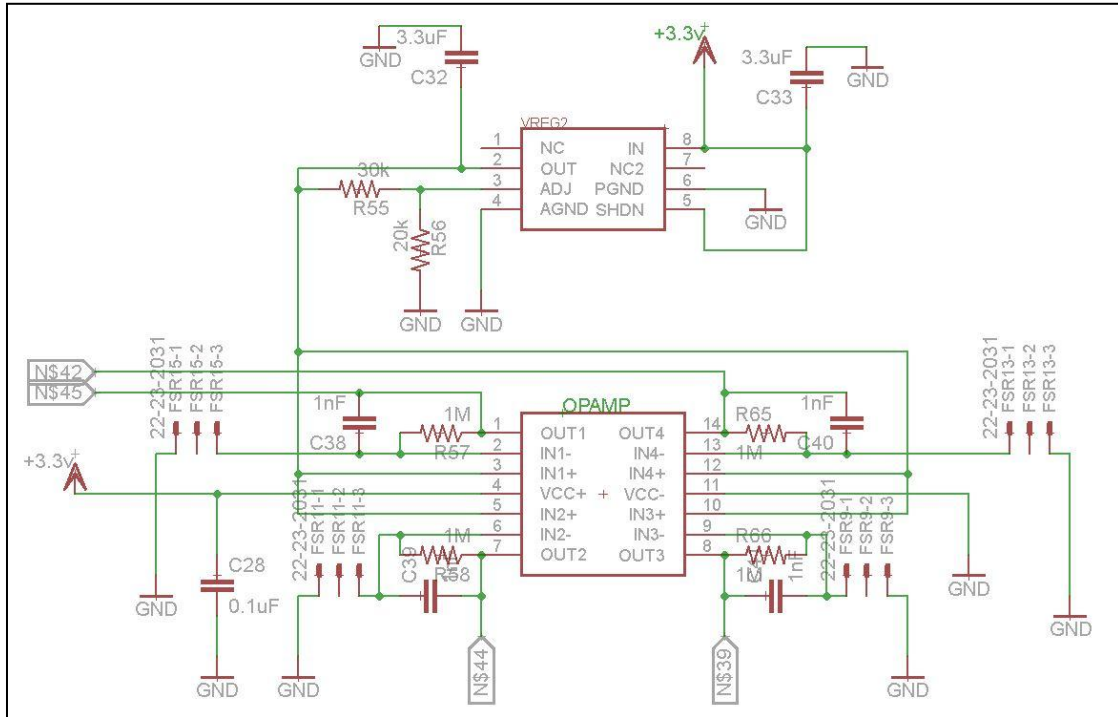


Figure A.1: Linearizing voltage amplification circuit for 4 pressure sensors.

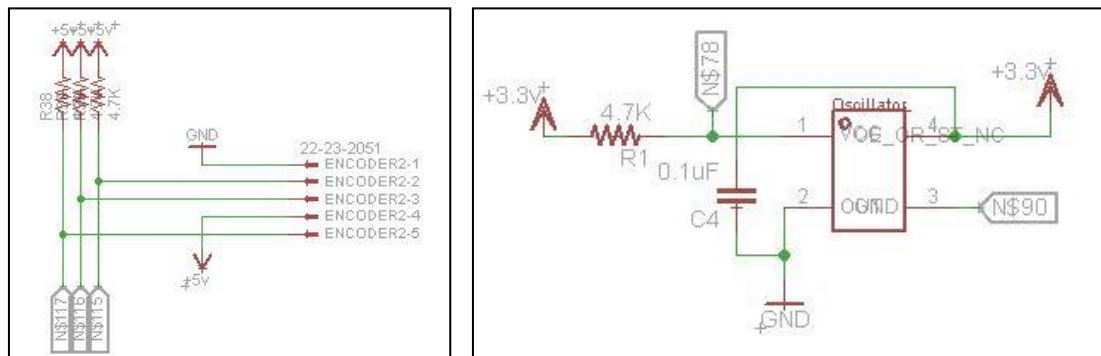


Figure A.2: Circuit design for a) one of the seven encoders and b) the oscillator.

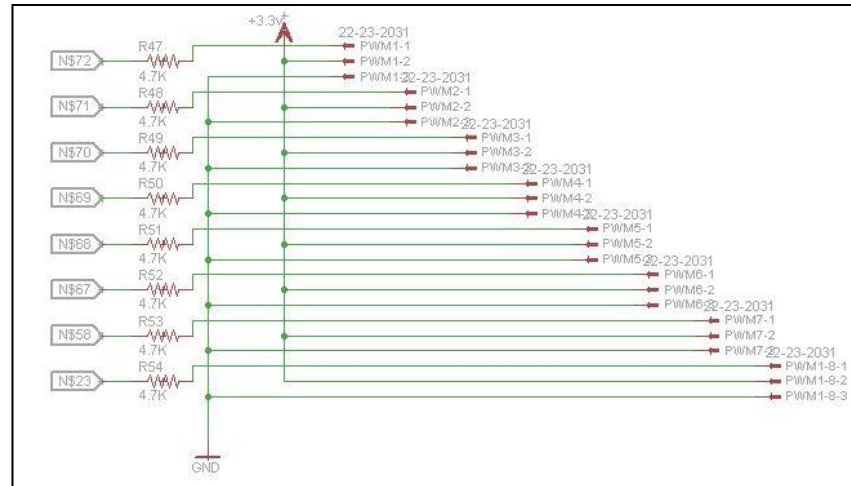


Figure A.3: Schematic for PWM

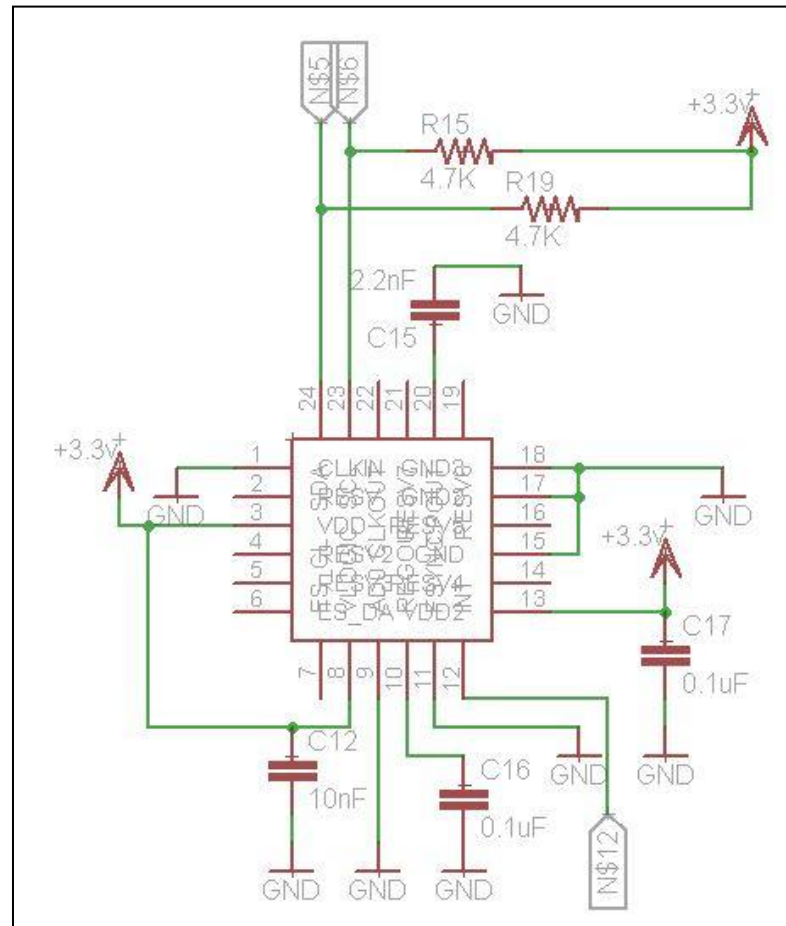


Figure A.4: Schematic for Accelerometer

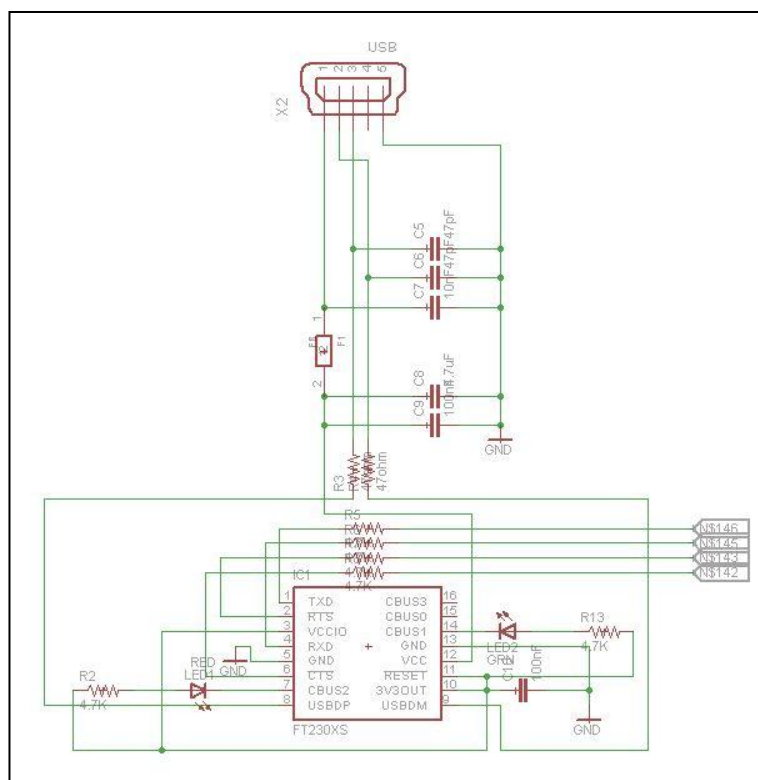


Figure A.5: Schematic for Serial communication

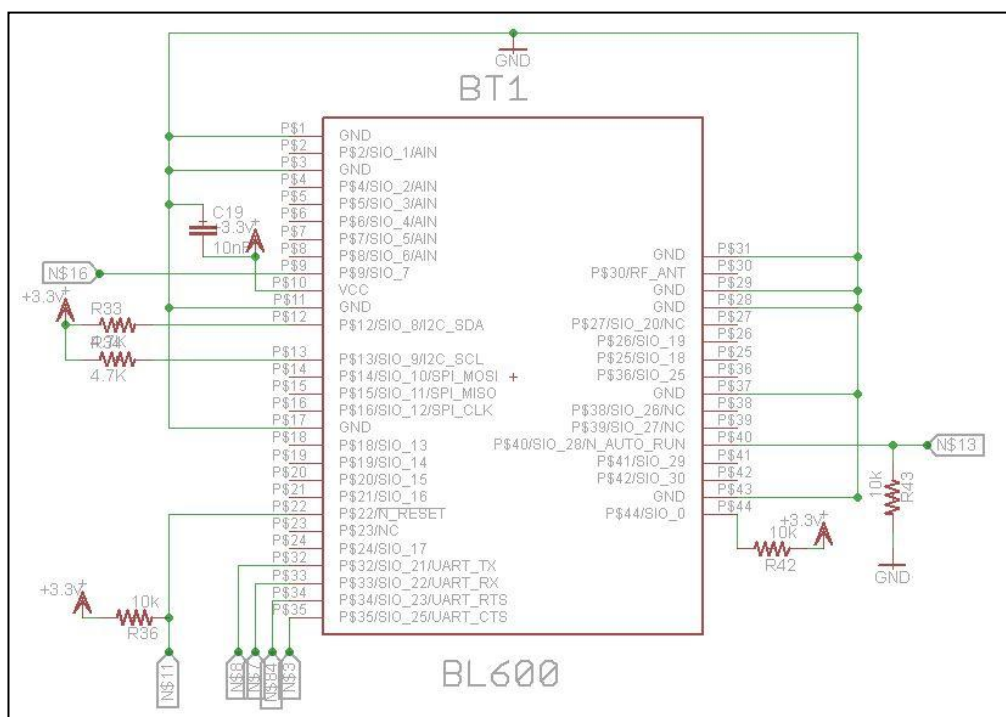


Figure A.6: Schematic for Bluetooth communication

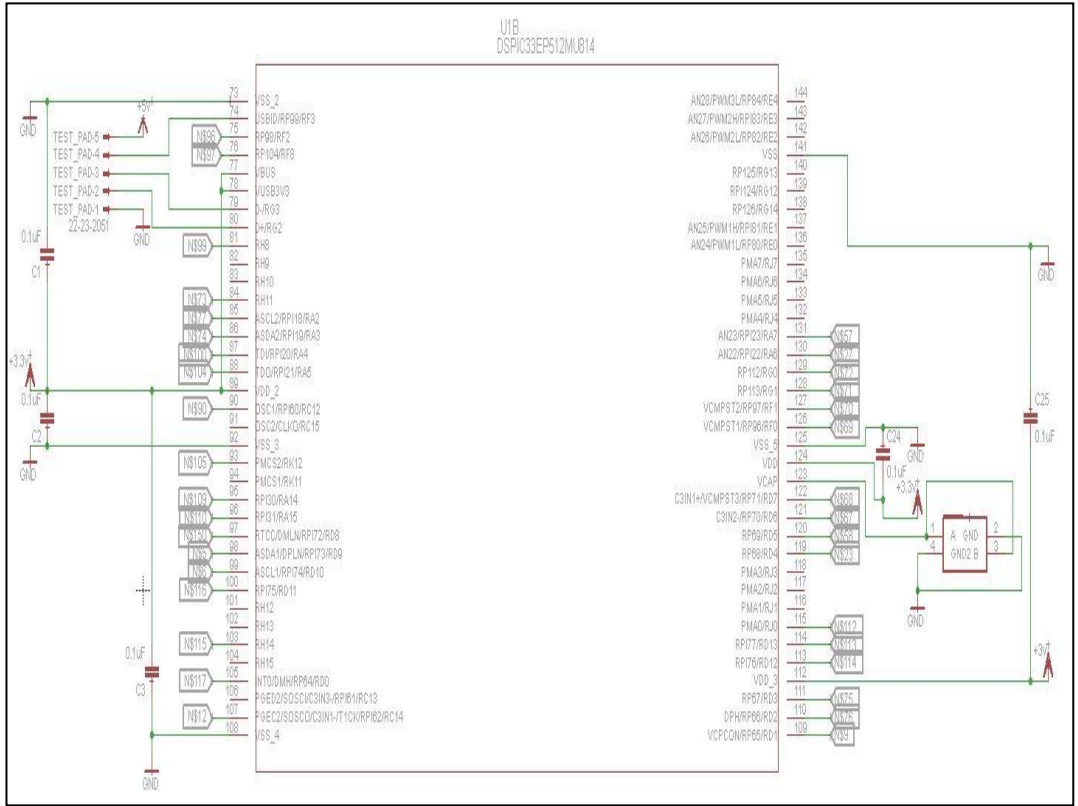
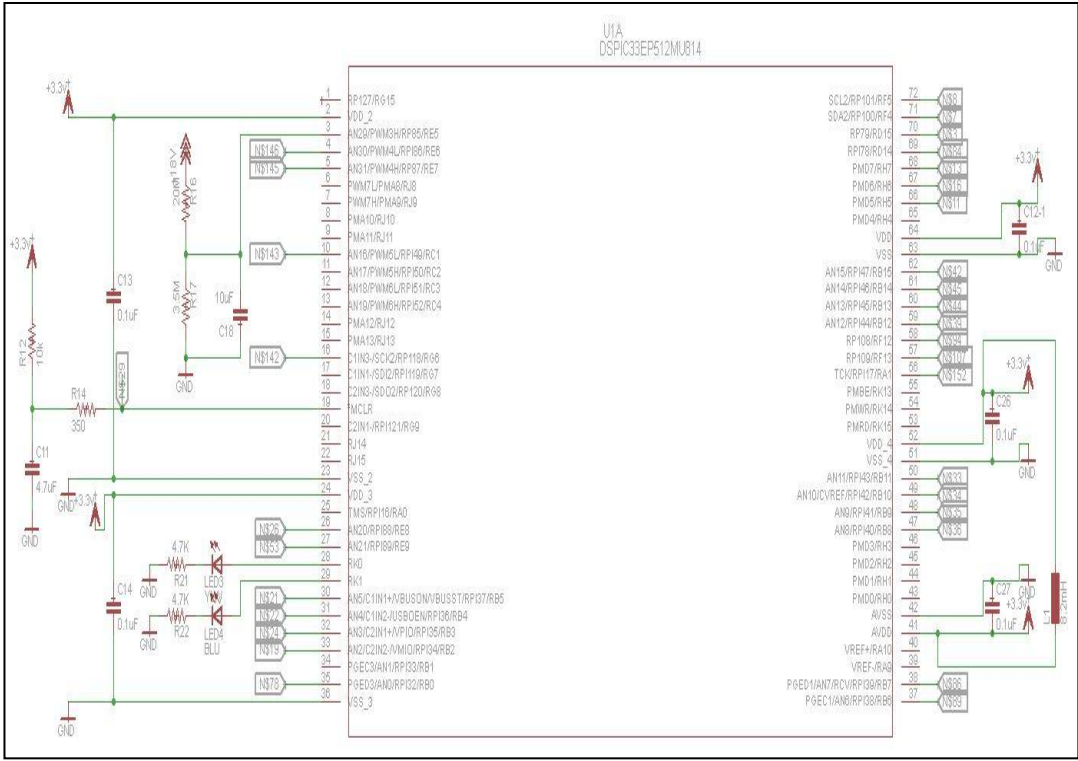


Figure A.7: Microcontroller Schematic

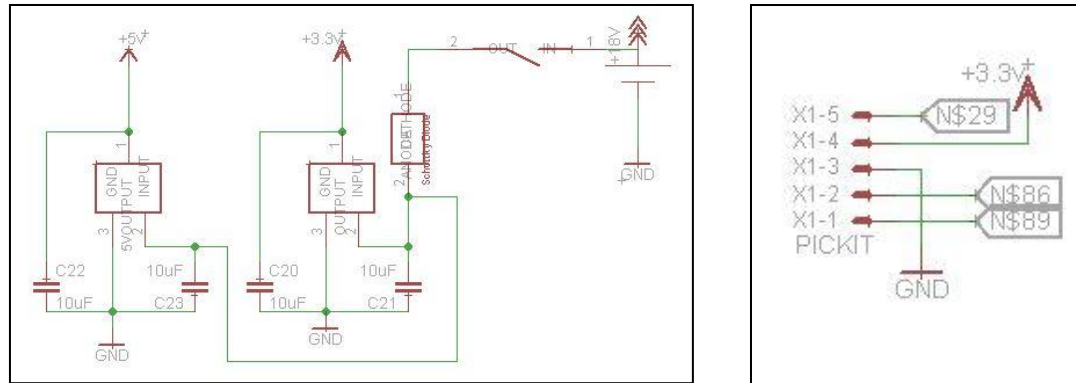


Figure A.8: Schematic for a) voltage regulators; b) microcontroller programmer

Appendix B: Costs Associated with Circuit Board and Six-DOF Lower-Limb Robot

Item #	Part Name	Unit price	Quan	Net Price
1	DSPIC33EP512MU814-X_P	13.5	1	13.5
2	Bluetooth	15.62	1	15.62
3	FTDI Chip	2.4	1	2.4
4	Mini USB	2.07	1	2.07
5	OP Amps	1.91	4	7.64
6	Adj Voltage Regulator	5.31	1	5.31
7	3.3V Voltage Regulator	1.22	1	1.22
8	5V Voltage Regulator	1.24	1	1.24
9	Oscillator	3.3	1	3.3
10	MPU3150	17.06	1	17.06
11	3pin PWM/FSR Connectors	1.11	24	26.64
12	3pin PWM/FSR Board Pins	0.853	24	20.472
13	5pin Encoder/Pickit Connec	2.02	8	16.16
14	5pin Encoder/Pickit Board P	1.59	8	12.72
15	Pickit board pins	0.48	1	0.48
16	Switch	6.73	1	6.73
17	FerriteBead	0.12	1	0.12
18	Schottky Diode	0.68	1	0.68
19	Green LED	0.43	1	0.43
20	Red LED	0.38	1	0.38
21	Yellow	0.43	1	0.43
22	Blue LED	0.52	1	0.52
23	8.2mH Inductor	1.24	1	1.24
24	10nF Capacitor	0.026	25	0.65
25	0.1uF Capacitor	0.038	25	0.95
26	2.2nF Capacitor	0.12	1	0.12
27	10uF Capacitor	0.29	5	1.45
28	3.3uF Capacitor	0.28	2	0.56
29	4.7uF	0.16	2	0.32
30	Low ESI Capacitor	0.52	1	0.52
31	1nF Capacitor	0.043	16	0.688
32	47pF Capacitor	0.12	2	0.24
33	4.7k Resistor	0.0124	45	0.558
34	10k Resistor	0.13	4	0.52
35	20k Resistor	0.13	1	0.13
36	30k Resistor	0.13	1	0.13
37	350 Resistor	0.13	1	0.13
38	3.3M Resistor	0.13	1	0.13
39	4.99M Resistor	0.028	16	0.448
40	2M Resistor	0.04	16	0.64
41	1M Resitos	0.04	16	0.64
42	47 Resistor	0.13	2	0.26
43	20M Resistor	1.2	2	2.4
Totals			262	167.846

Figure B.1: Circuit board components chart

Robot Subassembly: 3DOF Drive Train			
Structural Metal			
Laser Cut Parts			\$145.56
Hardware			
Fasteners			\$20.00
Gears			\$85.26
Wheels & Hubs			\$87.92
4 Motors			\$28.00
4 Gearboxes			\$240.00
Electrical			
Battery			\$38.44
Circuit Board			\$40.00
Circuit Board Components			\$167.00
Encoders			\$440.00
4 Motor Controllers			\$280.00
Circuit Breaker			\$30.00
Robot Subassembly: 3 DOF Parallel Manipulator			
Structural Metal			
Aluminum (machined in-house)			\$154.19
Laser Cut Parts			\$131.00
Hardware			
Lead screws, universal joints etc.			\$880.77
3 Motors			\$21.00
Electrical			
3 Encoders			\$150.00
3 Motor Controllers			\$210.00
Robot Subassembly: 6DOF Force Sensor			
Laser Cut Parts			\$100.00
Hardware			
Rubber, Fasteners			\$53.46
Sensors			
Pressure Sensors			\$234.00
Subassembly Cost Breakdown			
Total Cost of 3DOF Drive Train			\$1,602.18
Total Cost of 3DOF Parallel Manipulator			\$1,546.96
Total Cost of 6 DOF Force Sensor			\$387.46
Total Robot Cost			\$3,536.60

Figure B.2: Cost summary for six-DOF lower-limb rehabilitation robot

Curriculum Vitae

Name:	Aaron Yurkewich
Post-secondary Education and Degrees:	<p>University of Western Ontario London, Ontario, Canada M.E.Sc.(Electrical & Computer Engineering) 2013-2015</p> <p>The University of Western Ontario London, Ontario, Canada B.E.Sc.(Mechanical Engineering) 2009-2013</p>
Honours and Awards:	<p>NSERC Canadian Graduate Scholarship 2014-2015</p> <p>Province of Ontario Graduate Scholarship 2013, 2014(declined)</p> <p>Computer-Assisted Medical Interventions NSERC CREATE Grant 2013-2015</p> <p>John Foreman Gold Medal in Mechanical & Materials Engineering 2013</p> <p>NSERC Undergraduate Student Research Award 2012</p> <p>DELCAN Corporation Scholarship in Engineering Science 2012</p> <p>Lynn Fordham Award in Science and Engineering 2012</p> <p>Ontario Professional Engineers Education Scholarship 2012</p>
Related Work Experience	<p>Teaching Assistant, Digital Signal Processing, ECE 3331B Teaching Assistant, Intro to Electrical Instrumentation, MSE 2201A The University of Western Ontario 2013-2015</p>

Publications:

- Aaron Yurkewich, S. Farokh Atashzar, Ahmed Ayad, Dr. Rajni Patel. A Six-Degree-of-Freedom Robotic System for Lower Extremity Rehabilitation. IEEE International Conference on Rehabilitation Robotics (ICORR). Singapore. Accepted May 20, 2015. Presented August 13, 2015.
- Mahta Khoshnam, Aaron Yurkewich, Dr. Rajni Patel. Model-Based Force Control of a Steerable Ablation Catheter with a Custom-Designed Strain Sensor. IEEE International Conference on Robotics and Automation (ICRA). Karlsruhe, Germany. May 6, 2013. Accepted Jan. 7, 2013. Presented May 9, 2013.
- Ran Xu, Aaron Yurkewich, Dr. Rajni Patel. A Review of Modeling and Control of Concentric-tube Robots. Engineering Transactions of CAE, Frontiers of Mechanical Engineering. Submitted March 22, 2015.
- Ran Xu, Aaron Yurkewich, Dr. Rajni Patel. Curvature and Torsion Sensing for Pre-Curved Continuum Robots. SPIE BiOS. Submitted August 3, 2015.
- Kaspar Shazada, Aaron Yurkewich, Ran Xu, Dr. Rajni Patel. Sensorization of a Surgical Robotic Instrument for Force Sensing. SPIE BiOS. Submitted August 3, 2015.